

Spring 2009

A system model for the effect of Polarization Mode Dispersion on digital modulated optical signals in single mode fibers

Abhijit Shriram Chitambar
University of New Hampshire, Durham

Follow this and additional works at: <https://scholars.unh.edu/dissertation>

Recommended Citation

Chitambar, Abhijit Shriram, "A system model for the effect of Polarization Mode Dispersion on digital modulated optical signals in single mode fibers" (2009). *Doctoral Dissertations*. 470.
<https://scholars.unh.edu/dissertation/470>

This Dissertation is brought to you for free and open access by the Student Scholarship at University of New Hampshire Scholars' Repository. It has been accepted for inclusion in Doctoral Dissertations by an authorized administrator of University of New Hampshire Scholars' Repository. For more information, please contact nicole.hentz@unh.edu.

**A SYSTEM MODEL FOR THE EFFECT OF POLARIZATION MODE DISPERSION ON
DIGITAL MODULATED OPTICAL SIGNALS IN SINGLE MODE FIBERS**

BY

ABHIJIT SHRIRAM CHITAMBAR

B.E., University of Mumbai, May, 1997

M.S., Drexel University, May 2000

DISSERTATION

Submitted to the University of New Hampshire

in Partial Fulfillment of

the Requirements for the Degree of

Doctor of Philosophy

in

Electrical Engineering

May, 2009

UMI Number: 3363714

INFORMATION TO USERS

The quality of this reproduction is dependent upon the quality of the copy submitted. Broken or indistinct print, colored or poor quality illustrations and photographs, print bleed-through, substandard margins, and improper alignment can adversely affect reproduction.

In the unlikely event that the author did not send a complete manuscript and there are missing pages, these will be noted. Also, if unauthorized copyright material had to be removed, a note will indicate the deletion.

UMI[®]

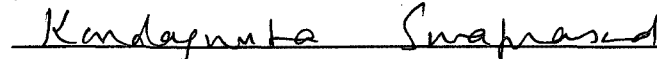
UMI Microform 3363714

Copyright 2009 by ProQuest LLC

All rights reserved. This microform edition is protected against unauthorized copying under Title 17, United States Code.

ProQuest LLC
789 East Eisenhower Parkway
P.O. Box 1346
Ann Arbor, MI 48106-1346

This dissertation has been examined and approved.



Dr. Kondagunta Sivaprasad,

Dissertation Director, Professor of Electrical and Computer Engineering



Dr. Kent Chamberlin,

Professor of Electrical and Computer Engineering



Dr. Allen Drake,

Associate Professor of Electrical and Computer Engineering,



Dr. Michael Carter,

Associate Professor of Electrical and Computer Engineering,



Dr. Charles Bianchi,

Affiliate Associate Professor of Electrical and Computer Engineering

April 8, 2009
Date

DEDICATION

This work is dedicated to God and to my patron saint Sai for his abundant blessings and grace. To my wife, Sarita; my parents Anuradha and Shriram; my in-laws Kumarie and Anisbert and my brother, Aniruddha for the encouragement that they provided during all these years of study.

Faith & Perseverance

ACKNOWLEDGEMENTS

This undertaking has been successful because of the help and goodwill that I have received from my friends, colleagues and my advisors.

Two people have been instrumental in guiding me through this endeavor and to whom I will forever be in debt. They deserve my special thanks: Dr. Sivaprasad - for his unwavering support and encouragement; Dr. Bianchi - who mentored me through my initial years at Lucent Technologies and who has been a true source of inspiration. His wisdom, knowledge and commitment to the highest standards, always have, and will continue to inspire and motivate me.

I would like to thank the members of my graduate committee at UNH for their time and effort in reviewing this dissertation.

I would like to thank my colleagues from Lucent Technologies and Tellabs: Andy Hamel, Rick Barrett, Jesse Pan, Paul Vanasse and Rick McCallough for sharing their knowledge and for their support. I would especially like to acknowledge the support of my present technical manager, Kenneth Fisher during the conclusion of the program.

Lastly, I would like to thank my family, especially my wife, Sarita, for her love, support and patience and my little son, Yash, for his bear hugs and kisses.

FOREWORD

The main topics of this dissertation are addressed as follows:

Chapter 1 provides an introduction to the PMD impairment in optical communication networks. Existing statistical models are defined and their limitations are discussed. Literature of the related work in the field is surveyed. The data shows that the existing models do not adequately represent the PMD impairment.

An overview of the basic building blocks of a simple optical network is provided in Chapter 2. The standard optical network performance indicators such as Optical Signal to Noise Ratio (OSNR), Inter symbol Interference (ISI) and eye closure, Bit Error Rate (BER), Q factor and performance penalty are discussed.

Chapter 3 provides an overview of the transmission medium of the optical networks along with the various channel impairments like, attenuation, which reduces the reach of optical networks and pulse broadening due to dispersion, which reduces the signal strength and degrades the performance of the optical network. Data from field measurements which highlights the significance of the channel impairments is reviewed.

Polarization Mode dispersion as a Channel impairment is analyzed in Chapter 4. As a part of this discussion, the first order and second order effects of the PMD impairment and its dependence on length are reviewed. The existing statistical model of PMD is analyzed and its limitations are discussed which provide the basis for a new approach to characterize the PMD impairment.

Results from sample simulations which highlight the impact of the PMD impairment on the performance of the optical communication system are illustrated. The new model which can be grown in a discrete way and which is able to capture the complete ensemble of discrete components of the output differential group delay distribution is described. The mathematical implementation of the new model to generate the output differential group delay distribution and the performance penalties is discussed.

Results from our various simulations that characterize the PMD impairment using the new systems model are shown in Chapter 6. Complete characterization of the discrete ensemble of the delay components at the output of a single mode fiber is demonstrated. The ability of the new model to sequentially grow the output distribution and to simulate fiber impairments in the form of mixed fiber sections and PMD artifacts is illustrated. The impact of the PMD impairment on optical networks in terms of Q penalty is evaluated and simulation results are compared against published results.

Conclusions and recommendations are discussed in Chapter 7.

TABLE OF CONTENTS

DEDICATION	iii
ACKNOWLEDGEMENTS	iv
FOREWORD	v
LIST OF FIGURES	xi
LIST OF TABLES	xvii
ABSTRACT	xviii

CHAPTER	PAGE
I INTRODUCTION & OVERVIEW	1
1.1 Introduction	1
1.2 Background	3
1.3 Motivation	11
1.4 Organization of the Dissertation	14
II COMPONENTS OF OPTICAL NETWORK	16
Introduction	16
2.1 Optical Network Overview	16
2.1.1 Transmitter Section	22
2.1.2 Intermediate Optical Amplification	24
2.1.3 Receiver Section	30
2.2 Optical Network Performance Parameters	31
2.2.1 Bit Error Rate	31
2.2.2 Optical Signal To Noise Ratio	33

2.2.3 Eye Diagrams	34
2.2.4 Performance Penalty	38
Summary	39
III IMPAIRMENTS IN OPTICAL FIBERS	40
Introduction	40
3.1 Attenuation	43
3.1.1 Rayleigh Scattering	44
3.1.2 Material Absorption	45
3.1.3 Waveguide Imperfections	47
3.1.4 Splices and Connectors	47
3.1.5 Optical Time Domain Reflectometer	49
3.1.6 Field Measurements on Continuity and Loss	51
3.2 Dispersion in Optical Fibers	52
3.2.1 Intermodal Dispersion	52
3.2.2 Chromatic Dispersion	53
3.2.3 Field Measurements for Chromatic Dispersion	57
3.2.4 Polarization Mode Dispersion	59
3.2.5 Field Measurements for PMD	63
Summary	65
IV THEORY OF POLARIZATION MODE DISPERSION	67
Introduction	67
4.1 Polarization in Optics	67
4.1.1 Generation of Polarized Light	68
4.1.2 Jones Vectors and Jones Matrix	72

4.1.3 Poincare Sphere	74
4.2 Propagation of Transverse Fields in an Optical Waveguide	76
4.3 Propagation of Polarization Modes in Single Mode Fibers	81
4.3.1 Birefringence and Beat Length	85
4.3.2 First Order PMD	87
4.3.3 Second Order PMD	91
4.3.4 Relationship between the First Order and Second Order PMD	93
4.4 Limitations of Existing Statistical Model of PMD	94
Summary	98
V MODEL AND SIMULATION OF POLARIZATION MODE DISPERSION	99
Introduction	99
5.1 Impact of PMD on Optical Systems	100
5.1.1 Impact of PMD on Network Data Rates	101
5.1.2 Performance Penalties due to PMD Impairment	111
5.2 The New Statistical Model for PMD	126
5.3 Numerical Implementation Of The New Model	133
5.3.1 Implementation of the Delay Distribution	133
5.3.2 Implementation of the DGD Model in an Optical System	138
Summary	148
VI SIMULATION RESULTS	149
Introduction	149
6.1 Configuration of Simulation Bin Size	150
6.2 Configuration of Concatenated Homogenous Channel	153

6.3 Configuration of Incremental Channel	163
6.4 Configuration of Concatenated Heterogeneous Channel	166
6.4.1 Mix of Distributed Effect	167
6.4.2 Mix of Distributed and Deterministic Effect	172
6.5 Impact of PMD Impairment on Network Performance	184
Summary	192
VII CONCLUSIONS AND RECOMMENDATIONS	194
Conclusions	194
Recommendations	197
LIST OF REFERENCES	200
APPENDIX	204

LIST OF FIGURES

<u>Figure</u>	<u>Page</u>	<u>Title</u>
1-1	7	PSP Evolution across Long Length of Single Mode Fiber
1-2	8	Sample Screen Shot of PMD Field Measurement
1-3	9	Field Measurement of PMD on Fiber Spool of Length 77 km
2-1a	17	Point to Point Optical Network
2-1b	17	Ring Network
2-1c	18	Meshed Network
2-2	19	Metro & Long Haul Networks
2-3	21	Wavelength Spectrum in CWDM & DWDM Systems
2-4	21	Basic DWDM Optical Network
2-5	23	Transmitter Section
2-6	24	NRZ-OOK & RZ-OOK Modulation Schemes
2-7	25	Erbium Doped Fiber Amplifier
2-8	26	Intermediate optical Amplification
2-9	29	Raman Amplification
2-10	29	Raman Gain Over a Fiber Span
2-11	30	Receiver Section
2-12	32	Bit Error Rate
2-13	35	Eye Diagram
2-14a	36	Eye Diagram With No Distortions
2-14b	37	Eye Diagram Chromatic Dispersion Under-Compensation
2-14c	37	Eye Diagram Ideal Chromatic Dispersion Over-Compensation

2-15	37	Eye Diagram for System with PMD Impairment
2-16	39	Performance Penalty
3-1	41	Optical Fiber
3-2	41	Multi Mode Fiber and Single Mode Fiber
3-3	45	Spectral Attenuation Curves For Different Loss Phenomenon
3-4	46	Absorption & Bending Losses in Fibers
3-5	48	Splices & Connectors
3-6	50	Optical Time Domain Reflectometer Block Diagram
3-7	50	Sample OTDR Trace
3-8	51	Span Length Discrepancy Statistics
3-9	52	Span Loss Discrepancy Statistics
3-10	56	Contributions to Chromatic Dispersion
3-11	56	Field Measurement of Chromatic Dispersion
3-12	57	Chromatic Dispersion Discrepancy in Measured Fiber Spans
3-13	58	Sample Chromatic Dispersion Penalty in Terms of Reduction in Reach
3-14	62	Interferometric PMD Measurement Block Diagram
3-15	63	Sample Interferometric Field Measurement for Distributed Effect of PMD
3-16	64	Polarization Mode Dispersion Field Measurement Statistics
3-17	65	Sample PMD Penalty in Terms of Reduction in Reach
4-1	69	Polarization Of Light
4-2	70	Electrical Field Intensity At Various Time Instants
4-3	71	Polarization States
4-4	73	Jones vectors And Jones Matrix

4-5	74	Poincare Sphere
		Wavelength Sweep On Poincare Sphere For A Highly
4-6	76	Birefringent Device
4-7	81	Orthogonal Modes
4-8	82	Orthogonal Pulses with No Group Delay
4-9	83	Accumulation of Deterministic effect of PMD
		Effect of Mode Coupling on $\Delta\tau$ and Energy Content of the Two
4-10	84	Orthogonal Modes
4-11	86	Phase transition over a Beat Length segment
4-12	95	Random Polarization States across Incremental Beat Lengths
4-13	96	Field Measurement of PMD
		Network Configuration to Measure Impact of PMD on Network
5-1	102	Data Rates
5-2	103	Mean PMD in Pico-Seconds v/s Bit Error Rate
5-3	105	Bit Error Rate Variation at 2.5 Gbps
5-4	105	Bit Error Rate Variation at 10 Gbps
5-5	106	Bit Error Rate Variation at 40 Gbps
5-6	109	Eye Diagrams at 10 Gbps Data Rate
5-7	109	Eye Diagrams at 40 Gbps Data Rate
5-8	110	Overall Performance System at 2.5 Gbps, 10 Gbps, 40 Gbps
5-9	112	Receiver Characterization Test Bed
5-10	113	Baseline Receiver Performance
5-11	115	System Performance with Distributed PMD
5-12	116	OSNR versus Mean BER for Distributed Effect PMD

5-13	118	Generating Deterministic PMD Using OptSim Simulation Test Bed
5-14	119	Deterministic PMD Setup
5-15	119	Deterministic Versus Distributed Effect 20 ps
5-16	120	Deterministic Versus Distributed Effect 30 ps
5-17	121	Deterministic Versus Distributed Effect 35 ps
5-18	122	Deterministic Versus Distributed Effect 40 ps
5-19	122	Deterministic Versus Distributed Effect 50 ps
5-20	123	Concatenation of Deterministic PMD (10 Gbps Data Rate)
5-21	124	Concatenation of 20 ps & 20 ps Deterministic Artifacts
5-22	124	Concatenation Of 20 ps & 30 ps Deterministic Artifacts
5-23	127	Fixed Birefringence of Beat length Segment
5-24	127	Concatenation of Two Beat Length Segments
5-25	129	Concatenation of Multiple Beat Length Segments
5-26	140	Sample Sinc Response Showing the Effect of Delays
5-27	140	Effect of DGD on the Zero Crossing Points
6-1	151	Effect of Sampling Bin Size on Output DGD Distribution curves
6-2	151	Q Penalty v/s Bin Size for Types of Fibers with Different Delay Variance
6-3	154	Plots of Output DGD Distribution for different Lengths of Same Fiber Type (Variance 0.001 ps)
6-4	156	Beat Length Segments versus RMS DGD for Fixed Fiber Type (Variance 0.001 ps)
6-5	157	Beat Segments Versus Q Penalty dB for Fixed Fiber Type (Variance 0.001 ps)

6-6	158	Plots of Output DGD Distribution for different Lengths of Same Fiber Type (Variance 0.5 ps)
6-7	159	Beat Length Segments versus RMS DGD for Fixed Fiber Type (Variance 0.5 ps)
6-8	160	Beat Length Segments versus Q Penalty dB for Fixed Fiber Type (Variance 0.5 ps)
6-9	161	PMD Field Measurement 7 km Fiber Spool
6-10	162	PMD Field Measurement 77 km Fiber Spool
6-11	162	PMD Field Measurement 124 km Fiber Spool
6-12	164	Output DGD Distribution for Different Fiber Types
6-13	165	Q Penalty for Different Fiber Types
6-14	168	Equal Parts Homogenous Mix with Variance 0.0001 ps & 0.1 ps
6-15	169	Equal Parts Homogenous Mix with Variance 0.0001 ps & 0.01 ps
6-16	171	Different Length Combinations of Homogenous Mix with Variance 0.0001 ps & 0.001 ps
6-17	174	Homogenous Fiber Delay variance 0.0001 ps With Single PMD Artifact 0.5ps. Simulation Bin Size = 0.0025 ps
6-18	174	Homogenous Fiber Delay variance 0.0001 ps With Single PMD Artifact 1ps. Simulation Bin Size = 0.0025 ps
6-19	175	Homogenous Fiber Delay variance 0.0001 ps With Single PMD Artifact 4ps. Simulation Bin Size = 0.0025 ps
6-20	175	Homogenous Fiber Delay variance 0.0001 ps With Single PMD Artifact 8ps. Simulation Bin Size = 0.0025 ps
6-21	176	Homogenous Fiber Delay variance 0.0001 ps With Single PMD Artifact 12ps. Simulation Bin Size = 0.0025 ps
6-22	177	5 ps PMD Artifact with Varying Lengths of Homogenous Fiber (Delay Variance 0.0001 ps), Sampling Bin Size 0.0025 ps

6-23	177	Q Penalty for 5 ps PMD Artifact with Varying Lengths of Homogenous Fiber (Delay Variance 0.0001 ps)
6-24	179	5 ps PMD Artifact Mixed with Different Types of Homogenous Fibers. Simulation Bin Size = 0.0025 ps
6-25	180	Simulation Result Output DGD Distribution of Two Artifacts of 8 ps and 5 ps
6-26	181	Field Measurement Snapshot of Resultant output DGD Distribution with 8 ps and 5 ps Artifact
6-27	182	Two PMD Artifacts of Value 2 ps & 3 ps with Different Fiber Types. Simulation Bin Size = 0.0025 ps
6-28	183	Two PMD Artifacts of Value 2 ps & 2 ps with Different Fiber Types. Simulation Bin Size = 0.0025 ps
6-29	185	Normalized RMS DGD versus Q penalty (dB) 10 Gbps Data Rate
6-30	188	Normalized RMS DGD versus Q penalty (dB) 40 Gbps Data Rate
6-31	190	Normalized RMS DGD versus Q penalty (dB) 100 Gbps Data Rate

LIST OF TABLES

<u>Figure</u>	<u>Page</u>	<u>Title</u>
5-1	106	Statistical Variations Over 100 Runs in Bit Error Rate 10 Gbps
5-2	107	Bit Error Rate over 100 Runs: 40Gbps Data Rate
5-3	117	Optical Signal to Noise Ratio Penalties for Bit Error Rate $5e-7$
5-4	143	Statistical Data from Output Simulation Results
6-1	152	Q Penalty Statistics: Different Fiber Types at Various Bin Sizes
6-2	155	Growth of RMS DGD (ps) with Length of Fiber (Delay Variance 0.001ps)
6-3	157	Growth of Q Penalty with Length for Fixed Fiber Type (Variance 0.001ps)
6-4	159	Growth of RMS DGD (ps) with Length of Fiber (Delay Variance 0.5ps).
6-5	160	Growth of Q Penalty with Length for Fixed Fiber Type (Variance 0.5ps)
6-6	166	Q Penalty for Different Fiber Types
6-7	169	RMS DGD for Case 1 of Fiber Mix
6-8	170	RMS DGD for Case 2 of Fiber Mix
6-9	172	RMS DGD for Case 3 of Fiber Mix
6-10	178	Q Penalty for Different Lengths: Fiber Section with 5ps PMD Artifact
6-11	186	Q Penalty Results 10Gbps Data Rate
6-12	189	Q Penalty Results 40Gbps Data Rate
6-13	191	Q Penalty Results at 100Gbps Data Rate

ABSTRACT

A SYSTEM MODEL FOR THE EFFECT OF POLARIZATION MODE DISPERSION ON DIGITAL MODULATED OPTICAL SIGNALS IN SINGLE MODE FIBERS

by

Abhijit Shriram Chitambar

University of New Hampshire May, 2009

A comprehensive systems model that retains the discrete nature of the output delay distribution in order to accurately characterize the pulse broadening due to Polarization Mode Dispersion (PMD) is developed in this thesis. PMD in optical channels has been a critical factor limiting high-speed data transmission over long distances in optical networks. PMD is a source of Inter Symbol Interference (ISI) and its impact increases with the transmission data rate. Since economical adaptive compensation schemes are currently unavailable, it is essential to characterize this impairment to completely understand its impact and develop effective countermeasures. An incremental approach has been developed to methodically grow the output DGD distribution of single mode optical fibers. It provides the flexibility to change individual beat segment delays and enables the simulation and characterization of the distributed and the deterministic effects of PMD. The model also accurately evaluates the impact of the PMD impairment on the performance of optical networks in terms of Q. Results from comparing performance penalties at 10G bps, 40G bps and 100 Gbps data rates of transmission are in agreement with published trends.

CHAPTER - 1

INTRODUCTION & OVERVIEW

1.1 Introduction

Optical fiber impairments are critical factors limiting high-speed data transmission over long distances in optical communication networks. Impairments in the channel caused by chromatic dispersion, Polarization Mode Dispersion (PMD) and transmission loss have a direct impact on the reach of a network or the quality of transmission at higher bit rates and narrowly spaced channels. The presence of PMD in optical fibers is one of the main factors limiting the capability of a channel to transport high-speed data. PMD reduces the reach of networks, and the increased regeneration requirements of optical signals result in expensive network designs.

A basic optical network consists of a transmitter Section, a transmission channel (optical fiber), optical amplifiers, regenerators and a receiver section. The transmitter section is a continuous wave laser source at a fixed wavelength. The laser source is fed to a modulator driven by the digital data source. The output of the modulator, which is a continuous beam of light switched ON and OFF at the data rate of the driver, is launched into the optical channel. As the signal propagating along the length of the fiber degrades in intensity and bandwidth due to attenuation and dispersion, it needs to be amplified and reshaped at periodic intervals.

To compensate for the degradation in the optical signal caused by these effects the signal may require reconstruction and regeneration over the length of transmission. The receiver section detects the optical signal, and the modulated information is recovered. The performance of such a typical optical network configuration is primarily a function of the system components and the transmission media. Physical measurements performed in order to characterize a fiber optic network include optical loss measurements, optical time-domain reflectometry (OTDR) measurements, chromatic dispersion and Polarization Mode Dispersion measurements. Data from OTDR measurements provides information on span length, span loss and the location and magnitude of defects which cause attenuation and reflectance. Chromatic dispersion causes distortion of the optical signal as it travels through the fiber. It is a critical performance parameter for designing dense wavelength division multiplexed (DWDM) and high bit rate (2.5Gbps, 10Gbps, 40Gbps, 100Gbps) Synchronous Optical Network (SONET) / Synchronous Digital Hierarchy (SDH) applications, where capacity is a function of channel spacing and spectral width. The measurement of chromatic dispersion is also required to optimize spacing between two optical nodes or terminals, to determine dispersion compensation, to maximize the channel count, and to identify nonlinear effects. PMD is a critical performance parameter for high bit rate SONET/SDH applications as it causes signal fading and inter-symbol interference which results in reach limitations due to degradation in network performance. A system with excessive chromatic dispersion and/or Polarization Mode Dispersion will have considerable inter-symbol interference which may result in an unacceptable bit error rate performance. Hence, a measurement of chromatic dispersion

and Polarization Mode Dispersion is necessary to evaluate the suitability of installed fiber for the transport of high bit rate optical signals.

Backbone and distribution networks are composed entirely of single-mode optical fibers, as it has reduced attenuation and multi-mode interference, which allow the propagation of high-speed broadband signals over long distances. Factors limiting the performance of the optical transport systems as a function of configuration (wavelength) and application (bit-rate) in single mode fibers are dispersion and the nonlinear effects of the fiber. As the rate of data transmission increases (2.5Gbps, 10Gbps, 40Gbps, 100Gbps), these factors result in an increase in ISI and a reduction in the signal-to-noise margin. Chromatic dispersion is a source of ISI that increases with the data rate and can be addressed by employing existing dispersion compensation techniques. PMD is also a source of ISI that increases with data rate, but the unpredictable nature of this impairment does not permit simple and cost effective compensation techniques. Hence, it is critical to devise a comprehensive model to characterize this impairment in order to understand the impact and develop performance improvements. This dissertation addresses the characterization and quantification of PMD in single mode optical fiber networks by creating a system model to simulate its effect and understand its impact on the optical network performance.

1.2 Background

In an optical transmission medium with a two-dimensional cross section, the arbitrarily polarized light may be expressed in two spatial dimensions, which are

orthogonal to each other and perpendicular to the direction of propagation. Thus, a single mode fiber with birefringence may support propagation of light energy within two so-called polarization modes. Energy excited in both dimensions may be represented by these two orthogonally polarized modes of propagation. If the transverse structure is physically and geometrically symmetrical, the two orthogonally polarized signals will travel physically equivalent paths. A medium that is longitudinally homogenous will not support the transfer of energy between orthogonally polarized modes. The signals will propagate with the same transit time or group delay and arrive at the receiver at the same time. On the other hand, birefringent fiber has a transverse propagation structure that is not quite symmetrical. In this case the two orthogonally polarized signals that are launched will travel along two physically separate paths having different optical lengths. Polarization Maintaining Fiber (PMF) is an example of such a transmission medium. The orthogonal modes in a PMF are defined by a fast and slow axis of propagation with unique refractive indices along the axes of propagation. The weak coupling between the two modes ensures that the signal energy launched along these axes will not couple with each other as they travel across the length of the PMF section. The two orthogonal modes will travel across the fiber with a speed defined by the unique refractive index along the axis. The intrinsic birefringence of this fiber is intentionally very high to minimize the influence of external variations (temperature, pressure) on the weak mode coupling. Such signals having different group delays will arrive at the receiver at different times. Since an optical intensity receiver does not discriminate polarization, these signals may interfere destructively, causing distortion and fading. Irregularities along a birefringent fiber, such as stress and strain, may give rise to longitudinal non-

homogeneity, resulting in continuous and random scrambling of the polarization states as the signal propagates. These irregularities allow the signal to spread across randomly polarized and concatenated paths, randomizing the Differential Group Delays (DGD) between various signal replicas arriving at the receiver. When the fiber is long enough to sufficiently spread the signal, a statistical distribution of DGD or distributed PMD is produced. The root mean square value of this distribution gives a measure of PMD impairment.

One of the earliest efforts toward understanding Polarization Mode Dispersion in single mode fibers was made by Rashleigh and Ulrich [1] in 1978. They explored the pulse broadening due to this dispersion impairment based on their understanding of two degenerate polarized eigen modes supported within a single mode fiber. Their experiments showed that birefringent single mode fibers exhibit significant mode dispersion and that this broadening is proportional to the fiber length for short sections of fiber and proportional to the square root of the fiber length for longer sections of the fiber. With the technology advancements and development of faster gigabit optical transmission systems there was a growing realization that the pulse broadening due to Polarization Mode Dispersion in single mode fibers would present an obstacle in deployment of high speed optical systems.

It was relatively straightforward to explain the propagation of these polarized eigen modes within a homogenous waveguide where the characteristic parameters of the two modes remained the same and the two modes were identical in all respects, but it became more complicated to understand their propagation when the two modes became

distinct [1]. If the waveguide geometry was disturbed by local stress or strain on the core of the fiber, the two Eigen modes acquired independent propagation characteristics. It was also observed that if a polarized light source were to be applied at the input of a long section of fiber (greater than 1 km) it was very difficult to observe the eigen modes as the output light appeared completely un-polarized. It was in 1986 that Poole and Wagner [2] came up with the first comprehensive model which adequately addressed the dispersion phenomenon and propagation through short and long lengths of single mode fibers. Assuming that the optical system suffers no loss due to polarization effects and that the pulse broadening due to PMD is much smaller than the bit period, Poole's model states that there exist input orthogonal states of polarization for which output states of polarization are orthogonal with no first order dependence to wavelength. These orthogonal modes at the input and the output are referred to as the Principle States of Polarization (PSP) and provide the basis for characterization of PMD in single mode fibers. An optical pulse aligned with the PSP's at the input of the fiber will emerge at the output with all its frequency components intact and the only distortion will be the time shift between the two orthogonal pulses. In short fibers the PSP's correspond to the polarization modes of the fiber; this is analogous to the earlier interpretation of eigen modes through a homogenous medium. For longer spans, the polarized light will couple with the PSPs at the input of the fiber and will evolve through various states of polarization across the length of the fiber according to waveguide variations [Figure 1-1].

Long Length of Birefringent Single Mode Fiber

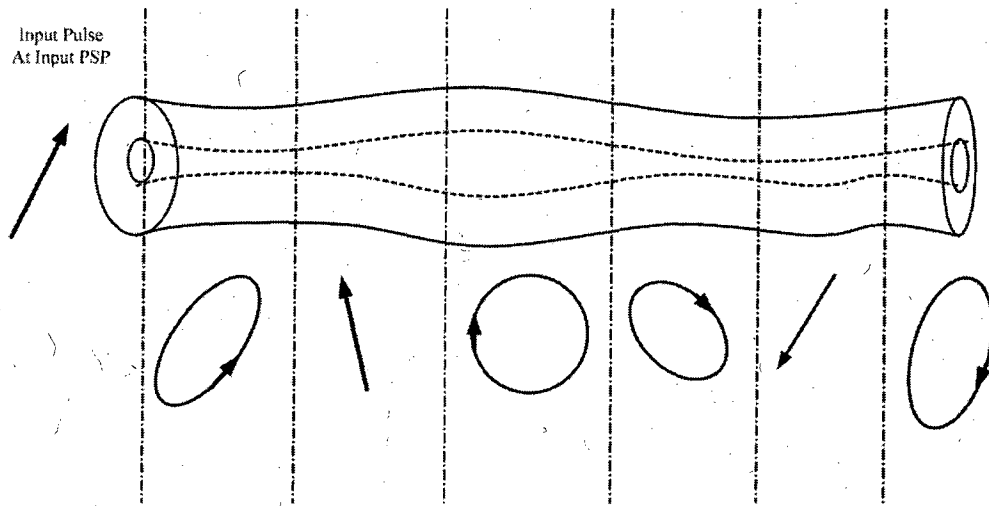


Figure 1-1 PSP Evolution across Long Length of Single Mode Fiber

Based on the new phenomenological approach using the PSP theory, Poole and Giles [3] in 1988 presented the analytical work on first order PMD and its dependence on length for short and long sections of single mode fiber. They concluded that the resultant output delay distribution appears to be nearly Gaussian and can closely be approximated as a continuous Gaussian envelope with a fixed mean and variance. In their later work, Poole and Nagel [4] offered a correction to their observation and indicated that the probability density function for the magnitude of the dispersion vector at long lengths of single mode fiber closely resembles a Maxwellian distribution and the PMD impairment could be approximated as a continuous Maxwellian envelope with a fixed mean and variance. Further work by Gisin and Pery [6] in 1993 measured the PMD impairment over increasing concatenations of fiber sections and confirmed that the observed output Differential Group Delay (DGD) distribution could be approximated as a Maxwellian

envelope. Field measurements of PMD use the interferometric technique [7] proposed by the Telecommunications Industry Association (TIA) and follow the Fiber Optic Test Procedure (FOTP-124) standard to capture a small sample of this statistical distribution in time. A Gaussian fit is imposed on this captured distribution as shown in Figure 1-2. The mean of the Gaussian envelope is interpreted as the root mean square value (PMD) of the distribution. The measured value of PMD in this case is 4.1 picoseconds.

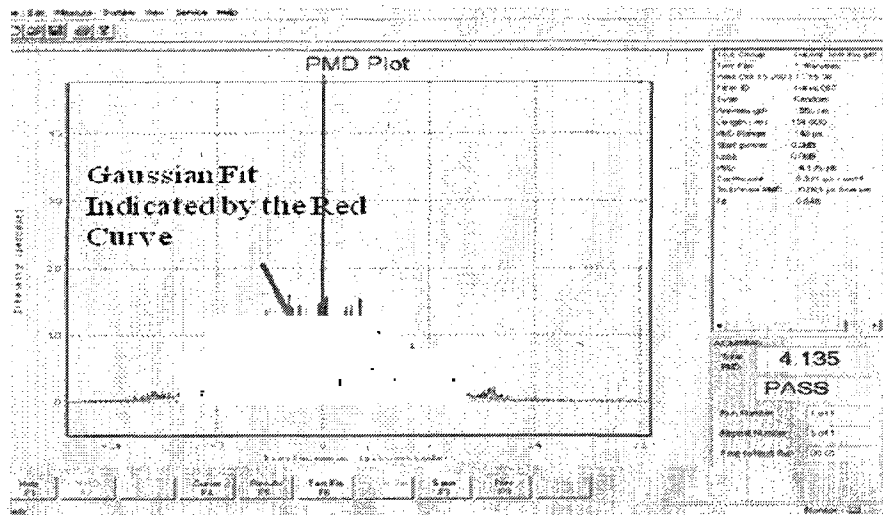


Figure 1-2 Sample Screen Shot of PMD Field Measurement

The output DGD distribution being a discrete ensemble of the delayed components at the receiver, an approximation of this collection in terms of a fixed mean and variance of a continuous Gaussian or Maxwellian envelope may not adequately represent or characterize the impairment. Figure 1-3 shows a field measurement on a fiber spool of length 77 km.

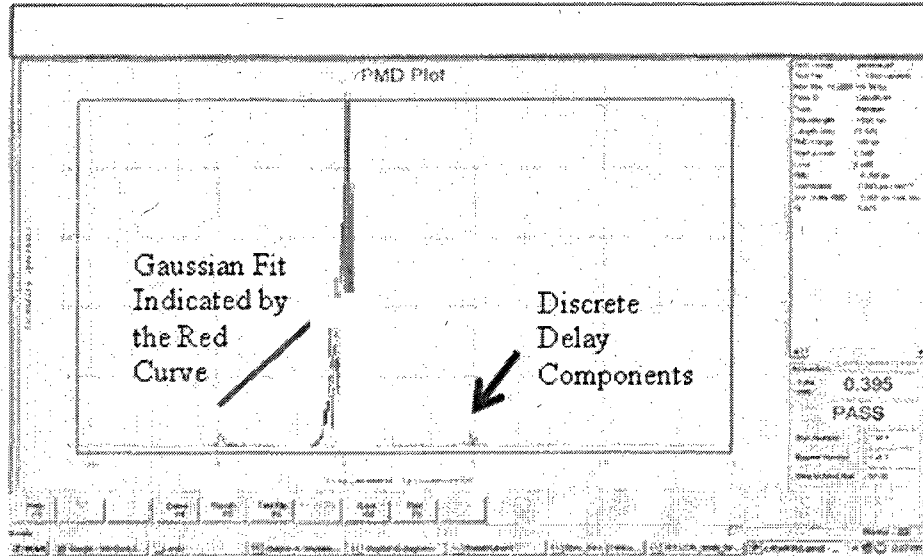


Figure 1-3 Field Measurement of PMD on Fiber Spool of Length 77 km

The field measurement imposes a Gaussian fit on the output DGD distribution and indicates the measure of the PMD impairment as 0.395 ps. The Gaussian envelope does not account for the small measure of the discrete delay components at 5 ps as shown in the figure. This results in gross under-estimation of the PMD impairment and results in incorrect network designs.

As technology advancements led to further development of high speed optical systems, it became necessary to assimilate the PMD impairment in a system model to understand the impact of this pulse broadening on the performance of optical networks. Poole and Fishman [8] investigated the fading caused by PMD in an optical system setup carrying data at 1.7 Gbps at wavelength of 1550 nm. Their experiments provided a quantitative estimate of the performance degradation for different values of PMD impairment. They compared their measured results against the analytical estimates and

found a good match in the trend of the results which showed a square law dependence of the penalty with respect to the PMD impairment. Subsequent work by Zhou and O'Mahony [9] show similar trends of the growth of penalty with respect to the PMD impairment. Poole found that his theoretical penalty results were much more optimistic than the actual measured results and he attributed this deviation to signal dependent noise in APD receivers or to discrepancies in the source spectrum. Later work by Zhou and Xie [10] on 10 Gbps optical systems further validated the square law trends and showed a penalty of less than 1db for PMD impairment of value less than 30% of the bit period. Although there could be contributions from other sources which were not considered in this comparison, it could also imply that continuous approximation of the discrete ensemble may not adequately represent the impairment and a more thorough characterization could lead to better representation of this impairment which will result in accurate estimate of the penalties.

Additional efforts have attempted to address the PMD impairment by developing compensation schemes [11, 12, and 13]. These efforts have been challenged by the time-varying nature of the PMD. Hakki [14] demonstrated the effect of adiabatic and isothermal changes on the measured value of the PMD impairments. Under adiabatic conditions the optical fiber was subjected to large variations in temperature which replicates the exposure of terrestrial fibers. These temperature variations give rise to varying stress along the length of the fiber which resulted in variation in the measured PMD impairment with time. Isothermal conditions replicate the environment of undersea cables where the variation in stress and strain is limited. Under these conditions Hakki [14] found that measured PMD impairment was strongly dependent on the frequency of

the signal. The variations in the measured value were also found to be a function of ambient temperature changes. This ambient environmental sensitivity of PMD adds to the challenge in designing compensation schemes. From an analytical point of view, a continuous approximation of this output distribution does not adequately represent the PMD impairment.

Accurate estimation of the dispersion penalty is critical to the design and optimization of optical communication systems. There has been significant effort toward establishing guidelines for PMD tolerance in optical network design [15, 16 and 17]. These generic guidelines suggest that a penalty greater than 1 dB is unacceptable. In terms of outage probability, this value translates to 1 in 18000. In terms of cumulative network outage time this translates to 30 minutes per year. Poole and Nagel [18] analytically correlate this 1 dB penalty stipulation to a normalized tolerance limit of 0.14, which implies that for a digital system to avoid a penalty of greater than 1 dB, the Polarization Mode Dispersion should be less than 14% of its bit period of data transmission. For a 10 Gbps system this translates to PMD tolerance of less than 14 ps.

1.3 Motivation

The commonly used network design metric [4, 18 and 19] for Polarization Mode Dispersion is quantified as the root mean square value of the output delay distribution. A survey of the literature [1-18] shows that the existing models are based on the theory of Principal States of Polarization and define the differential group delay as a continuous distribution. Some models approximate the shape of this continuous distribution as

Gaussian or Maxwellian in the time domain. For short fiber distances, polarization mode dispersion increases linearly with the length of propagation. For large fiber lengths the mean total polarization mode dispersion is proportional to the square root of the propagation length [1]. In practice, since a fiber span may accurately be viewed as a concatenation of a large number of discrete effects, the total PMD would be a function of the interaction of these discrete/individual effects. It is not clear that the mean value of a continuous distribution will thoroughly characterize the actual ensemble of concatenated polarization-scrambled paths.

Although the stochastic nature of this impairment necessitates the characterization of PMD over a large range of values to accurately estimate the distribution, an exhaustive Monte Carlo simulation of a large population of PMD values sufficient for the accurate prediction of low bit-error rates is both difficult and time-consuming. The extrema (end regions or “tails”) of such continuous distributions (Maxwellian or Gaussian) define the values of the impairment responsible for the worst-case performance degradation of the network. Proper characterization of the distribution is therefore critical. Also, the asymptotic nature of the distribution may necessitate the design of a system that is tolerant to large variations of the impairment. This in turn makes the design of successful compensation schemes very challenging. Accurate estimation of the dispersion penalty is critical to optical network design. Under-estimation of this penalty will result in significant degradation in network performance. Correction of this limitation may require expensive regeneration of the signal or even reduction in the reach of the optical network.

The literature survey shows that the existing statistical system models for PMD do not have the capability to account for the changes in birefringence induced in the fiber by the non-homogenous nature of the impairment over distance and they do not provide the capability to account for the pulse broadening accurately in such conditions. As a result they do not allow for dynamic analysis of the change in the output differential group delay distribution at the end of the fiber. The existing models do not have the capability to introduce and analyze anomalies such as differing sections of fibers or randomly occurring deviations. It is evident from these limitations that the existing statistical models do not adequately characterize the PMD impairment in single mode fibers and its impact on the performance of optical networks.

In this dissertation, a new approach is proposed and a comprehensive channel model is developed that retains the discrete nature of the output delay distribution in order to accurately characterize the pulse broadening due to PMD. The optical fiber can be visualized as a concatenation of a large number of beat length segments which are characterized by fixed individual delays and are joined along unique axes of polarization. Output delay components from one beat segment are the input to the next beat length segment where they couple with its unique delay and axis of polarization to generate new output delay components that are a function of the individual beat delays of all preceding beat length segments. The output delay distribution is sequentially grown across each successive beat segment to generate the total distribution at the end of the fiber span. This channel model is then integrated into a system model to evaluate the impact of the PMD impairment on the performance of optical network systems. The results are compared to data collected from the field and in the laboratory.

1.4 Organization of the Dissertation

The topics addressed in this dissertation are arranged into 7 chapters as follows:

Chapter 1 provides an introduction to the PMD impairment in optical communication networks. Existing statistical models are defined and their limitations are discussed. Literature of the related work in the field is surveyed. The data shows that the existing models do not adequately represent the PMD impairment.

An overview of the basic building blocks of a simple optical network is provided in Chapter 2. The standard optical network performance indicators such as Optical Signal to Noise Ratio (OSNR), Inter-symbol Interference (ISI) and eye closure, Bit Error Rate (BER), Q factor and performance penalty are discussed.

Chapter 3 provides an overview of the transmission medium of the optical networks along with the various channel impairments like, attenuation, which reduces the reach of optical networks, and pulse broadening due to dispersion, which reduces the signal strength and degrades the performance of the optical network. Data from field measurements which highlights the significance of the channel impairments is reviewed.

Polarization Mode Dispersion as a channel impairment is analyzed in Chapter 4. As a part of this discussion, the first order and second order effects of the PMD impairment and their dependence on length are reviewed. The existing statistical model of PMD is analyzed and its limitations are discussed, which provides the basis for a new approach to characterize the PMD impairment.

Results from sample simulations which highlight the impact of the PMD impairment on the performance of the optical communication system are illustrated in Chapter 5. The new model, which can be grown in a discrete way and which is able to capture the complete ensemble of discrete components of the output differential group delay distribution, is described in this chapter. The mathematical implementation of the new model to generate the output differential group delay distribution and the performance penalties is also discussed.

Results from our various simulations that characterize the PMD impairment using the new system model are shown in Chapter 6. Complete characterization of the discrete ensemble of the delay components at the output of a single mode fiber is demonstrated. The ability of the new model to sequentially grow the output distribution and to simulate fiber impairments in the form of mixed fiber sections and PMD artifacts is illustrated. The impact of the PMD impairment on optical networks in terms of Q penalty is evaluated and simulation results are compared against published results.

Conclusions and recommendations are discussed in Chapter 7.

CHAPTER - 2

COMPONENTS OF OPTICAL NETWORK

Introduction

This chapter provides an overview of the basic building blocks of a simple optical network. The optical network may be divided into four basic blocks: the Transmitter section, the Intermediate Optical Amplification section, the Receiver section and the Optical Transport Media section. Characteristics of each of these blocks or subsystems contribute towards the overall performance of the optical network. The standard optical network performance indicators such as Optical Signal to Noise Ratio (OSNR), Inter symbol Interference (ISI) and eye closure, Bit Error Rate (BER), Q factor and performance penalty are also discussed.

2.1 Optical Network Overview

Optical networks may be classified by network architecture, overall end to end reach or their wavelength density/capacity. In terms of network topology, they may be classified into

- Linear networks: Point to Point data transport applications [Figure 2-1a].

- Ring networks: Protected data applications where in case of failure on the active path the traffic will automatically switch to the protect path [Figure 2-1.b].
- Mesh networks: These are the next generation optical networks using the Wavelength Selective Switch technology (WSS) which allows seamless passage or blocking of one or multiple wavelengths. Mesh networks allow for path diversity between source and destination nodes. Thus in the case of any outage due to fiber cuts, data traffic can be easily re routed through diverse paths to reach the destination [Figure 2-1c].

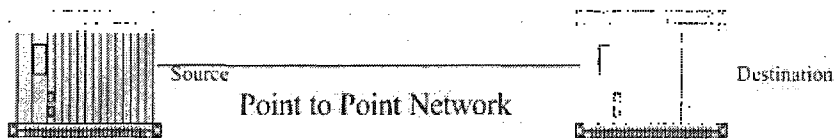


Figure 2-1a Point to Point Network

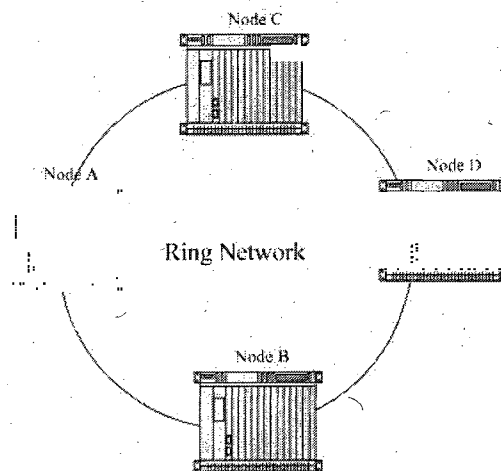


Figure 2-1b Ring Network

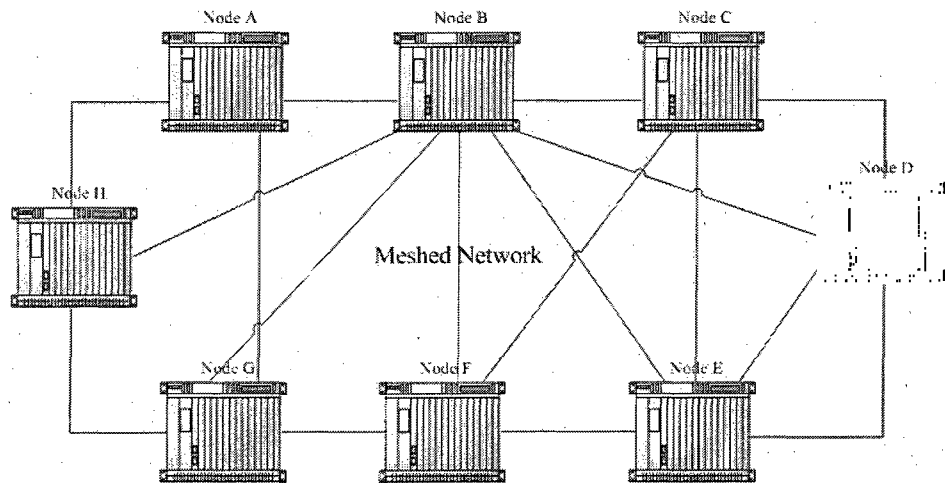


Figure 2-1c Mesh Network

Based on reach of the optical networks they may be classified into:

- Metro Optical networks: These networks are implemented within a city. Their overall reach may be close to 200 to 300 km. Metro environment is characterized by high density of a wide spectrum of traffic which includes voice (land line and wireless), data and video. Thus, Metro networks are responsible for aggregation and distribution of this wide spectrum of traffic. They also function as a bridge passing the aggregated local traffic on to the long haul networks which moves this traffic nationwide.
- Long Haul and Ultra Long Haul networks: These networks have an end to end reach of more than 1000 km. These networks are optimized to carry the data for long distances without regeneration. These networks can carry more than

100 wavelengths at either 10Gbps (1Tbps total capacity) each or 40Gbps (4Tbps total capacity) each respectively. The next generation of networks will be able to support 100Gbps data rates; thus 100 wavelengths at 100Gbps each will enhance the overall capacity of these networks to carry 10Tbps.

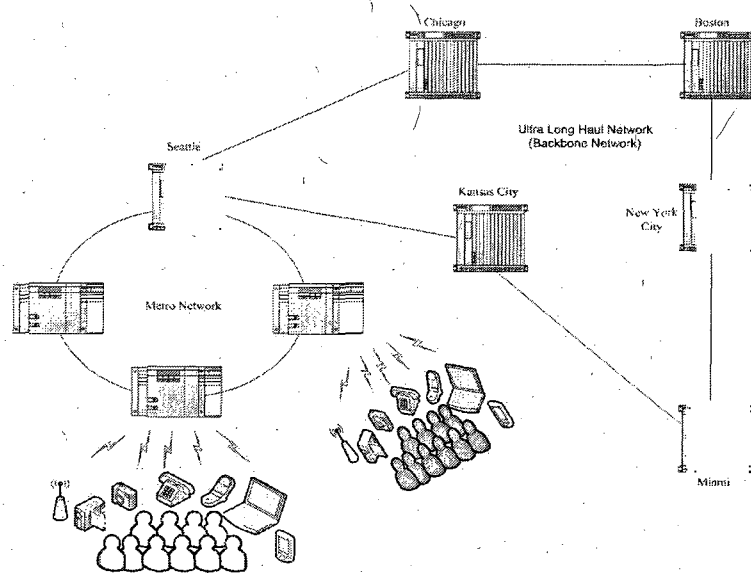


Figure 2-2 Metro and Long Haul Networks

Based on wavelength density optical networks are characterized into [Figure 2-3]:

- **Single Wavelength Networks:** These networks use a single optical wavelength to transport data from the source to the destination. These types of networks were seen over the early formative years of the optical networking technology. In today's technology the optical fiber offers a

large bandwidth by supporting the transport of multiple wavelengths across a single fiber.

- Coarse Wavelength Division Multiplexing (CWDM): In these applications typically 2 to 8 wavelengths are multiplexed onto the fiber. The spacing between the wavelengths is very wide (typically greater than 20nm). Fiber To The Premise (FTTP) and Fiber To The Home (FTTH) are applications where CWDM is used. Uplink from the Home or Premise to the central office is done at 1550nm while downlink from the central office is done at 1310nm.
- Dense Wavelength Division Multiplexing: DWDM systems utilize the C band (1525-1565 nm) or the L band (1570-1610 nm) or both for transporting a large number of wavelengths which are spaced very close to each other. Typical wavelength spacing's in commercial applications are either 100 GHz (0.8 nm) or 50 GHz (0.4 nm). This multiplexing scheme is used in long haul high capacity optical networks where data may be transported nationwide over optical backbones.

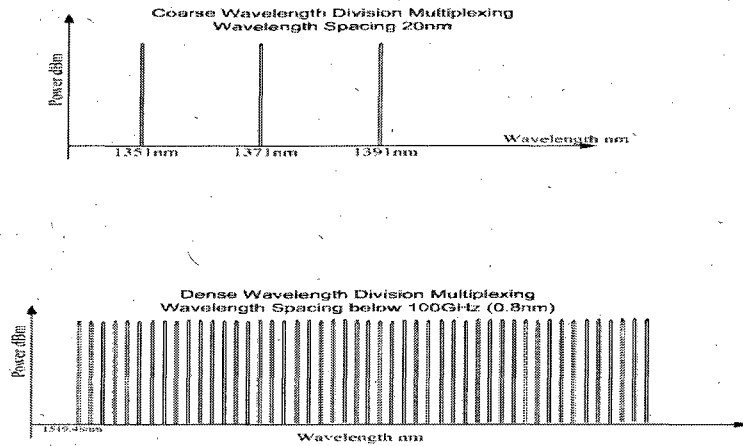


Figure 2- 3 Wavelength Spectrums in CWDM & DWDM Systems

Figure 2-4 shows the basic subsystems of a point to point DWDM optical network. It consists of a Transmit Section which injects multiplexed wavelengths into the transmission medium (single mode fiber). The wavelengths suffer loss as they propagate across the fiber spans and need optical amplification at regular intervals. The signals arrive at the destination and are de multiplexed and detected at the receiver section.

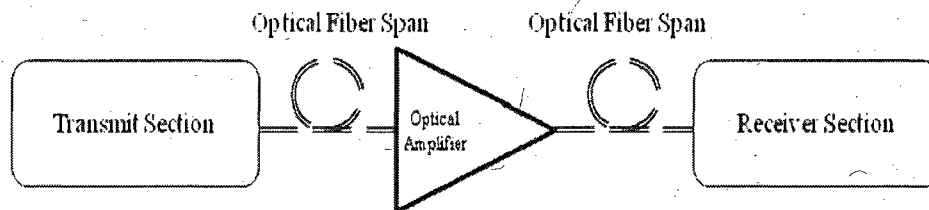


Figure 2- 4 Basic DWDM Optical Network

2.1.1 Transmitter Section

Figure 2-5 shows a detailed view of the Transmitter subsystem. Multiple electronic data streams may be interleaved into a single stream of high data rate for e.g. 10Gbps. There are two inputs to the external optical modulator. The first one is from a continuous laser source of specific wavelength and the second input is from its driver which is driven by the 10Gbps data stream. The output of the external optical modulator is a continuous beam of optical light at the wavelength of the laser source which is turned ON or OFF based on the input from the data stream. Current dense Wavelength Multiplexed (DWDM) systems requires stable laser sources whose operating wavelength and signal intensity do not change with external ambient conditions like temperature. The laser sources need to have narrow line width or spectral width and should be tunable across a wide range of wavelengths. Since the modulation of these laser sources involves turning the laser source ON and OFF most of the modulation schemes are referred to as ON - OFF Keying (OOK). The modulating digital pattern of 1's and 0's can either be directly applied to the laser source in which case the laser source itself is made to turn ON and OFF based on whether the modulating bit is a 1 or a 0, In which case it is referred to as direct modulation. The laser source can stay ON all the time and the modulating digital patterns of 1's and 0's can be used to drive an external modulating device (e.g. Mach Zehnder Modulator). This device will cause its output to turn ON or OFF based on the driving voltage pattern of either a 1 or a 0, this is referred to as external modulation of the laser source.

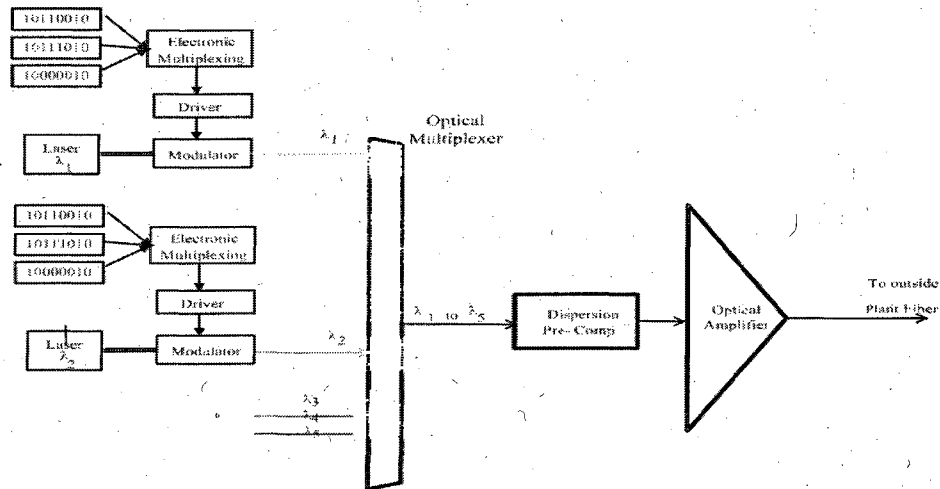


Figure 2- 5 Transmitter Section

Examples of some digital optical transmission schemes are Non Return to Zero On Off Keying (NRZ-OOK) and Return to Zero On Off keying (RZ-OOK) as shown in Figure 2-6. In the NRZ-OOK transmission scheme the laser source remains on for the entire duration of the pulse width for a bit 1. If two 1 bits are received consecutively, the laser will stay on for two consecutive pulse width durations. If a bit 0 is received it is turned off for one pulse width duration. If two consecutive 0 bits are received, the laser source will stay off for two consecutive pulse width periods. In RZ OOK scheme, the laser source will stay on for half the pulse width period for bit 1. If two 1 bits are received consecutively, the laser will turn on its laser source and will transition twice in the two pulse width periods. If a 0 bit is received the laser will stay off for the duration of pulse width and if two consecutive zeros are received the laser will stay off for two pulse width periods. Each modulation scheme has its advantages and disadvantages and the choice of modulation scheme is based on the design of the optical network. The optically

modulated signal is pre-amplified before being launched into the optical fiber span so that it can overcome losses over transmission and can travel a certain distance before it is either re-amplified or detected.

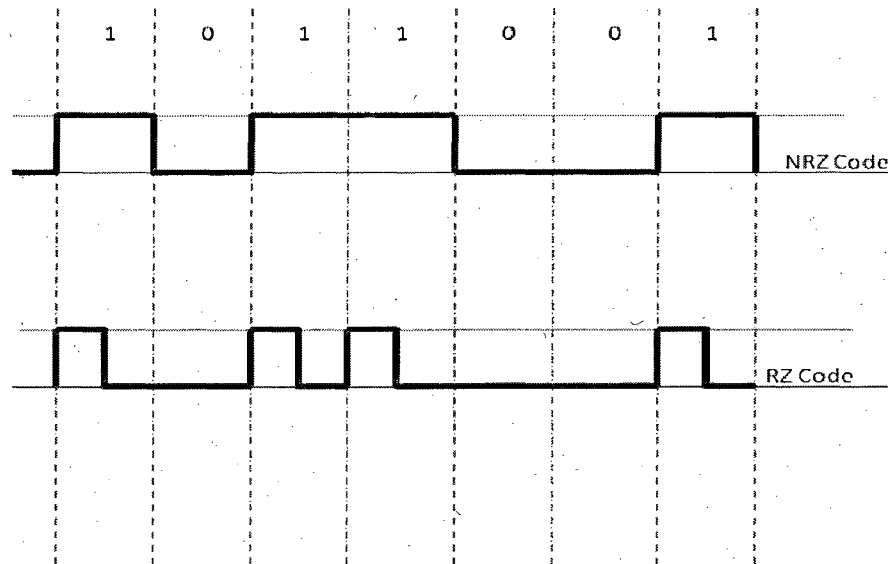


Figure 2- 6 NRZ-OOK & RZ-OOK Modulation Schemes

2.1.2 Intermediate Optical Amplification

Optical signals from the transmit section incur propagation losses as they travel over long lengths of fibers. As the optical signals degrade in strength, they need to be re-amplified at regular intervals of fiber spans. Optical amplification is often implemented using Erbium Doped Fiber amplifiers (EDFA) which does not require the signals to be converted into the electrical domain. These amplifiers are able to provide optical gain over the entire wavelength spectrum of the signal (C band 1525 nm - 1565 nm or L band 1570 nm to 1610 nm). In the erbium doped amplifiers the core of the silica fiber is doped with tri-valent Erbium ions (Er^{+3}) which can be excited by a pump laser source at 980nm

to produce gain in the 1550 nm range [19, 34]. The pump laser excites the ions into a higher state of energy from where they decay back to a lower energy level via stimulated emission. The photons from this stimulated emission have the same wavelength as the signal. The range of the signal spectrum which can be amplified or the gain bandwidth of the optical amplifier depends upon the spectroscopic properties of the dopant ions, the glass structure of the optical fiber, and the wavelength and power of the pump laser. EDFAs have broad gain bandwidth and a single amplifier can amplify all signals of the spectrum that are being carried on the fiber and which fall within the gain bandwidth. This makes them very useful in dense wavelength multiplexed systems Figure 2-7 shows a simple representation of the EDFA.

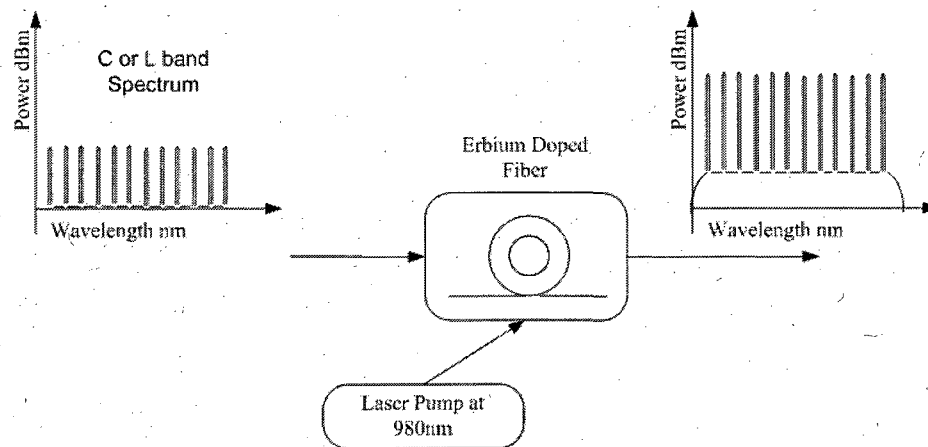


Figure 2- 7 Erbium Doped Fiber Amplifier

The disadvantage with these amplifiers is that they are also significant sources of broadband noise ASE (Amplified Spontaneous Emission). Although the gain is achieved through stimulated emission, this also accompanies spontaneous emission. A fraction of the spontaneous emission falling within the numerical aperture of the fiber is captured or guided by the fiber. These photons may interact with the dopants and be amplified along with the signal spectrum. The ASE which co-propagates with the direction of signal spectrum is responsible for degradation of the system performance. Although the amplifier has broad gain bandwidth, the gain provided to each wavelength is not equal [Figure 2-8]. The gain profile may have a positive tilt where the gain is larger for higher wavelengths or a negative tilt in which case the gain is less for higher wavelengths. Successive amplifications may introduce a significant positive or negative tilt which would need correction. This correction is implemented by loss equalization done using the gain tilt adjustment block of the amplifier.

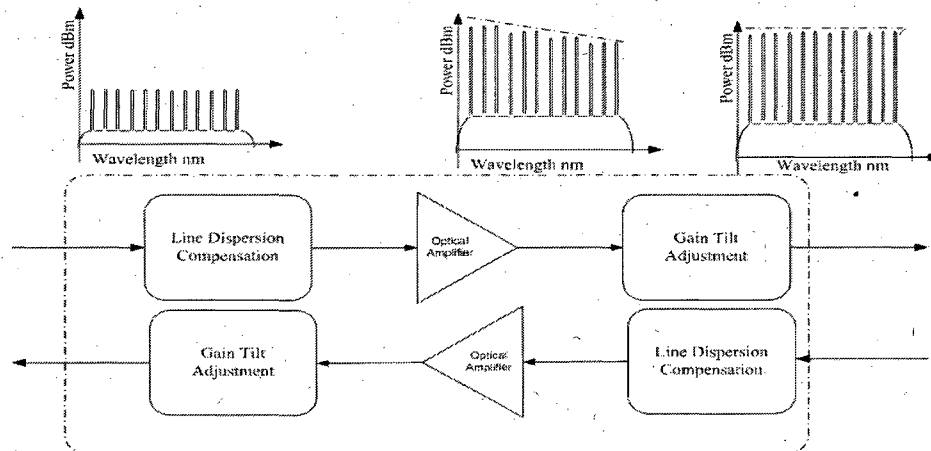


Figure 2- 8 Intermediate Optical Amplification

Another type of gain mechanism used today in ultra long haul optical communication networks is called Raman Amplification. Instead of the lumped or bulk gain provided by the EDFAs, this mechanism provides a distributed gain along the entire length of the transmission medium thus converting the optical fiber into a gain medium. Raman amplification can also be implemented in conjunction with lumped amplification of the EDFAs [19]. Raman amplification uses non-linear interaction between the light and the molecular vibrations of the silica to generate Stimulated Raman Scattering (SRS). Light of sufficiently high magnitude when launched inside the optical fiber, invokes the non-linear SRS phenomenon which converts a small fraction of the incident power from the input optical signal to another optical signal at a frequency down shifted by an amount determined by the vibrational modes of the medium [39]. If ω_p is the frequency of a laser pump propagating inside the fiber and ω_s is the frequency of the optical signal coincident with the pump at the fiber input, it will be amplified because of the Raman gain as long as $\omega_p - \omega_s$ is within the gain bandwidth of the Raman amplification [Figure 2-9]. SRS phenomenon generates photons across the entire gain bandwidth of the Raman-gain spectrum and this broad gain bandwidth allows all channels in the signal spectrum to be amplified at the same time. Figure 2-10 shows an example of the net gain across a 100km fiber span using co-propagating and counter propagating Raman pumps. The Raman gain of the co-propagating pumps increases with length and reaches a value of the maximum gain after which it starts decreasing due to the propagation loss within the fiber. The resultant gain across the length of the fiber span is the sum of gain from co-propagating and counter propagating Raman amplifiers. The advantage of Raman amplification over the EDFAs is the reduced generation of the broadband ASE noise.

This provides for a better noise margin for the signal spectrum at the receiver. The disadvantages are that generating the SRS requires very high levels of light to be injected into the fiber from the Raman pump lasers. This need for high power lasers makes the implementation expensive and increases the cost of deploying optical networks. This amplification scheme requires detailed characterization of the transmission medium to identify and resolve sources of attenuation (high loss in connectors and splices) and reflection (mis-aligned optical connectors with excessive air gaps) that can severely degrade the Raman gain and performance of the system. Lastly, the SRS phenomenon can itself become a source of cross talk between the channels of the signal spectrum as the shorter wavelengths may act as Raman pumps for the longer wavelengths; this phenomenon is referred to as Raman Induced Cross Talk which can affect the system performance considerably [40]. Ultra long haul optical communication networks generally use a combination of the two amplification schemes for network deployments and for extending the reach of networks.

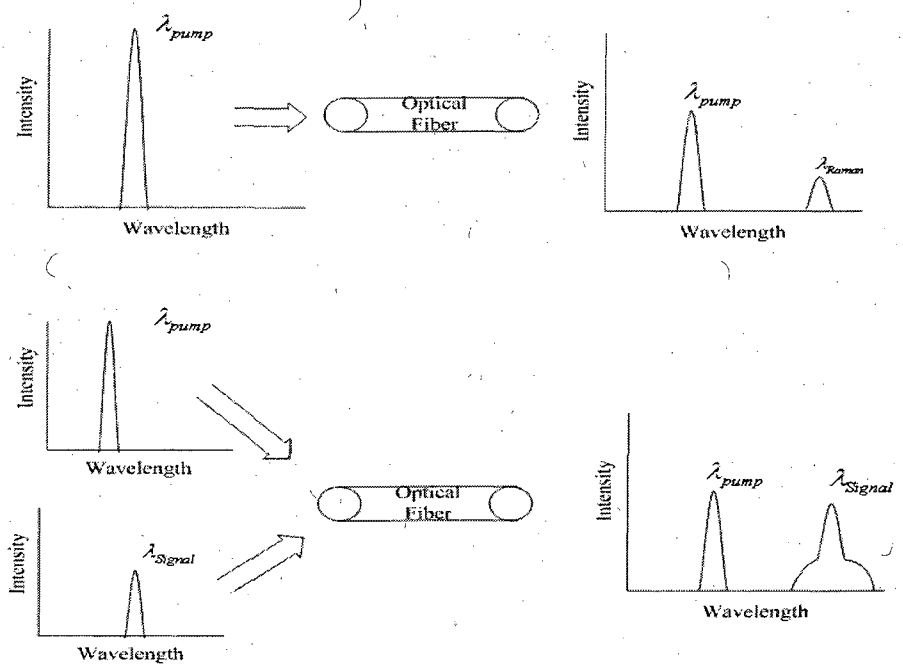


Figure 2- 9 Raman Amplification

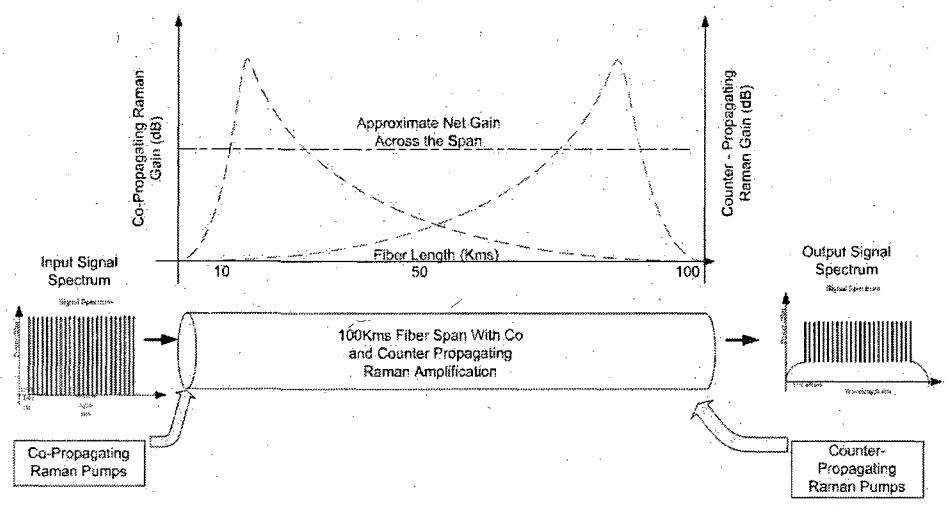


Figure 2- 10 Raman Gain Over a Fiber Span

2.1.3 Receiver Section

The optical signal spectrum travels across the network and reaches the destination where it enters the receiver section [Figure 2-11]. The signal spectrum is amplified to increase signal strength and overcome propagation losses. The optical de-multiplexer splits the optical spectrum into individual wavelengths which are detected using a photo detector. The photo detector converts the optical signal into an electrical signal from which individual data streams are derived. Few of the factors governing the performance of the receiver are Responsivity and Receiver Sensitivity. Responsivity of the receiver is the ratio of generated photocurrent to the incident light power and is measured in units of amps/watt or micro amps/micro watt. Performance criterion for digital communication systems is measured by the bit error rate (BER) which is the average probability of identifying a bit incorrectly. Typically digital optical receivers are measured for performance with BER of 10^{-9} corresponding to an acceptance of on average 1 error per 10^9 transmitted bits. The receiver sensitivity is then defined as the minimum optical power required at the input of the receiver to maintain a BER performance of 10^{-9} .

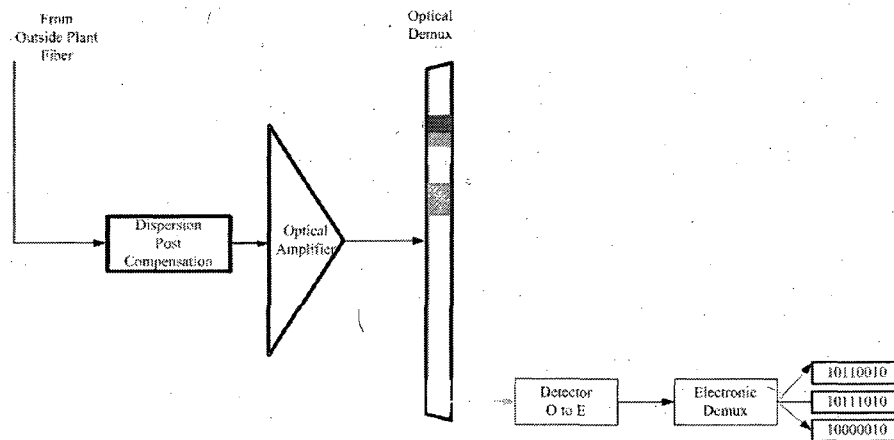


Figure 2- 11 Receiver Section

2.2 Optical Network Performance Parameters

In the previous section, we used the network performance parameter of Bit Error rate to define the sensitivity of the receiver. In this section we will look at different parameters which are commonly used to define the performance of the networks.

2.2.1 Bit Error Rate

The Bit error rate is defined as the average probability of identifying a zero bit as one and a one bit as zero. Figure 2-12 shows a visual indication of this probability. If I_1 is the level at which a One is detected and I_0 is the level at which a zero is detected the decision circuit compares the value of the arrived signal with a decision threshold value of I_D . If the value of time signal I is found to be greater than I_D then the bit is declared as one and if it is found to be less than I_D then it is declared as zero. An error will occur in detection of bit one if the value of I is less than the decision threshold of I_D in which case the one bit gets declared as zero. Similarly, an error will occur in detecting the arrival of the zero bit if the value of I is greater than I_D in which case the zero bit will be declared as 1. The BER is defined as:

$$\text{BER} = \frac{1}{2} [P(0/1) + P(1/0)] \quad \dots\dots[2.1]$$

σ_1 = Standard deviation of the normal distribution for probability of a 1 bit

σ_2 = Standard deviation of the normal distribution for probability of a 0 bit

Then the BER may be expressed as [19]

$$\text{BER} = \frac{1}{4} \left[\text{erfc} \left(\frac{I_1 - I_D}{\sigma_1 \sqrt{2}} \right) + \text{erfc} \left(\frac{I_D - I_0}{\sigma_0 \sqrt{2}} \right) \right] \quad \dots\dots[2.2]$$

Bit Error rate may also be expressed in terms of the Q parameter where:

$$\text{BER} = \frac{1}{2} \text{erfc} \left(\frac{Q}{\sqrt{2}} \right) \quad \dots\dots[2.3]$$

Where

$$Q = \frac{I_1 - I_0}{\sigma_1 - \sigma_0} \quad \dots\dots[2.4]$$

The Q factor is described as the ratio of difference in one and zero levels versus difference in standard deviations of their probability distribution curves. It can be seen that for higher values of Q BER improves.

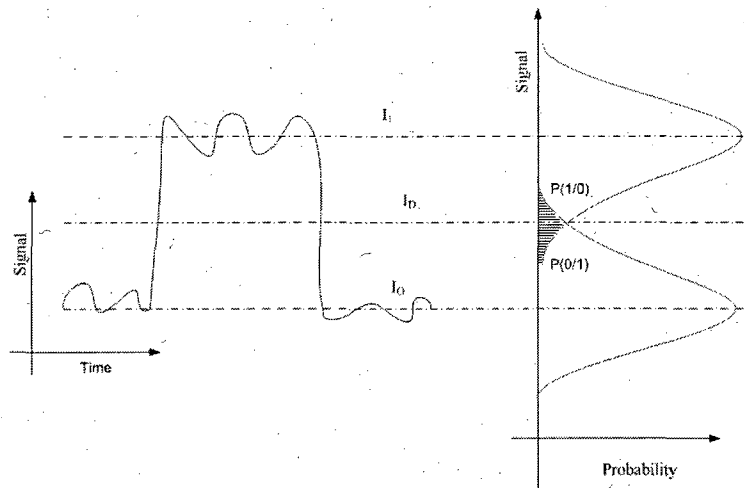


Figure 2- 12 Bit Error Rate

2.2.2 Optical Signal to Noise Ratio

The Optical Signal to Noise Ratio (OSNR) is a common way of expressing the quality of the optical signal spectrum in the network. It is expressed as the ratio of average signal power to average noise power.

$$\text{OSNR (dB)} = 10\text{Log}\left(\frac{P_{av.Signal}}{P_{av.Noise}}\right) \dots\dots[2.5]$$

The BER and OSNR are related such that a better OSNR typically produces a smaller BER in the absence of other impairments not related to signal loss. Establishing a mathematical relationship between BER and OSNR is complicated as BER also depends upon different network design parameters such as forward error correction algorithm implementation, data encoding formats, receiver design and so forth. Simple optical systems are based on Intensity Modulation with Direct Detection Scheme (IM/DD) where the transmitter modulates the optical carrier (OOK) with its digital data stream [19] and the modulated optical signal is directly detected by the photo detector to recover the digital data stream. In multi-channel systems this detection scheme requires wider channel spacing to ensure accurate signal recovery. Advanced detection schemes based on RF technology can enhance the receiver sensitivity by using the coherent nature of the optical carrier. For example, the optical signal at the input of the receiver may be mixed with a stronger optical signal from a local laser source before photo detection takes place. The generated photo current is proportional not only to the input optical signal but also to the optical component obtained from the beating process of the input optical signal and the local laser source. This results in increasing the total input signal level and thus

enhances the receiver sensitivity. Such systems are called Coherent Lightwave Systems and the detection scheme is referred to as Coherent detection. In coherent receivers Q is approximated in terms of OSNR as [19]

$$Q \cong \frac{1}{2} \sqrt{OSNR} \quad \dots\dots[2.6]$$

In the previous section, Equation 2.3 relates BER with Q , this along with Equation 2.6 indirectly relates BER to OSNR.

2.2.3 Eye Diagrams

Digital pulses in lightwave systems may be distorted by noise, pulse spreading or by other impairments. These distortions reduce the ability of the receiver to correctly identify the presence of 1 or 0 within the binary data. Eye diagrams provide a convenient way to measure these distortions and to examine the inter symbol interference and noise in digital communication systems [36, 37 and 38]. The eye diagram is formed by random superposition of long stream of bits using an electronic oscilloscope [Figure 2-13]. The resultant oscilloscope display of the superimposed stream of a digital data sequence resembles a human eye and is called an eye pattern or eye diagram. The middle region of the eye pattern is called the eye opening and defines the separation between the 1 and the 0 levels of the signal. Clear or larger eye opening makes it easier for the receiver to decide whether the received bit is a one or a zero. The decision is made by the receiver by comparing the input signal level against a fixed decision threshold at a fixed sampling time.

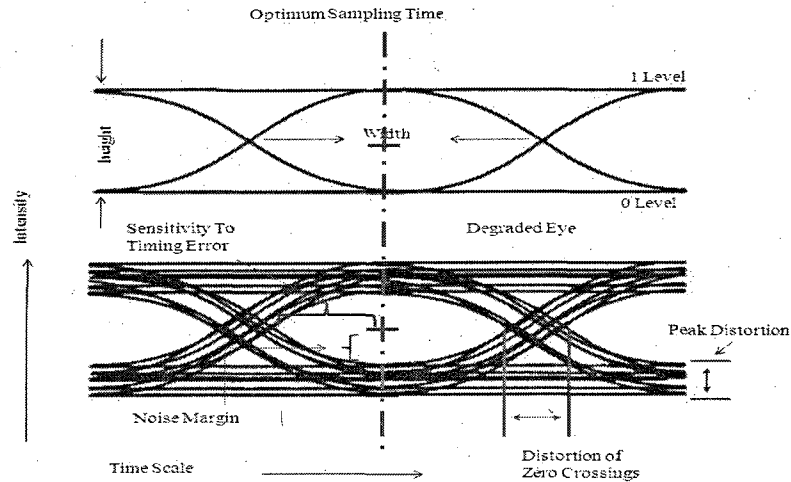


Figure 2- 13 Eye Diagram

If the level of the signal sampled by the receiver is above the decision threshold, the bit is declared as 1. If the level of sampled signal is lower than the decision threshold the received bit is declared as 0. Signal distortion leads to degradation of the eye opening which can result in a received 1 bit being read as zero or a received 0 bit being read as 1. The eye pattern can provide significant information about the performance of the digital transmission system. It gives a measure of the rise and the fall times of the pulses. The width of the eye opening defines the time interval over which the signal can be successfully sampled without the influence of inter symbol interference. Ideal sample time would be at the largest width of the eye opening. Sensitivity of the system to timing errors is defined by how fast the eye closes as the sampling time is varied from the optimum sampling time. The height of the eye opening defines the noise margin or the distance of the decision threshold from the noise level.

It has been observed that different types of signal distortions have their distinct way of degrading the eye opening. This makes it probable to identify the type of

impairment in the optical system based on the measured eye pattern. For example, Figure 2-14a shows the eye pattern for an ideal transmission system with clear and wide eye opening. In a system that is under compensated for chromatic dispersion impairment the measured eye pattern shows a reduction in the height of the eye opening [Figure 2-14b]. On the other hand, in a system which is over compensated for chromatic dispersion compensation, the measured eye pattern shows a reduction in the width of the eye [Figure 2-14c]. Figure 2-15 shows the eye pattern for a system with large amount of PMD. The eye pattern shows random traces of the pulses across the eye opening limiting the decision making ability of the receiver.

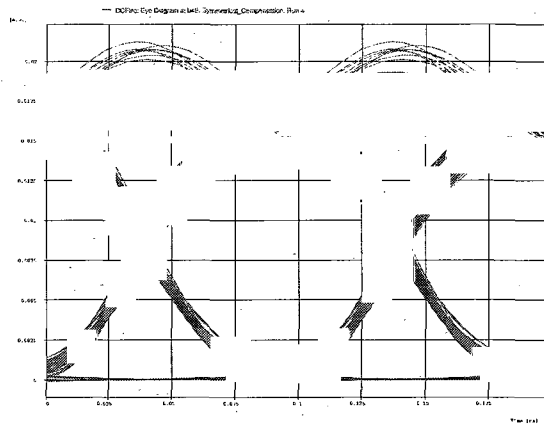


Figure 2- 14a Eye Diagram with No Distortions

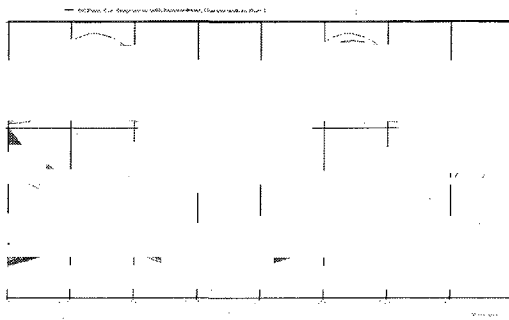


Figure 2- 14b Eye Diagram Chromatic Dispersion Under-Compensation

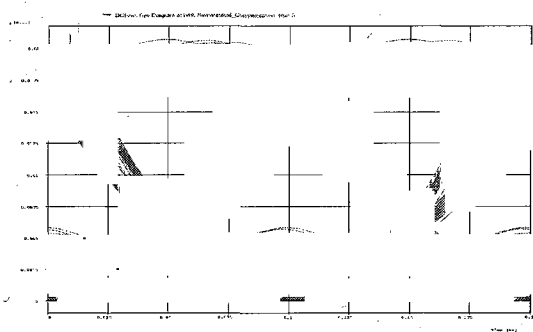


Figure 2- 14c Eye Diagram Ideal Chromatic Dispersion Over-Compensation

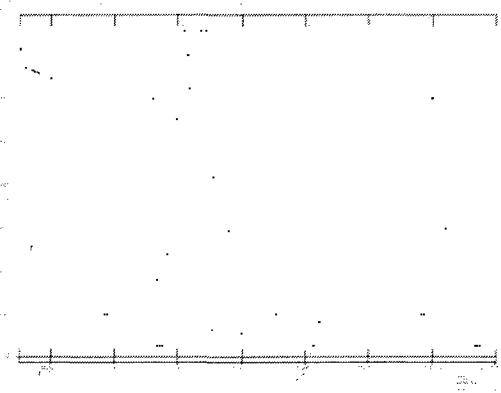


Figure 2- 15 Eye Diagram for a System with PMD Impairment

2.2.4 Performance Penalty

A performance characteristic for a component or system may be obtained by plotting the BER as a function of the OSNR. This allows characterization of the performance penalty incurred in the presence of impairment in the network. Initially, baseline performance of the receiver is generated in the absence of the impairment of interest. This is done by introducing different levels of noise and measuring the OSNR and BER at the receiver. A plot of OSNR versus BER is generated for different values of noise levels. A small value of the impairment is then introduced in the network and another plot of OSNR versus BER is generated at the same values of noise levels as before. An example of the performance characterization is shown in Figure 2-16. If a BER of 10^{-7} is desired the receiver baseline performance indicates a minimum required OSNR of 5dB. After introducing the small fixed value of the impairment, the OSNR required to maintain the network performance at a BER of 10^{-7} is 8.8 dB. Therefore a performance penalty of 3.8 dB is incurred to maintain the performance of the network at a BER of 10^{-7} in the presence of the fixed value of impairment in the network.

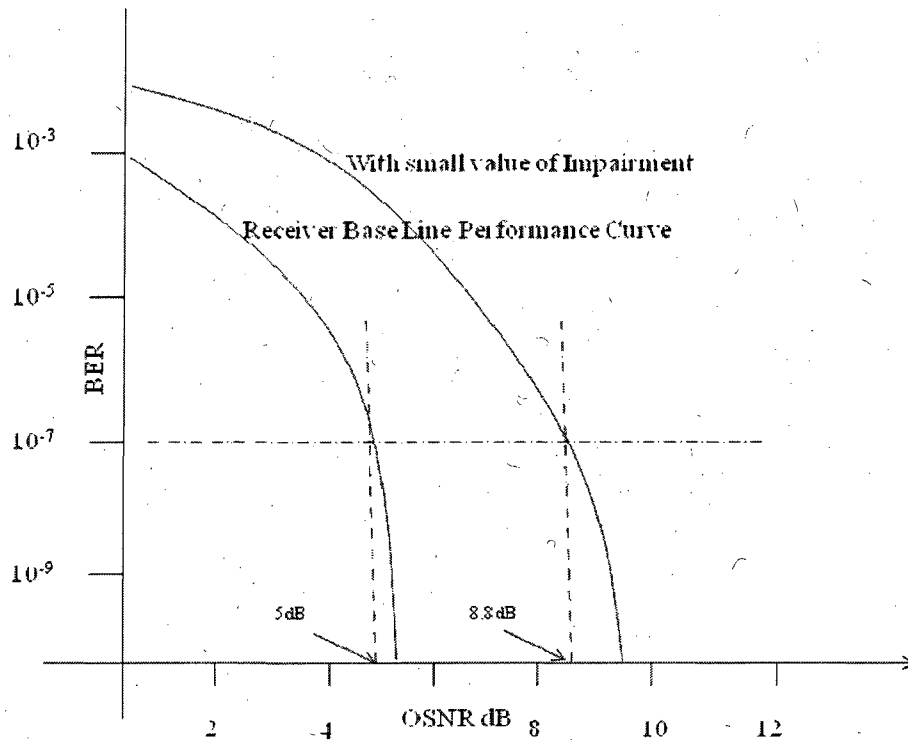


Figure 2- 16 Performance Penalty

Summary

In this chapter the different classifications of optical networks were presented. The various components of optical networks; the transmitter, the receiver and the amplification subsystem were reviewed. Network performance metrics and measures such as Bit Error Rate (BER), Optical Signal to Noise ratio (OSNR), eye diagrams and performance penalty were introduced. In the next chapter the optical fiber as a transmission medium will be discussed.

CHAPTER -3

IMPAIRMENTS IN OPTICAL FIBERS

Introduction

The previous chapter discussed the basic building blocks of the optical network: the transmitter, the optical amplifier and the receiver. This chapter will provide an overview of the transmission medium of the optical networks along with the various channel impairments like: attenuation which reduces the reach of optical networks and pulse broadening due to dispersion which reduces the signal strength and degrades the performance of the optical network.

A conventional optical fiber consists of a circular glass core surrounded by a concentric glass cladding which is enclosed within a buffer coating [Figure 3-1]. Based on the core size, optical fibers are classified as Multi Mode Fibers (MMF) or Single Mode Fibers (SMF). Multimode fibers may have a core size of 50 micro meters with a cladding of 125 micro meters where as single mode fibers may have a core size of 5 micro meters with a cladding of 125 micro meters [Figure 3-2]. Optical networks designed using multimode fibers are less expensive since the large core size greatly reduces the complexity of coupling light sources into the fiber. The distance over which the optical signal can travel down the length of a multimode fiber is primarily affected by

the signal strength and intermodal dispersion. An input pulse launched into the large core size of the MMF will have larger pulse spreading and a high value of propagation loss.

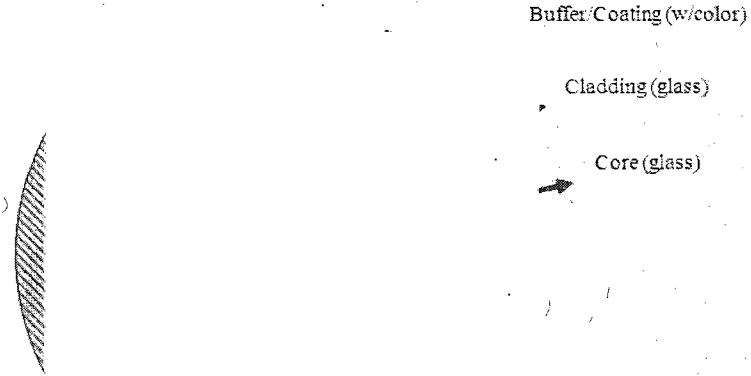


Figure 3-1 Optical Fiber

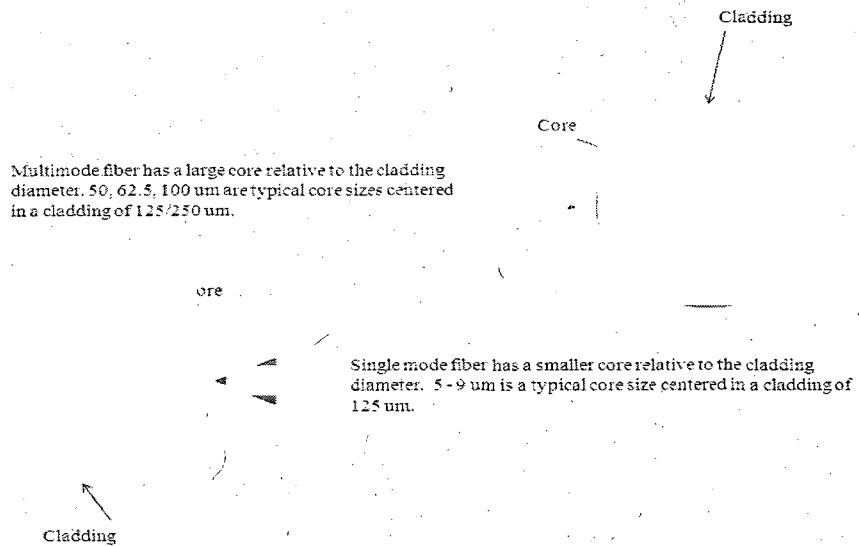


Figure 3-2 Multimode and Single Mode Fiber

The large core size of the waveguide also supports multiple modes of propagation and hence the launched pulse will have more than one propagation path to the receiver. Thus, multiple phase shifted replicas of the signal will arrive at the receiver resulting in inter-symbol interference. This is referred to as intermodal dispersion. Intermodal dispersion reduces the bandwidth and distance of transmission through multi mode fibers. The manufacturers of the multimode fibers specify the dispersion rating based on a figure of merit called the bandwidth-length product. This figure of merit defines the tradeoff in transmission associated with the use of the MMF. The larger the requirement on the bandwidth to be transmitted, the shorter would be the distance that it could be transported over the multi mode fiber. Due to these inherent reach limitations multimode fiber networks find their applications within buildings where they can typically support gigabit data rates up to 500 meters. Single Mode fibers have a small core size as compared to multi mode fibers. This ensures that multiple paths are not available across the length of propagation and therefore are not susceptible to intermodal Dispersion. Their low loss profile over a conventional range of wavelengths makes them appropriate for use in long distance optical network applications.

For the purpose of this study, impairments in optical fibers are broadly characterized into two categories: attenuation and dispersion. Attenuation includes all transmission losses that result in reduction of the optical power of the signal as it propagates across the transmission medium. If these impairments are not controlled the signal strength arriving at the destination may fall below the level that can be detected at the receiver. Dispersion includes impairments which tend to spread the optical signal pulse power distribution in time, reducing the instantaneous peak signal power at any

instant in time along the length of the fiber. These impairments may not only cause the input power to fall below the minimum level required for detection but may also introduce inter-symbol interference in which case a bit one or zero may be interpreted incorrectly.

3.1 Attenuation

Losses in optical fibers reduce the average power that reaches the receiver and thus are one of the critical factors responsible for the reduction in the reach of optical networks. Factors that contribute to the loss may be intrinsic to the fiber, such as Rayleigh scattering and material absorption and micro bending due to waveguide defects, or they may be extrinsic in nature such as misaligned splices and connectors, micro bends due to incorrect fiber spooling techniques and macro bends introduced by poor routing of optical fibers. The attenuation coefficient of the fiber is defined as the loss of the fiber per kilo meter. It is commonly expressed in dB/km as;

$$\alpha(dB / Km) = -\frac{10}{L} \log_{10} \left(\frac{P_{OUT}}{P_{IN}} \right) \quad \dots\dots[3.1]$$

P_{IN} = Input power launched into the fiber in watts

P_{OUT} = Output power received at the end of the fiber in watts.

L = Length of the fiber in km.

3.1.1 Rayleigh Scattering

Rayleigh scattering is one of the fundamental loss mechanisms in optical fibers. As the molten silica in the core of the optical fiber cools down over the manufacturing process, its density may not be the same at all points across the length of the optical fiber. This results in a small variation of the refractive index in the core across the length of the fiber. These changes are extremely small as compared to the wavelength of the light that propagates through the fiber. When incident light encounters these changes in the refractive indices light is scattered in all directions. The fraction of the light that scatters back towards the source is called backscatter. Thus, the forward propagating light is weaker as it travels across the length of the fiber as a fraction this light is lost in backscatter. Rayleigh scattering is the most dominant intrinsic effect resulting in loss of light and its intrinsic loss can be approximated as [19]

$$\alpha_R = \frac{C}{\lambda^4} \text{ db / km} \quad \dots\dots[3.2]$$

Where;

C = Constant whose value depends on the constituents of the fiber core.

λ = wavelength of the incident light.

Figure 3-3 shows the attenuation profile due to Rayleigh scattering in an optical fiber across the wavelength spectrum between 800nm and 1600nm. The attenuation coefficient of the Rayleigh scattering decreases with increase in wavelength from 800nm and is less than 0.2 dB/km in the 1550 nm band of wavelengths. Although Rayleigh scattering

decreases in higher wavelengths greater than 2000nm, high values of fiber losses due to Infra Red absorption make silica fibers unusable in these wavelength ranges.

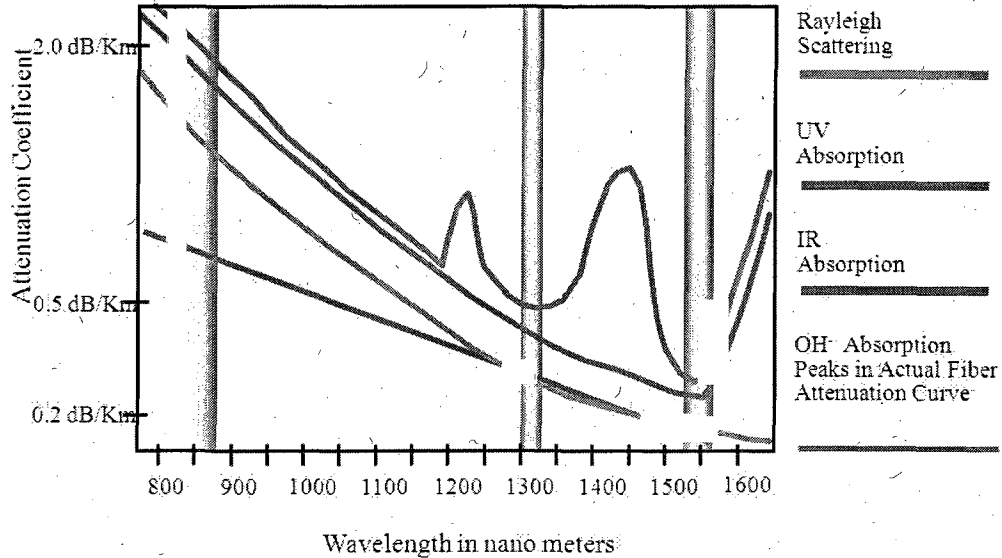
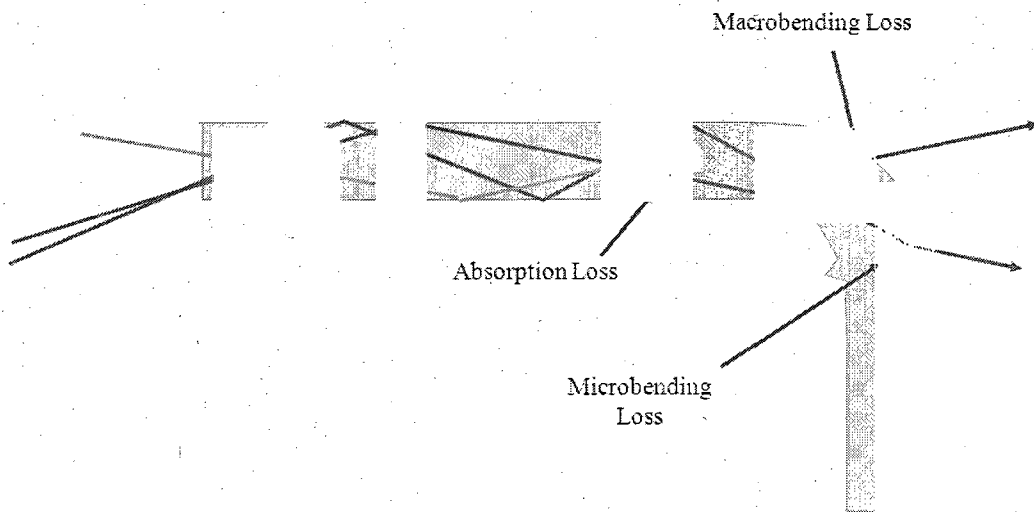


Figure 3-3 Spectral Attenuation Curves For Different Loss Phenomenon within the Fiber

3.1.2 Material Absorption

All materials absorb some amount of incident electromagnetic radiation and convert it into another form (e.g. heat). Intrinsic material absorption in optical fibers relates with absorption of some amount of incident light due to the vibration resonances of the silica molecules. Electronic resonances contribute to high fiber losses in the ultra violet region where as vibration resonances dominate fiber losses in the infra red region as shown in Figure 3-4. Extrinsic material absorption results from impurities in the silica core that may be introduced over the manufacturing of the optical fiber. Amount of

absorption across the wavelength spectrum depends on the type of impurities for e.g. traces of iron, Copper or Nickel may increase the loss due to material absorption in the 600 to 1600nm wavelength range. Water vapor is the most significant extrinsic cause of material absorption. Vibrational resonance of the hydroxyl ions (-OH) occurs near 2730nm and its harmonics with silica produce strong absorption peaks close to 1400nm and 1240nm [19] as shown in Figure 3-3. The large absorption peak at 1410nm is also referred to as the “water peak”. Technology advancements have led to the development of special fibers which eliminate the water peak and make the entire spectrum from 1330 to 1550nm available for optical transmission.



Note: Only the fiber core is shown.

Figure 3-4 Absorption & Bending Losses in Fibers

3.1.3 Waveguide Imperfections

Imperfections in waveguide geometry may be introduced over the manufacturing process or due to external effects. This may cause leakage of light from the core resulting in loss of signal power [Figure 3-4]. Imperfections in the waveguide may be introduced over the manufacturing process if a sudden drop in temperature occurs resulting in defects in the form of wrinkles near the core and cladding interfaces. This may break the phenomenon of total internal reflection at the core-cladding interface resulting in the leakage of light into the cladding of the fiber. Micro bends may be introduced if the fiber spools get squeezed or stretched while being installed under the ground or over power lines or if they suffer extreme external temperature variations (e.g. desert conditions) resulting in different materials in the cable structure that expand or contract at different rates. Losses due to Macro bending may occur if fiber cables are wound too tightly. Tight bending of fiber cables may cause light rays in the core of the fiber to exceed the critical angle. This will allow light to leak out of the core and into the cladding and to the outer buffer. Macro bending loss is more severe at longer wavelengths. For example, a nickel-sized bend may leak out 0.5 dB of light at 1310 nm, but may cause a loss of 2.0 dB at 1550 nm. Macro bending losses can be reduced by eliminating tight bends in the fiber and cable. Cable manufacturers recommend a minimum bend radius of 5-10 times the outer diameter to prevent excessive bending loss.

3.1.4 Splices and Connectors

Optical fibers are joined together to form long length of fibers by fusion splicing them together or by joining them using mechanical connectors. Each such interface adds

some amount of loss to the fiber. The splicing technique introduces a very small amount of loss and back reflection since the core and claddings of the two fibers are fused with each other at the coupling interface. Typical fusion splice loss is between 0.02 ~ 0.2 dB. In the case of poor alignment over the splicing, the cores of the fiber may not align resulting in additional loss [Figure 3-5]. Poor splicing that results in high splice losses may also occur due to the presence of impurities during the splicing process at the interface between the two fibers.

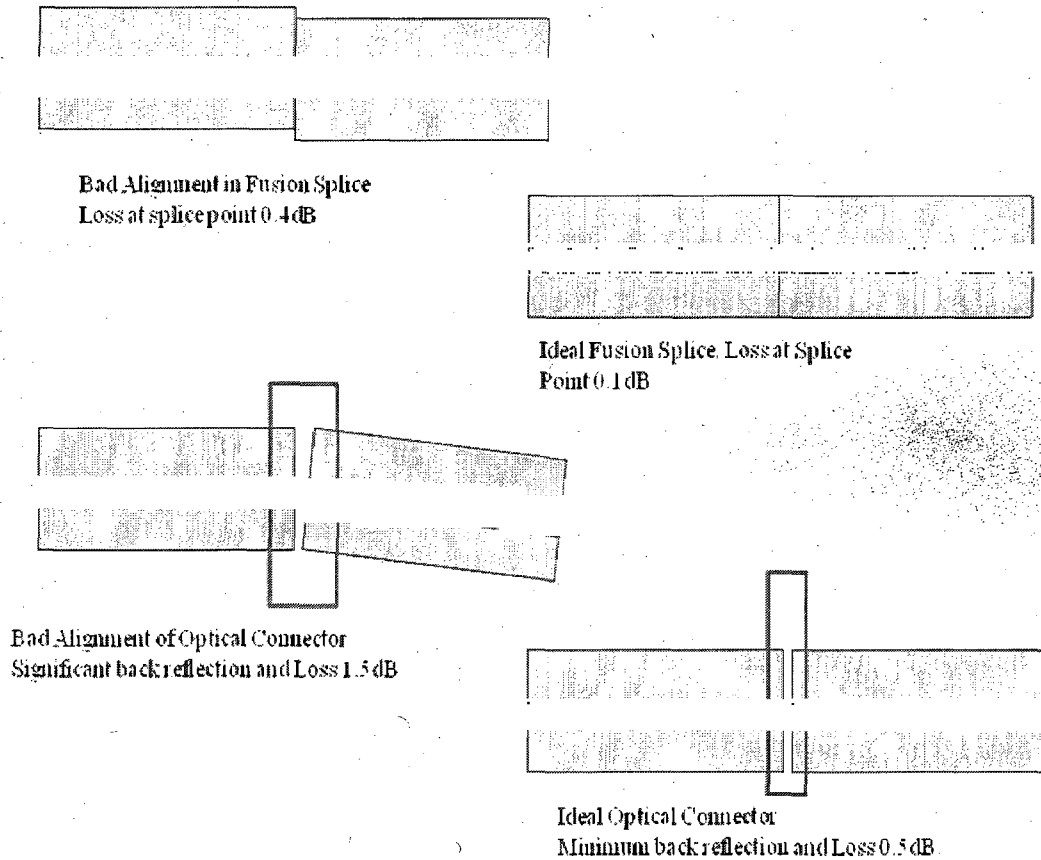


Figure 3-5 Splices and Connectors

Mechanical connections between the fibers introduce air gap between the cores. This results in back reflection of light at the connection interfaces which may degrade the signal and impact the performance of optical networks. Typical connector losses are 0.5 dB ~ 1 dB with low back reflectance. Poor mechanical connections between the fibers can be a source of high loss and reflectance if these connectors are not plugged in properly or if they have accumulated dirt on their surface. Appropriate cleaning and polishing of the connector surfaces can eliminate these high losses.

3.1.5 Optical Time Domain Reflectometer

In order to help identify the sources of fiber loss along the length of the fiber in real optical networks an Optical Time Domain Reflectometer (OTDR) is used. The OTDR can measure the overall length of the fiber span and the average loss across the length of the fiber. It can accurately point out the location of splices and connectors and also provide information about the loss of each individual splice or connector. It can indicate reflectance at individual connectors and provide an estimate of the optical return loss. Figure 3-6 shows a simple block diagram of an OTDR. It uses the radar principle to measure distance by creating a plot of the return signal versus distance. The distance or length of the fiber is calculated on the basis of the time at which a light pulse of fixed width was sent and the level of back scatter that is received at the receiver. Figure 3-7 shows a sample OTDR trace of a fiber. The trace is a plot of distance on the x-axis versus optical power on the y-axis. The overall trace has a negative slope which indicates that the power decreases across the length of propagation. Event 1 on the trace is an OTDR representation of a mechanical connector. A mechanical connector is characterized by

loss along with back reflectance. The x-intercept indicates the location of the connector from the source and the y-intercept indicate the loss of the connector. Event 2 represents a fusion splice followed by the end of the fiber.

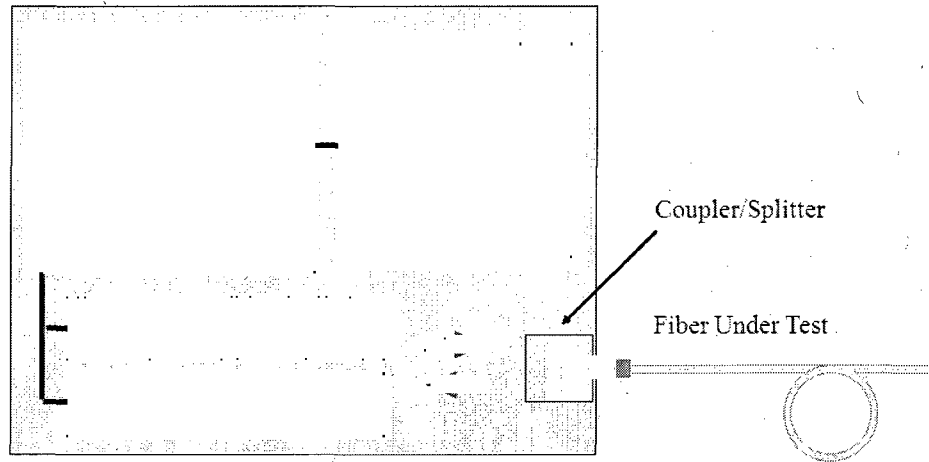


Figure 3-6 Optical Time Domain Reflectometer Block Diagram

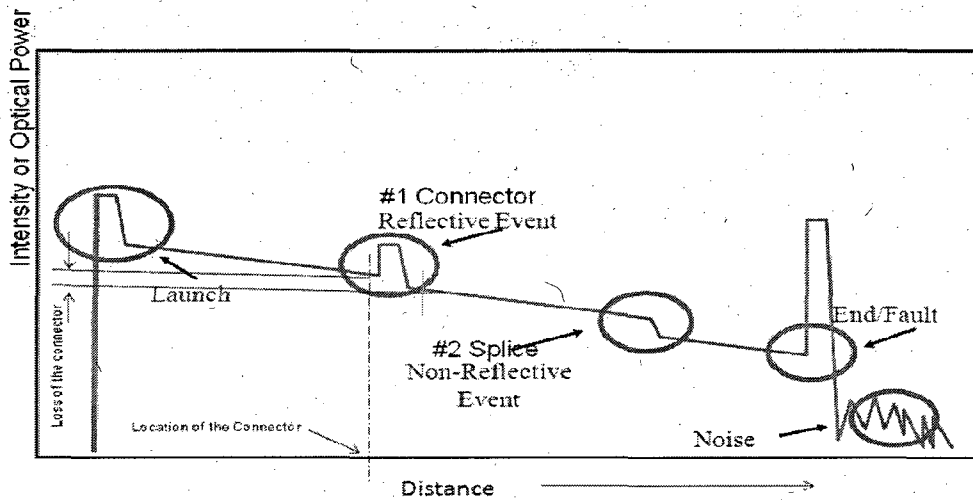


Figure 3-7 Sample OTDR Trace

3.1.6 Field Measurements on Continuity and Loss

Analysis of data collected from field measurements over 700 fiber spans indicate that more than 20% of spans differ from expected length by greater than 10 km [Figure 3-8]. This suggests a significant impact on the loss budget of more than 2 dB [27].

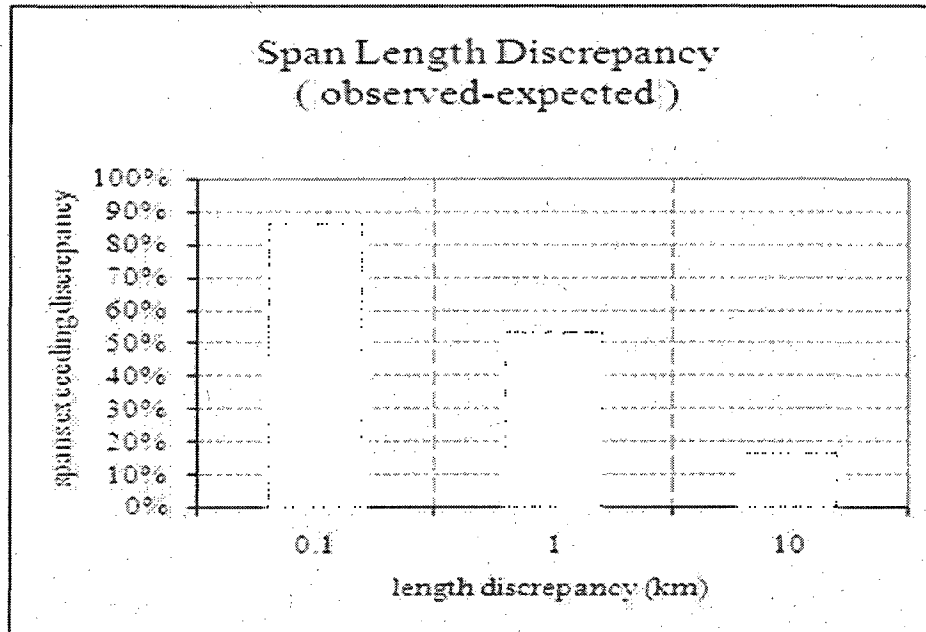


Figure 3- 8 Span Length Discrepancy Statistics

The statistics of measured (and recorded) fiber span loss indicate that more than 20% of measured spans are found to differ from expectation by more than 5 dB [Figure 3-9]. These statistics demonstrate how field measurements are beneficial in identifying and resolving excess loss issues in high performance optical transport networks.

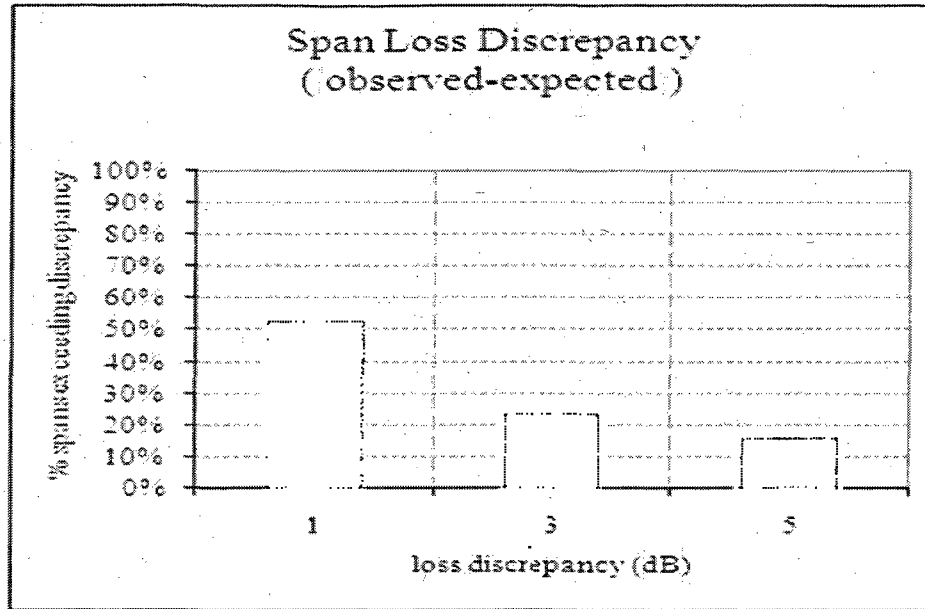


Figure 3- 9 Span Loss Discrepancy Statistics

3.2 Dispersion in Optical Fibers

Dispersion in optical fibers results in the broadening of the pulse in the time domain as it propagates across the length of the fiber. With respect to the impact of dispersion on digital communications, multimode fiber transmission is primarily limited by intermodal dispersion, whereas single mode fiber transmission is currently limited by chromatic and polarization mode dispersions. The focus of this study is on polarization mode dispersion.

3.2.1 Intermodal Dispersion

In multimode fibers, intermodal dispersion is the main limiting factor restricting the networks reach and data rate of transmission. It is caused because of the large size of

the MMF core which can support multiple modes of transmission with varying group delays. Therefore an optical pulse at its input may split into different modes and each mode will propagate over a different path within the fiber arriving at the receiver at different times thus resulting in the spread and eventual destructive superposition of the replicas of the transmitted optical pulse and subsequent reduction loss of instantaneous peak optical power at the receiver. Single mode fibers do not support multiple modes and therefore are not limited by intermodal dispersion.

3.2.2 Chromatic Dispersion

Chromatic dispersion in single mode optical fibers is caused by the wavelength dependence of the fundamental mode of propagation within the fiber. Due to their dependence, each wavelength or the spectral component of the pulse is subjected to a different refractive index and as a result travels across the fiber with a slightly different group velocity. All laser sources in optical networks have a defined center wavelength λ with a small spectral width $\Delta\lambda$ (typically less than 2nm). As an optical pulse of time period T at center wavelength λ and spectral width $\Delta\lambda$ travels through an conventional single mode fiber the pulse spreading in time domain ΔT may evaluated as [19];

$$\Delta T = \frac{d}{d\lambda} \left(\frac{1}{v_g} \right) \Delta\omega = DL\Delta\lambda$$

where

$$\text{Dispersion parameter } D = \frac{d}{d\lambda} \left(\frac{1}{v_g} \right) = -\frac{2\pi c}{\lambda^2} \beta_2 \text{ ps/nm.km}$$

$$\text{GVD Parameter } \beta_2 = \frac{d^2\beta}{d\omega^2}$$

v_g = group velocity

ω = angular frequency = $2\pi/\lambda$

L = Length of the Fiber

β = Propagation Constant

.....[3.3]

D is the dispersion parameter of the fiber expressed in ps/nm.km. It has two principle components: Material and Waveguide dispersion. Material dispersion is caused because the refractive index offered by the silica core of the waveguide is different for the different frequencies of the signal spectrum. Figure 3-10 shows the plot of material dispersion D_M for the wavelength range 1.1 micro meters to 1.7 micro meters. For the conventional single mode fiber, D_M is negative for shorter wavelength. Its value is zero at 1.2 micro meters which is defined as the zero dispersion wavelength λ_{ZD} . D_M becomes positive after λ_{ZD} and continues to increase in value with wavelength. The waveguide dispersion is much smaller in comparison to material dispersion. It is caused by the dependence of the phase and group velocities on core radius, numerical aperture, and wavelength of propagation. Shorter wavelengths are completely confined to the fiber core, while a fraction of the optical power at longer wavelengths propagates through the cladding. Since the index of the core is slightly greater than the index of the cladding, this difference in spatial distribution causes a change in propagation velocity. As shown in

Figure 3-10, the value of the waveguide dispersion parameter D_w is negative all across the wavelength range. Its effect is to push the zero dispersion wavelength of pure silica from 1.2 micrometer to 1.31 micrometer. The resultant dispersion D is sum of contributions from D_M and D_w as shown in Figure 3-10.

$$D = D_M + D_w \quad \dots\dots[3.4]$$

Since the contribution of waveguide dispersion depends on the waveguide parameters such as core radius and the difference in refractive index between the core and the cladding, these parameters are varied to design fibers with different dispersion profiles. Single mode fibers can be characterized on the basis of their zero dispersion wavelength and dispersion value at 1.55 micro meters. For example a conventional single mode fiber will have $\lambda_{ZD} = 1.31$ micro meters with D at 1.55micro meter = 16.7 ps/nm.km. A positive dispersion shifted fiber may have $\lambda_{ZD} = 1.49$ micro meter with D at 1.55micro meter = 3.25 ps/nm.km. A negative dispersion shifted fiber may have $\lambda_{ZD} = 1.59$ micro meter with D at 1.55 micro meter = -3 ps/nm.km. Chromatic dispersion impacts the reach of the optical network and the network performance. Impairment from Chromatic Dispersion can be overcome by measuring the dispersion profile of the fiber [Figure 3-11] and planning for dispersion compensation along the length of the optical network. This will ensure that the pulse spreading does not cause excessive inter-symbol interference.

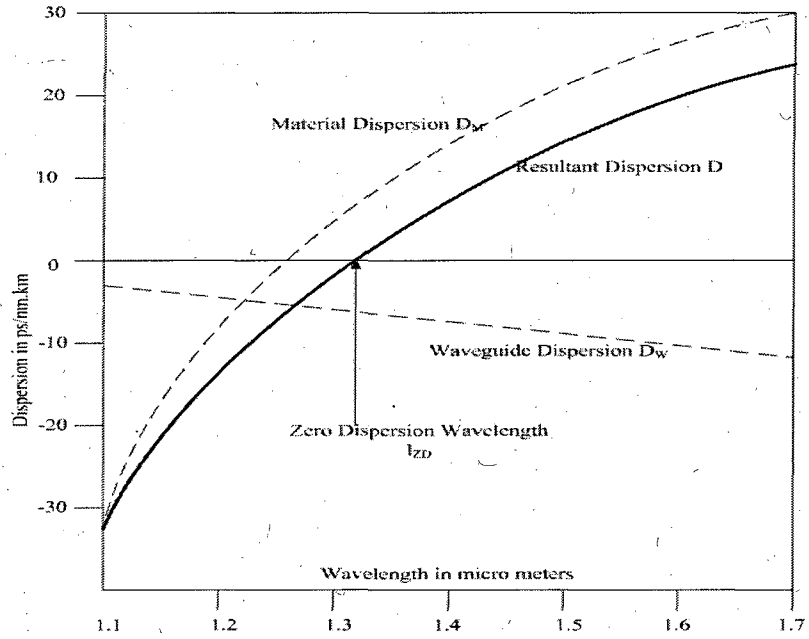


Figure 3-10 Contributions to Chromatic Dispersion

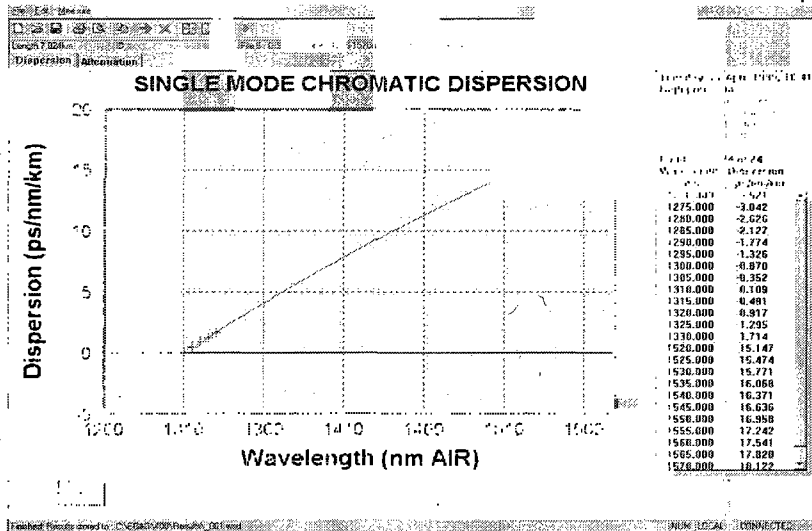


Figure 3-11 Field Measurement of Chromatic Dispersion

3.2.3 Field Measurements for Chromatic Dispersion

Analysis of the chromatic dispersion data from the field collected over 700 fiber spans involved comparison of the observed zero-dispersion wavelength to customer expectation. [Figure 3-12] [27].

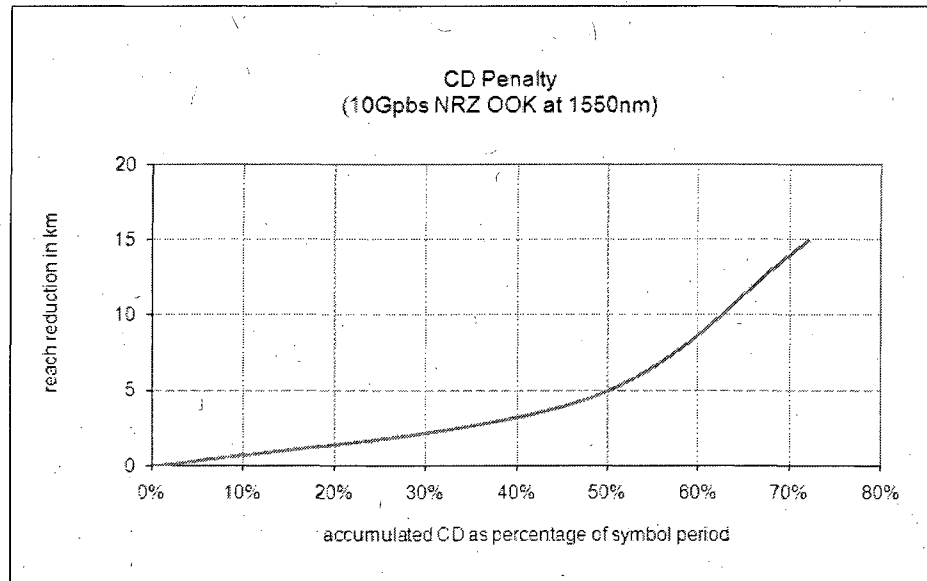


Figure 3- 12 Chromatic Dispersion Discrepancy in Measured Fiber Spans

It is observed that nearly 5% of the measured fibers are found to differ from the expected type (λ_0 discrepancy exceeds 25nm). Such deviations in expected results could result in significant design errors which could violate the engineering rules for 10 Gbps and higher rates in medium and long reach optical systems. The performance penalty from Chromatic dispersion impairment may be viewed as the difference of the actual signal-to-noise ratio from the ideal value at a specified level of performance (e.g. bit error ratio of 10^{-7}). Since this impairment is characterized in the time domain (psec/nm), it may be

expressed as a percentage of the symbol period for a specified channel bandwidth. Since both the loss and the chromatic dispersion of a fiber are stable at a specific frequency or wavelength, the penalty may be translated from power margin (dB) to reduced reach (km). A comparison of the reach reduction for various CD regimes is shown in Figure 3-13.

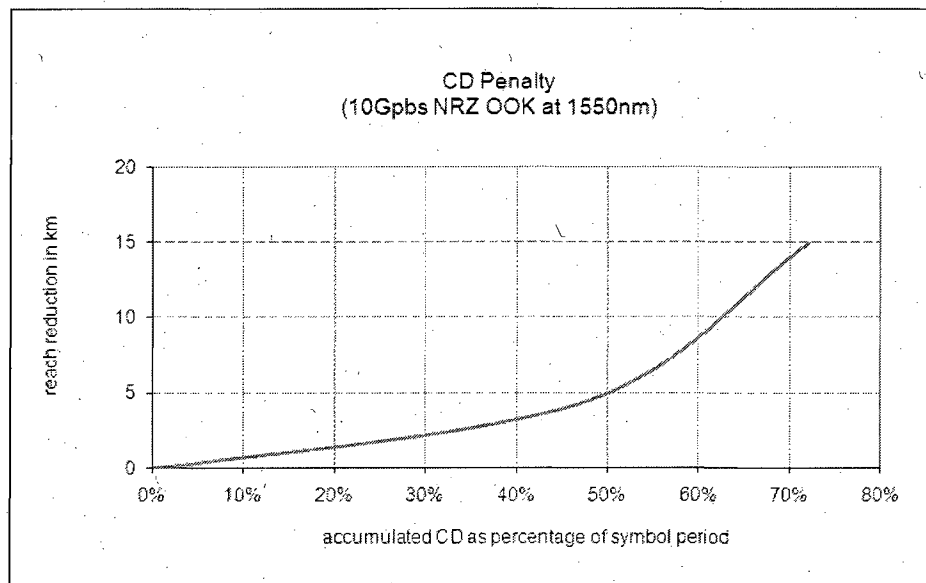


Figure 3- 13 Sample Chromatic Dispersion Penalty in Terms of Reduction in Reach

This is estimated from a sample simulation at 10 Gbps for a non return to zero (NRZ) encoded on off keyed (OOK) link design with an ideal transmitter and sensitivity receiver. The trend is parabolic and increases with chromatic dispersion in relation to the symbol duration. Penalty at an impairment value of 30% of the bit period is observed to be around 2.5 km of reach reduction. The delay limits of newer high bit-rate (40 Gbps, 100 Gbps) systems are less tolerant to chromatic dispersion that is inherent to many of

the existing long-haul networks constructed with conventional single-mode fibers. In some cases, even the small total chromatic dispersion accumulated in non-zero dispersion-shifted fibers must be addressed. The residual dispersion creates an excess delay budget that is generally reduced by the use of dispersion-compensating modules (DCMs). However, the difference between the fiber dispersion and the DCM (i.e. residual dispersion or compensation error) is not equal at all wavelengths. This error results in part from the use of fixed-length dispersion-compensating modules and in part from the dispersion slope mismatch of the DCM to the transport fiber. As the reach is extended and the transmission window is widened, knowledge of the wideband channel response is essential in order to minimize the power, delay, and nonlinearity penalties in a DWDM network design.

3.2.4 Polarization Mode Dispersion

A single mode fiber is said to support only one dominant mode of transmission. However, a single mode fiber that is not symmetrical across its cross-section supports two polarization modes which are perpendicular to each other in the plane of the fiber cross section and are therefore referred to as orthogonally polarized modes. When a randomly polarized pulse of light is incident on the slightly asymmetrical core of the optical fiber, the transverse wave front may be expressed by its two orthogonal modes of polarization. If the single mode fiber is ideal with perfect cylindrical core geometry and waveguide geometry across the length of the fiber, the two orthogonal modes will travel across the fiber and arrive at the receiver at the same time. The intensity photo-detector will detect this as a single pulse and convert it into an electrical signal. If the single mode

fiber is not ideally uniform in cross-section and length, the two orthogonal modes of propagation will be subject to different refractive indices and will travel through the fiber with different propagation times. The receiver will detect a distorted pulse due to the delay between the replicas of the input signal pulse. A sufficiently distorted signal may be inaccurately interpreted as zero instead of 1 or 1 instead of zero and may degrade the performance of the optical networks. This phenomenon of pulse spreading due to cross-sectional asymmetry and in-homogeneity along a fiber is referred to as Polarization Mode Dispersion (PMD).

In optical network systems, single mode fibers are subjected to random changes in stress and strain due to temperature and pressure variations which lead to non uniformity along the waveguide structure and break down in the symmetry of the cylindrical shape of the core. These random perturbations in waveguide symmetry remove the degeneracy between the orthogonally polarized modes. Variation across the length of the fiber results in interaction between the two orthogonal modes where energy is exchanged at periodic intervals. Since the birefringence changes randomly across the length of the fiber, a linearly polarized light at the input of the fiber will quickly become completely depolarized as it travels through the fiber. The intensity photo detector at the end of the fiber thus receives a delay distribution of the signal replicas and the PMD is characterized by the root mean square value of this distribution. The PMD is measured in picoseconds increasing linearly in length for short sections of fiber and increasing as the square root of length for longer lengths.

Intrinsic PMD may be introduced in fibers over the manufacturing process which may introduce variant stress on the core or introduce defects in the symmetrical shape of the waveguide. Extrinsic factors which could contribute towards the PMD impairment may include stress on fiber spools during installation of the fiber. The fibers may be subjected to strain due to excessive bends or twists of the cables or due to extreme environmental variations in the case of optical fibers routed over transmission power lines. Intrinsic causes of PMD can be minimized by ensuring quality control and by using advanced techniques in manufacturing processes which can monitor waveguide symmetry and residual thermal stress of the core within acceptable tolerances. Mode coupling or the interaction between the orthogonal modes can be controlled by constantly spinning the fiber as it is drawn from the molten silica and by varying the spins in clockwise and anti clock wise directions. External causes that could contribute to the impairment can be controlled through use of stronger cabling structures which can limit the impact of environmental variations and also through better installation techniques that can prevent stress related to bends and twists within a cable.

Optical network design requires PMD measurements of the installed fiber. Field measurements of PMD are done using Interferometric measurement techniques [20], which conforms to the TIA FOTP-174 dispersion measurement standard [21]. Figure 3-14 shows a simple block diagram of the interferometric PMD measurement.

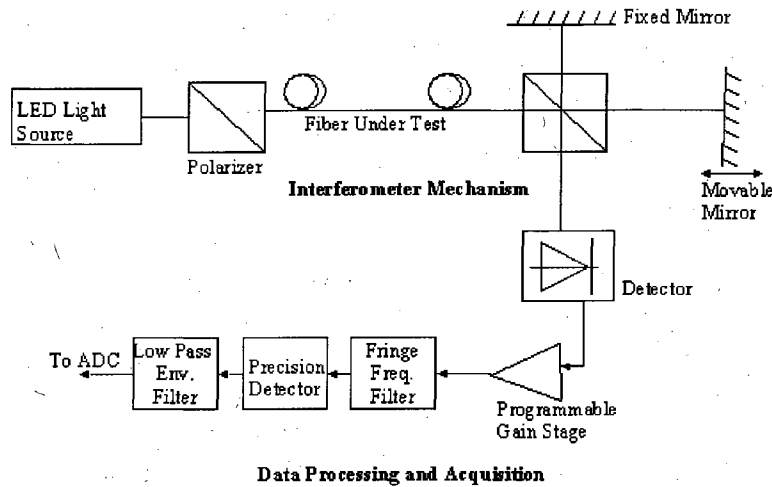


Figure 3-14 Interferometric PMD Measurement Block Diagram

In this technique, the test fiber is excited by a linearly polarized light source, typically a 1550nm LED with a polarizer that is effective over the operating wavelength range. The source spectral shapes are approximately Gaussian to ensure a smooth auto correlation function that may be subtracted from the measured fiber results. The receiver consists of a Michelson interferometer that is implemented mainly in fiber but the variable optical path is accomplished in air by moving a mirror over a range of approximately 55mm. As the mirror is moved, the detector will measure fringes of varying amplitude. The envelope of these detected fringes is utilized to provide PMD information. When two arms of the interferometer are of equal length the amplitude of the interference fringes will reach maximum. This maximum corresponds to the central autocorrelation peak, which is used to determine the zero time delay position for the interferometer. Existence

of PMD in a fiber under test will cause the interferogram to broaden proportionally. Figure 3-15 shows a sample screen shot of a lab measurement on a 3.1 km fiber spool using this technique and the measure of PMD is recorded as 6.1ps.

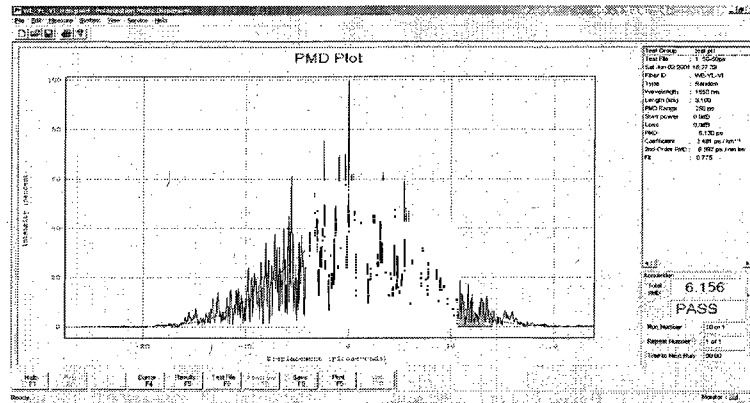


Figure 3-15 Sample Interferometric Field Measurement on a 3.1 km Fiber Spool.

3.2.5 Field Measurements for PMD

The statistics of measured PMD and the PMD coefficient collected over 700 fiber spans are presented in Figure 3-16. More than 6% of the spans were found to exceed 5 ps of mean PMD and more than 3% of the spans exceeded 10 ps mean PMD [27]. For intermediate reach networks at 40 Gbps or 100 Gbps and for long-haul networks at 10 Gbps, identifying excessive PMD is critical.

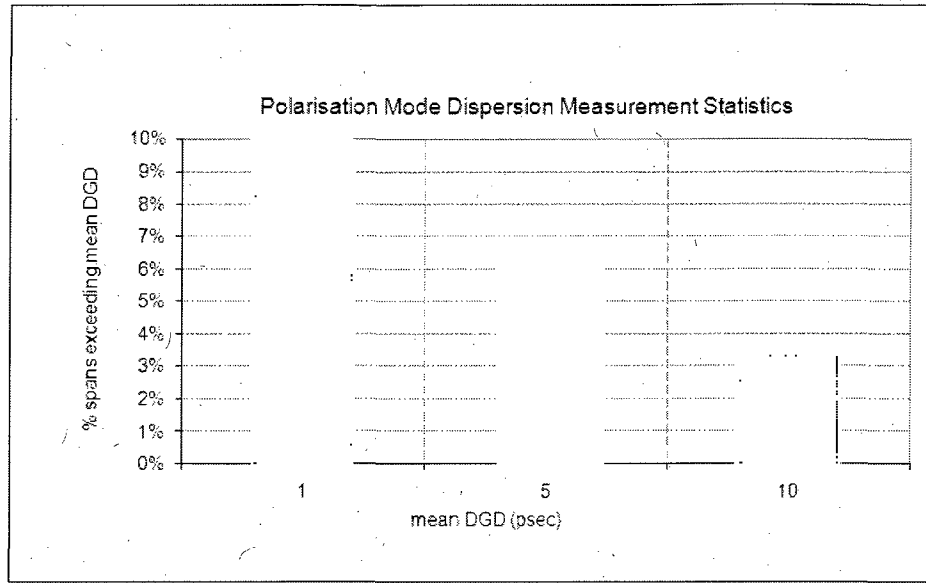


Figure 3- 16 Polarization Mode Dispersion Field Measurement Statistics

The performance penalty from impairment may be viewed as the difference of the actual (impaired) signal-to-noise ratio from the ideal (unimpaired) value at a specified level of performance (e.g. BER of approximately 10^{-7}). Since this particular impairment (DGD) is characterized in the time domain (ps), it may be expressed as a percentage of the symbol period. Since the loss of a fiber is stable at a specific frequency or wavelength, the penalty may be translated from power margin (dB) to reduced reach (km). However, the reliability of path penalty estimation is limited by the range and dimension of the simulation due to the statistical nature of PMD. A comparison of the worst-case reach reduction for various PMD regimes is shown in Figure 3-17. This is estimated from a finite simulation of possible bit sequences at 10 Gbps for an NRZ - OOK link design with ideal transmitter and sensitivity receiver. With PMD impairment at 30% of bit period a reduction in reach of 1.5 km is observed. With a PMD impairment at 40% of the bit

period there is a reduction in reach of close to 5 km. PMD remains a limitation to bit rate and system reach for which there is no attractive, inexpensive, or simple solution. It is therefore necessary to verify the PMD for high-speed long reach applications, especially with older and/or unknown fibers. The eventual migration to 40 Gbps transmission may also increase the design sensitivity to PMD impairment.

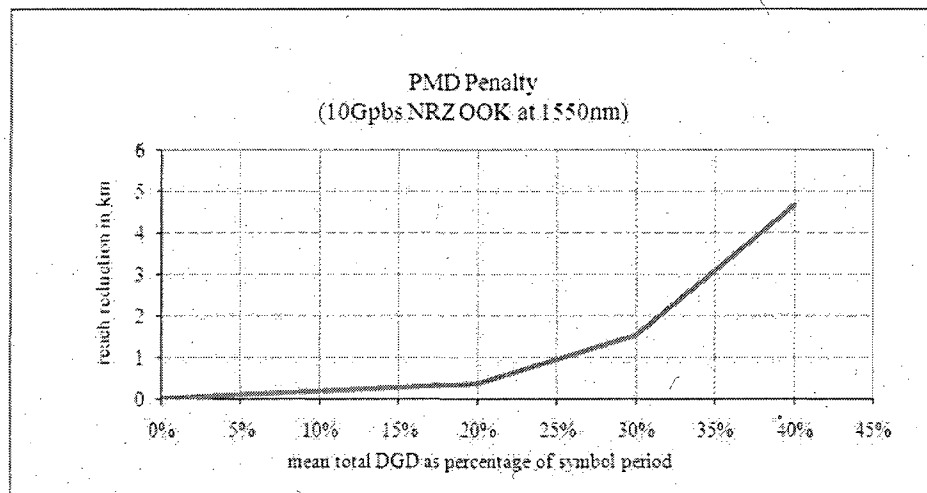


Figure 3- 17 Sample PMD Penalty in Terms of Reduction in Reach

Summary

In this chapter an overview of impairments in the optical fibers was provided. The impairments were grouped into two categories of attenuation and dispersion. The impact of fiber losses on the reach of optical networks and various impairments like Rayleigh scattering, Material absorption, Waveguide imperfections, splices and connectors which contribute towards this degradation were discussed. A review of the dispersion

impairments including Chromatic Dispersion and Polarization Mode Dispersion was provided. The pulse spreading due to these dispersion impairments and the factors that contribute to it were discussed. The next chapter explores in detail the PMD impairment and its impact on optical network performance.

CHAPTER - 4

THEORY OF POLARIZATION MODE DISPERSION

Introduction

This chapter provides an introduction to polarization in optics and the methods used toward its quantification. Propagation of the polarization modes in the optical waveguide is discussed and as a part of this discussion the first order and second order effects of the PMD impairment and its length dependence are reviewed. The existing statistical model of PMD is analyzed and its limitations are discussed.

4.1 Polarization in Optics

Polarization is a phenomenon observed in waves that vibrate in a direction perpendicular to their direction of propagation. Light can be treated as a transverse electromagnetic wave and a light wave traveling forward may vibrate in the vertical plane, in the horizontal plane or in an intermediate direction. Polarization is defined in terms of the pattern traced out in a transverse plane by the electric field vector of this wave as a function of time. A ray of light consisting of a mixture of waves vibrating in all possible directions perpendicular to the line of propagation is called natural or un-polarized light. Examples of this type of light are sunlight and firelight. Un-polarized

light may be represented as an electric field that from moment to moment vibrates and occupies random orientations in a plane that is transverse to the line of propagation. If the vibration of the light wave is restricted to a particular direction, light is said to be polarized in that particular direction. The transverse plane that captures the oscillation is defined as the plane of polarization. Output of a laser diode may be completely polarized whilst the output of a Light Emitting Diode may be partially polarized (10 % to 20 %). The extent of polarization in light is often expressed in terms of the degree of polarization.

$$DOP = \frac{P_{Polarized}}{P_{Polarized} + P_{Un-Polarized}} \quad \dots\dots(4.1)$$

where:

$P_{Polarized}$ = Power in the polarized component of light

$P_{Un-Polarized}$ = Power in un-polarized component of light.

4.1.1 Generation of Polarized Light

Figure 4-1 shows a simple setup to generate and understand polarization of un-polarized light. In this setup, an un-polarized light source is incident upon a polarizer with a horizontal slit to produce a horizontal linear polarization. This horizontally polarized light is then passed through a quarter wave retarder, which resolves this into two components which have an absolute phase difference of 90 degrees. If the z-axis is considered as the direction of light propagation, then x and y components of the polarization vector at time 't' can be expressed as [42]:

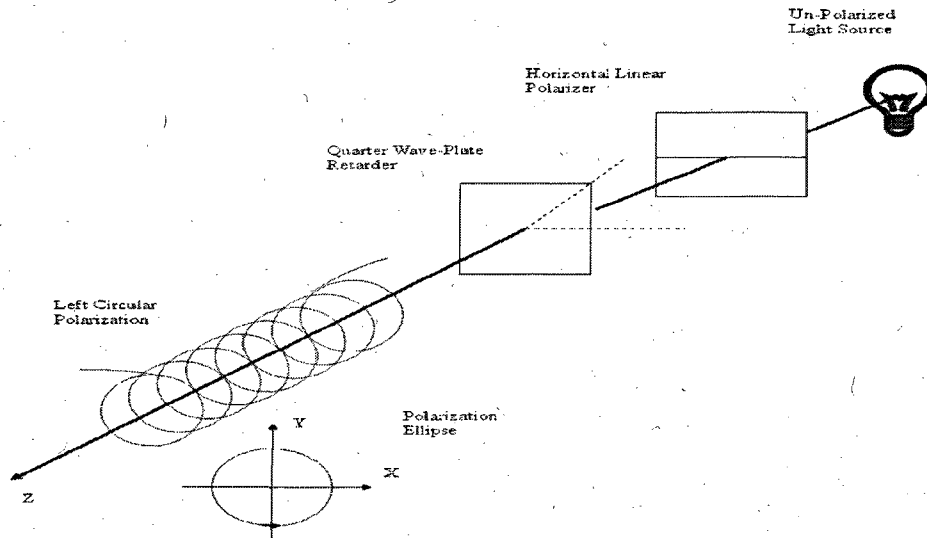


Figure 4- 1 Polarization Of Light

$$\begin{aligned}
 E(t) &= \hat{E}_{0X} \cos(\omega t + \delta_X) + \hat{E}_{0Y} \cos(\omega t + \delta_Y) \\
 E_X(t) &= \hat{E}_{0X} \cos(\omega t + \delta_X) \\
 E_Y(t) &= \hat{E}_{0Y} \cos(\omega t + \delta_Y) \\
 \delta &= \delta_Y - \delta_X
 \end{aligned}
 \quad \left. \vphantom{\begin{aligned} E(t) \\ E_X(t) \\ E_Y(t) \\ \delta \end{aligned}} \right\} \dots\dots (4.2)$$

where,

$E_X(t)$ and $E_Y(t)$: Electric field intensities in the x and the y direction respectively

\hat{E}_{0X} and \hat{E}_{0Y} : Maximum amplitudes of the electric field intensities in the x and y direction

δ_X and δ_Y : Phase of the electric field intensities in the x and y direction

δ : Phase difference

ω : Angular frequency

Assuming that the two components \hat{E}_{0x} and \hat{E}_{0y} are equal and $\delta_x = 180$ and $\delta_y = 90$ ($\delta = -90$), then $E_x(t)$, $E_y(t)$ and $E(t)$ can be calculated and a visual representation can be made as shown in Figure 4-2. In this case, the head of the resultant electric field intensity vector $E(t)$ moves in an anti-clockwise direction on the periphery of a circle if the wave is propagating towards the reader.

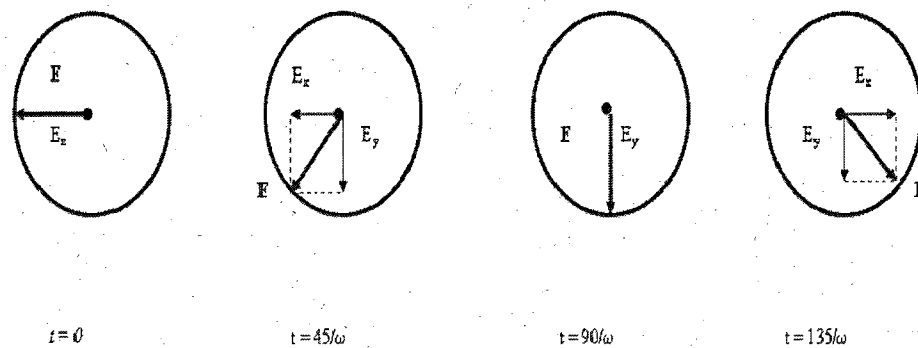


Figure 4- 2 Electrical Field Intensity At Various Time Instants

If the two components \hat{E}_{0x} and \hat{E}_{0y} are unequal, the vector head would move around an ellipse. If the phase difference δ is zero, the ellipse or the circle would become a line and linear polarization would be obtained as shown in Figure 4-3.

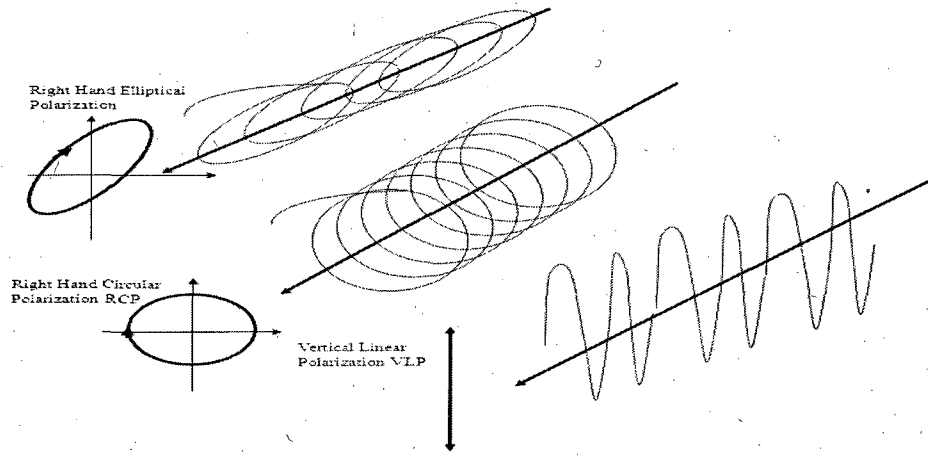


Figure 4- 3 Polarization States

The frequency domain manifestation of PMD is a direct consequence of the frequency dependence of the differential phase velocities. For a fixed input state of polarization, the PMD causes the output state of polarization to vary with the frequency in a cyclic fashion. As the frequency is increased the output polarization evolves and returns to its original state after a characteristic frequency shift $\Delta\omega_{cycle}$. The differential delay $\Delta\tau$ can be defined in terms of this characteristic frequency shift as follows [18]:

$$\Delta\tau = \frac{2\pi}{\Delta\omega_{cycle}} \dots\dots[4.3]$$

The next few subsections discuss the different ways in which the output polarization can mathematically be expressed and quantified. The Jones Matrix method and the Poincare sphere are commonly used to express the polarization states of the fibers and are briefly discussed in the following sections.

4.1.2 Jones Vectors and Jones Matrix

The Jones vector and matrix developed by R. Clark Jones provided a simpler mathematical expression of polarization, which in turn helped in the description of interference effects. The Jones vector describes polarized light by a two element complex vector, the elements of which, specify the magnitude and phase of the x and y components of the electric field at a particular point in space [18].

$$E = \begin{pmatrix} E_x \\ E_y \end{pmatrix} = \begin{pmatrix} E_{0x} e^{i\delta_x} \\ E_{0y} e^{i\delta_y} \end{pmatrix} \quad \dots\dots[4.4]$$

The normalized form of the Jones vector would express linear horizontal polarized light as:

$$E = \begin{pmatrix} E_{0x} e^{i\delta_x} \\ 0 \end{pmatrix}$$

or

$$E = \begin{pmatrix} 1 \\ 0 \end{pmatrix} \quad \dots\dots[4.5]$$

Right hand circularly polarized light would be expressed as:

$$E = \frac{1}{\sqrt{2}} \begin{pmatrix} 1 \\ +i \end{pmatrix} \quad \dots\dots[4.6]$$

The Jones Matrix is a complex two by two matrix, which describes the polarization properties of two port optical devices by relating the input and output Jones vectors. The Jones matrix representation of unknown devices can be found by measuring

three output Jones Vectors in response to three known polarization stimuli are shown in Figure 4-4 (whose Jones vector representation is known).

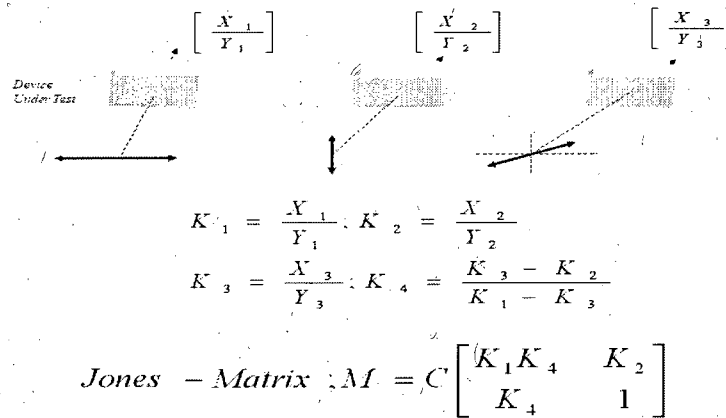


Figure 4- 4 Jones Vectors and Jones Matrix

For a short length L of birefringent fiber, Jones matrices can be used to relate the input and the output field amplitudes as described below [33];

$$\begin{bmatrix} E_{x-output} \\ E_{y-output} \end{bmatrix} = \begin{bmatrix} \exp(jk_0 n_x L) & 0 \\ 0 & \exp(jk_0 n_y L) \end{bmatrix} \begin{bmatrix} E_{x-input} \\ E_{y-input} \end{bmatrix} \quad \dots\dots[4.7]$$

where, n_x and n_y are the refractive indices of the two orthogonal components. This can be re written in terms of the birefringence $B=n_x-n_y$ as:

$$\begin{bmatrix} E_{x-output} \\ E_{y-output} \end{bmatrix} = \exp(jk_0 n_x L) \begin{bmatrix} 1 & 0 \\ 0 & \exp(jk_0 B L) \end{bmatrix} \begin{bmatrix} E_{x-input} \\ E_{y-input} \end{bmatrix} \quad \dots\dots[4.8]$$

4.1.3 Poincare Sphere

The Poincare Sphere is a three-dimensional graphical tool that provides a convenient description of polarized signals and polarization transformations caused by propagation through devices (like optical fibers) [18]. The Poincare sphere is a unit sphere centered on the rectangular xyz – coordinate system [Figure 4-5]. The coordinates of any point within or upon this sphere define the Stokes parameters.

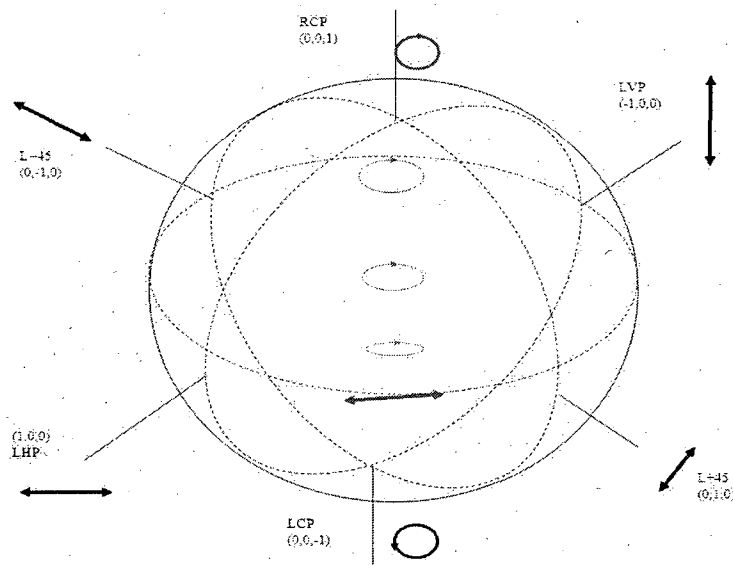


Figure 4- 5 Poincare Sphere

The characteristics of Poincare Sphere are:

- a. Completely polarized light is represented by a point on the surface of the Poincare sphere.
- b. Partially polarized light is represented within the volume of the Poincare sphere. The distance of the point from the origin gives the degree of polarization.
 - i. A point at the origin would define completely un-polarized light.
 - ii. A point at the surface would define completely polarized light.
- c. Circular states of polarization are represented at the poles.
- d. Intermediate elliptical states of polarization are distributed between the equator and the poles of the Poincare Sphere.
 - i. Curves above the equator are right handed (in the northern hemisphere).
 - ii. Curves below the equator are left handed (in the southern hemisphere).
 - iii. Elliptical states slowly change to circular states (at the poles) over the journey from the equator to the poles.
- e. Orthogonal polarizations are located diametrically opposite to one another on the sphere.

The state of polarization is represented as a point on the Poincare sphere and the evolution of polarization is represented as a continuous trace. The evolution of polarization emerging from a highly and uniformly birefringent device (Polarization Maintaining Fiber PMF) as the wavelength is changed is shown in Figure 4-6. The circular trace characterizes the wavelength sweep of the tunable laser and the radius of

the concentric circle is determined by the polarizer orientation at which the wavelength sweep has occurred. The end points of the diameter locate the eigenmodes of the device under test. Eigenmodes are polarization states that propagate unchanged through a device. In a linearly birefringent device the eigenmodes correspond to the fast and slow axes of the device. For a lightly birefringent device, the polarization evolution would trace a random path on the Poincare Sphere as the wavelength is changed.

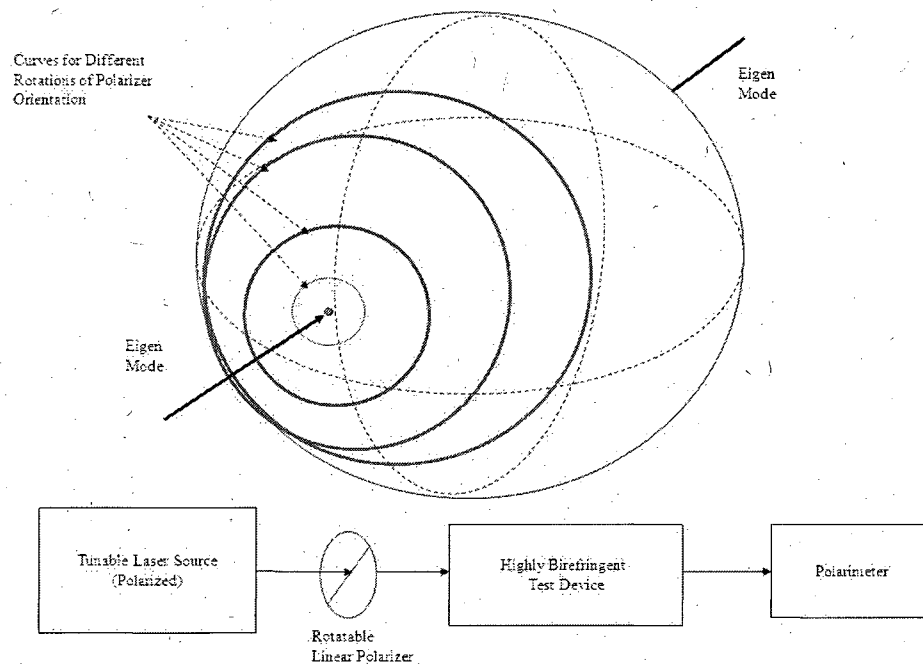


Figure 4- 6 Wavelength Sweep On Poincare Sphere For A Highly Birefringent Device

4.2 Propagation of Transverse Fields in an Optical Waveguide

Source free solutions to the Maxwell's equations for a time harmonic field are given by the following vector wave equation [32]:

$$\begin{aligned} \{\nabla_t^2 + n^2 k^2 - \beta_j^2\} e_j &= -\{\nabla_t + i\beta_j \hat{z}\} \{e_{ij} \cdot \nabla_t \ln n^2\} \\ \{\nabla_t^2 + n^2 k^2 - \beta_j^2\} h_j &= -(\nabla_t \ln n^2) \times (\{\nabla_t + i\beta_j \hat{z}\} \times h_j) \end{aligned} \quad \dots\dots[4-9]$$

In the above equations an implicit time dependence of $\exp(i\omega t)$ is assumed in the field vectors where ω is the angular frequency and;

β is the propagation constant.

$n = n(x, y, z)$ is the refractive index profile.

$k = 2\pi / \lambda$ is the free space wave number.

λ is the free space wavelength.

A step index optical waveguide with a refractive index of n_{co} for the core and a refractive index of n_{cl} for the cladding and with a profile height parameter of Δ may be defined as a weakly guiding optical waveguide if $\Delta \ll 1$ (or equivalently when $n_{co} \approx n_{cl}$).

The profile height parameter Δ is defined as;

$$\Delta = \frac{1}{2} \left\{ 1 - \frac{n_{cl}^2}{n_{co}^2} \right\} \cong \frac{n_{co} - n_{cl}}{n_{co}} \quad \dots\dots[4-10]$$

In a weakly guiding homogenous step index waveguide the $\nabla_t \ln n^2$ term can be ignored in the vector wave equation. Therefore, each longitudinal field component within the waveguide will satisfy the following equations [32]:

$$\{\nabla_t^2 + n^2 k^2 - \beta_j^2\} e_{zj} = 0 \quad \dots\dots[4-11]$$

$$\{\nabla_t^2 + n^2 k^2 - \beta_j^2\} h_{zj} = 0$$

Their transverse electric and magnetic fields are related as follows:

$$h_t = \left(\frac{\epsilon_0}{\mu_0} \right)^{\frac{1}{2}} n_{co} \hat{z} \times e_t \quad \dots\dots[4-12]$$

The propagation constant $\beta = n_{co} k$ is independent of the orientation of the transverse electrical field. The transverse electric field e_t can be expressed in unit vectors parallel to the Cartesian axes as:

$$e_t(x, y) = e_x(x, y)\hat{x} + e_y(x, y)\hat{y} \quad \dots\dots[4-13]$$

It then follows that that e_x and e_y will satisfy the Equation 4-14:

$$\{\nabla_t^2 + n^2 k^2 - \beta_j^2\} e_x = 0 \quad \dots\dots[4-14]$$

$$\{\nabla_t^2 + n^2 k^2 - \beta_j^2\} e_y = 0$$

For circular fibers with no azimuthal variation, the fundamental modes will satisfy the above equations and can be expressed as [32]:

x – Polarized Mode

$$E_x = F_0(r) \exp(i\beta z)$$

$$H_y = \left(\frac{\epsilon_0}{\mu_0} \right)^{\frac{1}{2}} n_{co} E_x$$

y – Polarized Mode

$$E_y = F_0(r) \exp(i\beta z)$$

$$H_x = - \left(\frac{\epsilon_0}{\mu_0} \right)^{\frac{1}{2}} n_{co} E_y$$

.....[4-15]

where, $F_0(r)$ is the axis-symmetric solution of Equation 4.15 and the propagation constant is identical for both the polarization modes.

For a non-homogenous waveguide characterized by a non-uniform refractive index profile $n(x,y)$, the propagation constant depends on the orientation of the electric field. The modes are solutions of the complex vector wave equation given by Equation 4.10. In this case $\nabla_t \ln n^2$ is a nonzero term that couples the electric and magnetic terms of the vector wave equation. The two polarization modes will have distinct propagation constants β_x and β_y and the difference between the two defines the birefringence of the waveguide. The two modes are expressed as [32]:

x- Polarized Mode

$$E_x = \psi(x, y) \exp\{i(\beta + \delta\beta_x)z\}$$

$$H_y = \left(\frac{\epsilon_0}{\mu_0}\right)^{\frac{1}{2}} n_{co} E_x$$

.....[4-16]

y- Polarized Mode

$$E_y = \psi(x, y) \exp\{i(\beta + \delta\beta_y)z\}$$

$$H_x = -\left(\frac{\epsilon_0}{\mu_0}\right)^{\frac{1}{2}} n_{co} E_y$$

where, $\delta\beta_x$ and $\delta\beta_y$ are small corrections to the propagation constant β and $\psi(x, y)$ is the solution of Equation 4.16 for the largest value of β . The corrections to the propagation constant β have been found by solving the vector wave equation for a weakly guiding waveguide using simple perturbation methods and are given by [32];

$$\delta\beta \cong \frac{\rho(2\Delta)^{\frac{3}{2}} \int_{A_{co}} (\nabla_t \cdot e_t) e_t \cdot \nabla_t f(x, y) dA}{2V \int_{A_{co}} e_t^2 dA} \quad \text{.....[4-17]}$$

Where:

Δ is the profile height parameter.

V is the waveguide parameter.

A = infinite cross section

$f(x, y)$ = variable part of the profile (profile function).

The corrections $\delta\beta_x$ and $\delta\beta_y$ are evaluated from the above equation using the following substitutions $e_x = \psi(x, y)\hat{x}$ and $e_y = \psi(x, y)\hat{y}$, where \hat{x} and \hat{y} are unit vectors along the axes.

4.3 Propagation of Polarization Modes in Single Mode Fibers

Optical waveguides support signal excitation that may be expressed by two orthogonal spatial dimensions in the plane transverse to propagation. As a result orthogonally polarized modes of propagation are said to be possible [Figure 4-7]. If the transverse structure of the transport medium is physically and geometrically symmetrical, the two modes will travel identical optical path lengths. If there is no interaction between the modes, they will suffer identical propagation delays and arrive at the receiver at the same time and with the same amplitude [Figure 4-8].

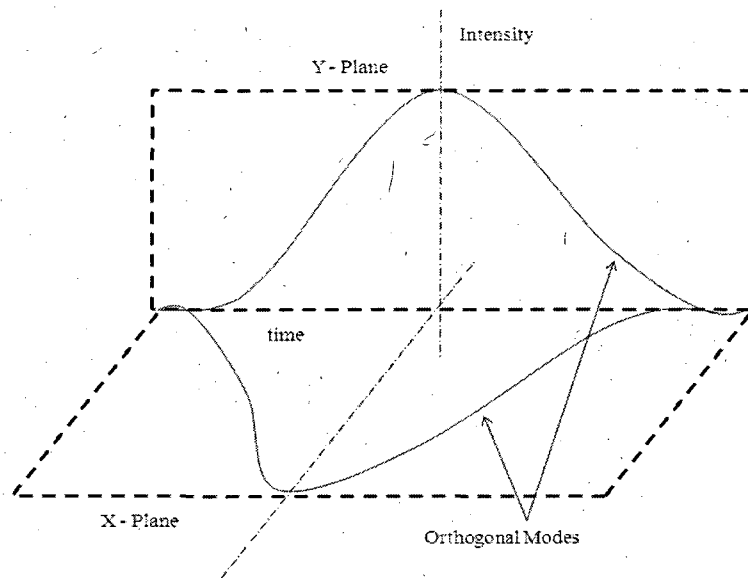


Figure 4-7 Orthogonal Modes

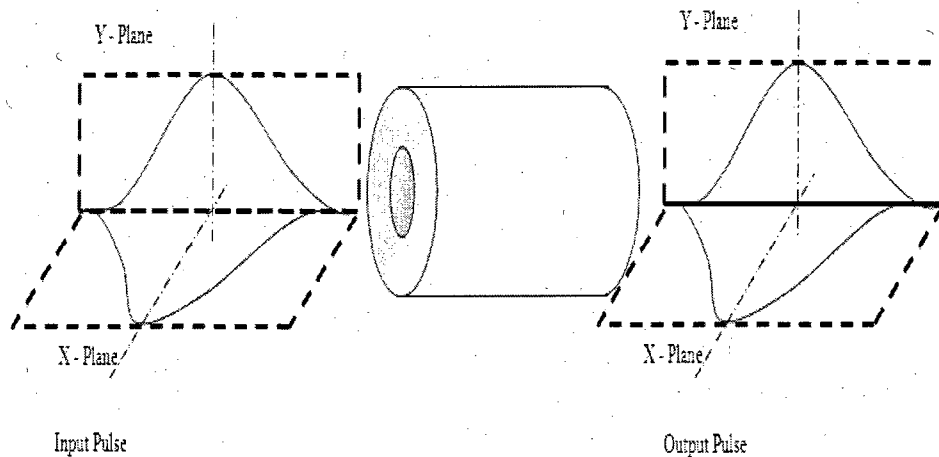


Figure 4- 8 Orthogonal Pulses with No Group Delay

Birefringent fibers have transverse propagation structure which is physically and geometrically asymmetrical. This offers different optical path lengths for the two modes. Thus, they suffer a differential group delay and arrive at the receiver at different times, thus causing pulse distortion. If the propagation of the two modes is not accompanied by any energy exchange or interaction between them, then the group delay is non-varying and will accumulate linearly with distance. This differential group delay corresponds to the deterministic effect of PMD and the unit of its coefficient is ps/km [Figure 4-9].

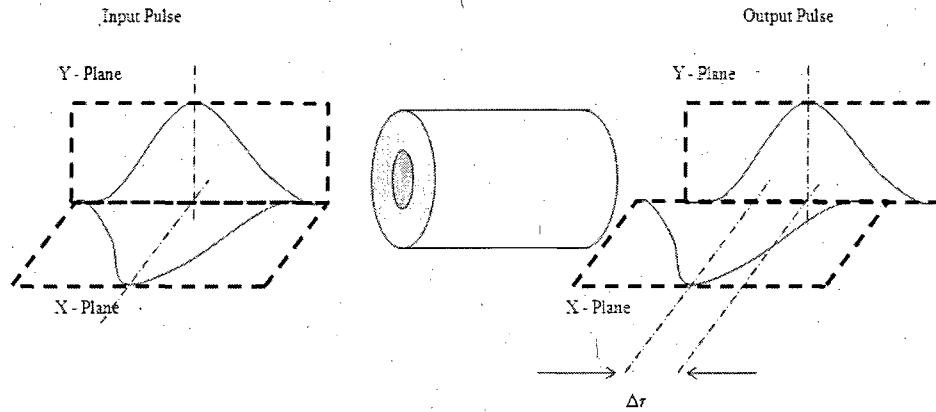


Figure 4- 9 Accumulation of Deterministic effect of PMD

If the transport medium is subjected to continuous irregularities due to stress and strain along the length of propagation, energy exchange or mode coupling is initiated between the modes at each point of transition in propagation characteristics that occurs because of fiber irregularity [Figure 4-10]. The fiber can be visualized in terms of a large number of infinitesimal sections of deterministic effects, each joined to the next section by a different mode coupling function block whose response varies with the stress/strain on that section of the infinitesimal element. Mode coupling causes migration of energy between the two modes and a change in the differential group delay ' $\Delta\tau$ ' of the infinitesimal segment. Since the irregularities occur over a significantly long length of fiber, the effect of mode coupling is to grow and scramble the accumulated polarization modes at the far end, thus randomizing the distribution of differential group delay. Hence, the measure of the impairment is obtained from a statistical distribution of values of $\Delta\tau$ measured. For long lengths of fibers this statistical distribution has been proposed to be

Maxwellian and, therefore, the measure of differential group delay is obtained from calculating the mean of this Maxwellian envelope [6].

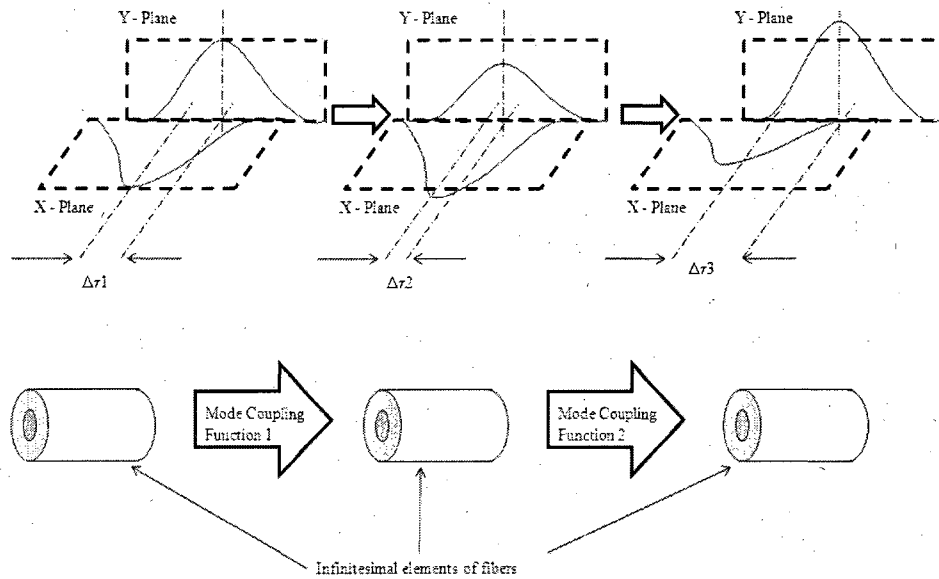


Figure 4- 10 Effect of mode Coupling on $\Delta\tau$ and energy content of the two orthogonal modes

This is referred to as the distributed effect of PMD. The mean value is not representative of the instantaneous value, but is used as a benchmark for comparison, given the assumption that the distribution is Maxwellian. Distributed PMD has been proposed to accumulate as the square root of the distance of propagation and its unit is defined in terms of $\text{ps}/\sqrt{\text{km}}$ [5].

4.3.1 Birefringence and Beat Length

Consider a short section of fiber where the non-uniformity or perturbation is constant across its length. When an input pulse of a linearly polarized light source with random orientation is incident on such a fiber section, it may couple into two orthogonal modes of polarization. Each mode will have its distinct refractive index and travel across the next short section of fiber with different speeds. The difference in their propagation constants can be expressed as [18]:

$$\beta_s - \beta_f = \frac{\omega n_s}{c} - \frac{\omega n_f}{c} = \frac{\omega \Delta n_{eff}}{c} \quad \dots\dots[4.18]$$

where;

β_s, β_f are the propagation constants of the two modes.

$\omega = \frac{2\pi}{\lambda}$ is the angular frequency of the light.

c is the speed of light in vacuum.

$\Delta n_{eff} = n_s - n_f$, n_s and n_f are the refractive indices of the slow and the fast modes.

The difference in the propagation constant [Equation 4.18] or the differential refractive index Δn_{eff} between the two orthogonal modes is referred to as the birefringence.

Typically values of birefringence are between 10^{-5} and 10^{-7} (and are much smaller than the index difference between the core and the cladding, which is approximately 10^{-3}).

Figure 4-11 illustrates the evolution of polarization within the fiber due to birefringence

for a linearly polarized input signal at an angle of 45 degrees, with the axes of the linearly birefringent short section of fiber.

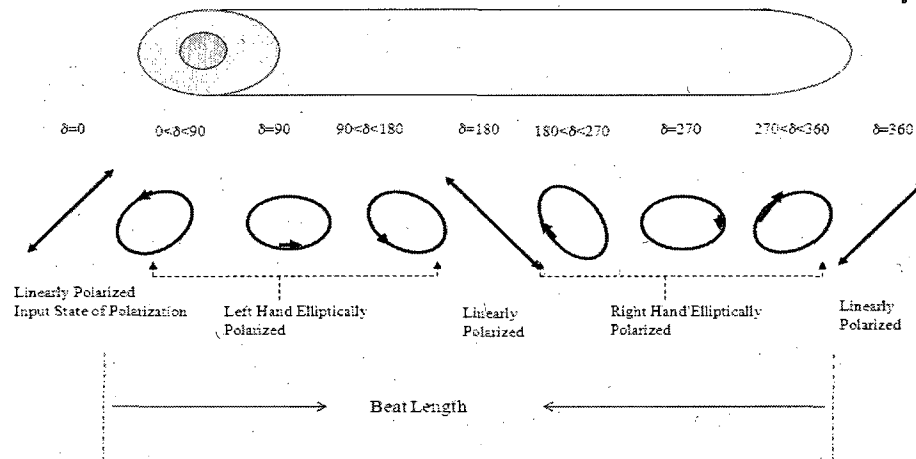


Figure 4- 11 Phase transition over a Beat Length segment

The phase difference between the orthogonal modes due to birefringence causes the polarization to evolve cyclically from its initial linear state through various elliptical states returning to its original state after a characteristic length called the beat length L_b .

The beat length is directly related with the birefringence by [18];

$$L_b = \frac{\lambda}{\Delta n_{eff}} \quad \dots\dots[4.19]$$

Thus, a beat length of a fiber is the characteristic length across which the birefringence remains constant and the input and output states of polarization are the same.

Conventional single mode optical fibers are random concatenations of a large number of

such beat length sections. The polarization state of one incremental length section is coupled randomly with the input polarization axes of the next section. This randomizes the output polarization state at a length referred to as the correlation length L_c or the coupling length h . The randomized polarization coupling of incremental sections also generates a distribution of the group delay. This is because the x and y modes of each section couple with the randomly oriented input polarization states of the next section. The group delay is then no longer linear and becomes difficult to calculate as the output is now a delay distribution.

4.3.2 First Order PMD

The two orthogonal modes supported by the fiber travel with different phase velocities due to birefringence and this gives rise to mode dispersion. The intrinsic birefringence is often a result of core ovality or ellipticity or asymmetrical thermal stress imposed onto the fiber over the manufacturing process. In small sections of fiber the birefringence is constant and there is no mode coupling. In polarization maintaining fibers (PMF), high birefringence is intentional in order to dominate the variations due to external effects. In such cases, the intrinsic birefringence generates two distinct optical pulses corresponding to the “slow” mode and the “fast” mode of the PMF. Since the high birefringence prevents the influence of the external factors, there is only a very weak coupling between the two modes and consequently the composite PMD is approximately equal to the intrinsic PMD. Hence, PMFs are also referred to as Hi-Bi (highly birefringent) fibers. In the literature, this behavior is referred to as deterministic effect of PMD or artifact PMD. This can be expressed as [18];

$$\frac{\Delta\tau}{L} = \frac{d}{d\omega}(\beta_s - \beta_f) = \frac{\Delta n_{eff}}{c} - \frac{\omega}{c} \frac{d}{d\omega} \Delta n_{eff} \quad \dots\dots[4.20]$$

It can be observed from Equation 4.20 that the deterministic effect of PMD has a linear dependence with length. This linear dependence is observed over short sections of fibers or in the case of PMF, and is also referred to as the intrinsic PMD of the fiber. Intrinsic factors imply that the PMD is innate to the fiber and is caused during the manufacturing process by introduction of imperfections in the waveguide geometry. Extrinsic factors include stresses on the fiber during installation, from twisting and bending pressure, or strains induced from temperature variations. In conventional fibers, birefringence is low. Hence, the intrinsic and extrinsic effects are nearly equal in magnitude and they act as a random set of disturbances to the fiber. Each of these disturbances is capable of causing significant coupling between the polarization modes of the fiber. The mode coupling will depend on the strength and spatial positioning or the orientation of the external effects relative to the internal birefringence of the fiber. Since mode coupling is a random phenomenon, the group velocity differences are also random. The pulses reach the end of the fiber with random magnitudes and a random distribution of arrival times. This is referred to as the distributed effect and the pulse distribution is referred to as the Differential Group Delay Distribution (DGD). The strength of mode coupling has a significant effect on the width of the pulse propagating along the fiber and hence on the bandwidth of the transmission medium. Weak coupling has little effect on the intrinsic birefringence of the fiber. It results in a relatively larger composite PMD, nearly equal to the intrinsic PMD. Conversely, strong mode coupling may interact frequently with the intrinsic birefringence, increasing the mixing of the fast and slow modes. This results in a

smaller composite PMD. Strong mode coupling therefore, decreases the mean value of fiber PMD.

The temporal behavior of PMD can be attributed to the changes in environmental conditions such as ambient temperature, local vibrations or slow changes such as fiber aging. These conditions may affect the stress or strain across the fiber sections resulting in a change in their birefringence over time.

The DGD is said to follow a Maxwellian probability density function [4, 6 and 22].

$$p(\tau) = \sqrt{\frac{2}{\pi}} \frac{\tau}{\alpha^3} e^{-\frac{\tau^2}{2\alpha^2}}, \text{ where } \tau = \sqrt{\frac{8}{\pi}} \alpha \quad \dots\dots[4.21]$$

The random coupling between the two principal states of polarization induced by the random perturbations of birefringence along the fiber tends to equalize propagation time for the two states. The PMD is characterized by the root mean square (RMS) value of $\Delta\tau$ obtained after averaging over random variations [19].

$$\langle \Delta\tau \rangle = \sqrt{\frac{\Delta\beta^2 \cdot h^2}{2} \left[\frac{2L}{h} - 1 + e^{-\frac{2L}{h}} \right]} \quad \dots\dots[4.22]$$

where;

$\Delta\beta$ = average modal birefringence parameter.

h = coupling length

L = length of the fiber

$\Delta\tau$ = dispersion group delay

For polarization maintaining fibers there is no mode coupling, and so the coupling length (h) is infinitely larger than the length of the fiber ($h \gg L$) and the PMD increases linearly with fiber length. For standard or non-polarization maintaining fibers whose length L is larger than the coupling length h ($L \gg h$), Equation 4.22 will reduce to:

$$\text{PMD} = \Delta\beta_1 \sqrt{hL} = D_p \sqrt{L} \quad \dots\dots[4.23]$$

where D_p is the dispersion parameter or the coefficient of PMD whose units are in $\text{ps}/\sqrt{\text{km}}$. Thus, the PMD increases with the square root of length. When cable sections are concatenated, the PMD value for the entire link is calculated as the root-mean-square of the sum of PMD values of individual cable sections [23]. When large fiber links are joined, the effect of concatenation on the overall DGD distribution is statistical and can be explained in terms of convolution of these individual distributions. Poole's statistical analysis of concatenation for arbitrary elements [5] in terms of Stokes vectors and their behavior on the Poincare' sphere shows that the Polarization Dispersion Vector (pdv) of a concatenation of random pdv's will be the sum of those random pdv's. The variance of the distribution of PMD for the total link is equal to the sum of variances of the individual segments. Hence the total PMD for the link is treated as the square root of the sum of squares of the individual PMD values:

$$\tau(L) \triangleq \sqrt{\Omega_1^2(L) + \Omega_2^2(L) + \Omega_3^2(L)} \quad \dots\dots[4.24]$$

where,

$\Omega_1(L)$, $\Omega_2(L)$, $\Omega_3(L)$ are the polarization dispersion vectors of the three links whose magnitude equals the PMD of each link.

$\tau(L)$ is the total PMD of the link.

4.3.3 Second Order PMD

In a segment of fiber having some non-vanishing random birefringence, two orthogonal polarization modes are generated which propagate through the length of the fiber segment. The energy content in these two principal states of polarizations varies randomly over the propagation length due to random coupling between the two modes. The time difference between these two states gives us the measure of first order PMD. The concept of second order PMD may then be understood by introducing the effect of chromatic dispersion on these two polarization states. The optical frequencies constituting the two polarization states encounter differing transit delays. This distorts the principal modes of polarization of a pulse propagating along an optical fiber, and the distortion is similar to either a delay spread or a compression suffered by a finite bandwidth signal propagating along a dispersive fiber as observed with chromatic dispersion. Therefore, the coefficient of second order PMD is defined in such a way that it has the same units as the chromatic dispersion coefficient (ps/nm/km).

If $\vec{\Omega}_+$ and $\vec{\Omega}_-$ represent the two mutually orthogonal polarization state vectors whose magnitudes equal the differential group delay ($|\vec{\Omega}| = \Delta\tau$), then the second order PMD vector $\vec{\Omega}_\omega$ is defined as [24]:

$$\vec{\Omega}_\omega = \frac{d\Omega}{d\omega} \quad \dots\dots[4.25]$$

The second order PMD vector $\vec{\Omega}_\omega$ is introduced as the derivative of the principal polarization state vector with respect to optical frequency 'ω'. This vector has zero mean and hence is characterized by its root mean square value.

$$PMD_{\text{SECOND ORDER-COEFF}} = \frac{2\pi c}{\lambda^2 l} \sqrt{\langle \Omega_\omega^2(\omega) \rangle} \frac{ps}{nmKm} \quad \dots\dots[4.26]$$

Where;

$\langle \dots \rangle$ = Statistical mean

l = length of the fiber (assumed to be very large with respect to polarization mode coupling length h).

Using the dynamical equations for first and second order PMD, the fiber length dependence of second order PMD has been calculated by Gisin et.al [5] as:

$$\langle \Omega_\omega^2 \rangle = \frac{B^4 h^4}{3} \left[\frac{l^2}{h^2} - \frac{5l}{2h} + \frac{17}{8} - 2 \left(\frac{l}{h} + 1 \right) e^{-\left(\frac{2l}{h}\right)} - \frac{1}{8} e^{-\left(\frac{4l}{h}\right)} \right] \quad \dots\dots[4.27]$$

where;

$B^2 = \langle \vec{\beta}^2 \rangle$ is the root mean square birefringence.

l = length of the fiber.

h = polarization mode coupling length.

When the length of the fiber 'l' is very large with respect to polarization mode coupling length 'h';

$$\lim_{\frac{l}{h} \rightarrow \infty} \langle \vec{\Omega}_\omega^2 \rangle = \frac{B^4 h^4}{3} \left(\frac{l}{h} \right)^2 \quad \dots\dots[4.28]$$

$$\text{Therefore, the total second order PMD} = \sqrt{\langle \vec{\Omega}_\omega^2 \rangle} = \frac{B^2 hl}{3} \quad \dots\dots[4.29]$$

The second order PMD has a linear dependence with the fiber length 'l'.

4.3.4 Relationship between the First Order and Second Order PMD

As observed from above, for fibers with very large length 'l' with respect to the polarization mode coupling length 'h', the second order PMD increases linearly while the first order increases with the square root of the fiber length 'l'. This result helps establish a simple relationship between first and second order PMD [5]:

$$\left. \begin{aligned} \langle \bar{\Omega}_\omega^2 \rangle &= \frac{1}{3} (\langle \bar{\Omega}^2 \rangle)^2 \\ \sqrt{\langle \bar{\Omega}_\omega^2 \rangle} &= \frac{1}{\sqrt{3}} (\langle \bar{\Omega}^2 \rangle) \\ \sqrt{\langle \bar{\Omega}_\omega^2 \rangle} &= \frac{1}{\sqrt{3}} (PMD_{\text{First-Order-Coefficient}} \cdot \sqrt{l})^2 \\ PMD_{\text{Second-Order-Coefficient}} &= \frac{1}{\sqrt{3}} (PMD_{\text{First-Order-Coefficient}})^2 \end{aligned} \right\} \dots\dots[4.30]$$

4.4 Limitations of Existing Statistical Model Of PMD

The most widely accepted phenomenological model, which aided the description and the characterization of PMD in long fiber lengths, was based on the concept of the Principal States of Polarization. This model assumes large coherence times of the source and that the polarization dependent loss (PDL) is negligible. This model states that over an arbitrary length of the fiber, there exists an orthogonal input state of polarization for which the corresponding output states of polarization are also orthogonal and are independent of wavelength to the first order. These input states of polarization are known as the Principal States of Polarization (PSP), and provide the base for the characterization of PMD in single mode fibers of arbitrary lengths and configurations. As the birefringence of a single mode fiber varies along the length of propagation, a long fiber may be represented as a concatenation of birefringent sections with random orientations of polarization (Fast and Slow) axes. Electric fields emerging from each segment are projected onto the polarization axes of the following segment. The linearly polarized input polarization states are transformed into composite elliptical polarization states by the distributed mode coupling and the random polarization scrambling effects of concatenation in long birefringent fibers as shown in Figure 4-12. This incremental coupling and scrambling phenomenon randomizes and distributes the resulting differential group delay. The root mean square value of this DGD distribution provides a measure of the PMD impairment.

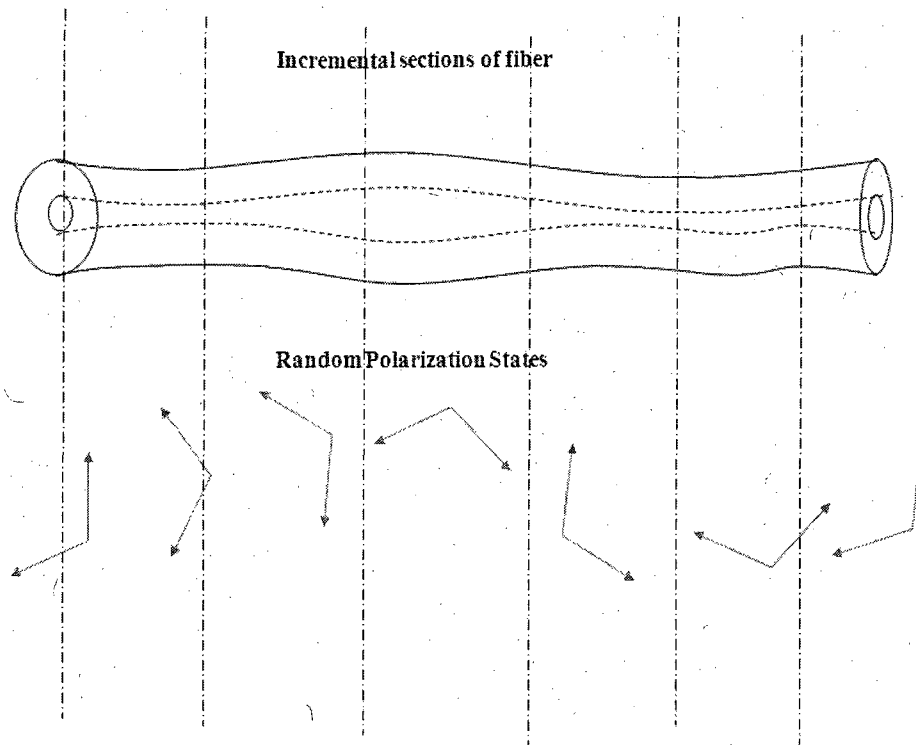


Figure 4- 12 Random Polarization States across Incremental Beat Lengths

The statistical approach to model this impairment is applied within two length domains: short range domain when the length of propagation is very small compared to the correlation length and long range domain when the length of propagation is very large compared to the correlation length. The correlation length L_c is the length after which output polarization becomes uncorrelated with the initial input polarization state and it becomes equally probable to observe any state of polarization at the output. In short length regimes ($L \ll L_c$), the PMD varies linearly with the length of propagation and for large length regimes ($L \gg L_c$) PMD varies as the square root of the length of propagation.

Field measurements of PMD using interferometric techniques capture only a small sample of the statistical distribution and only over a brief observation time, forcing a Gaussian fit [Figure 4-13] to the measured distribution [7]. The mean of this Gaussian fit is used to represent the mean PMD; in this case it is 4.1 picoseconds.

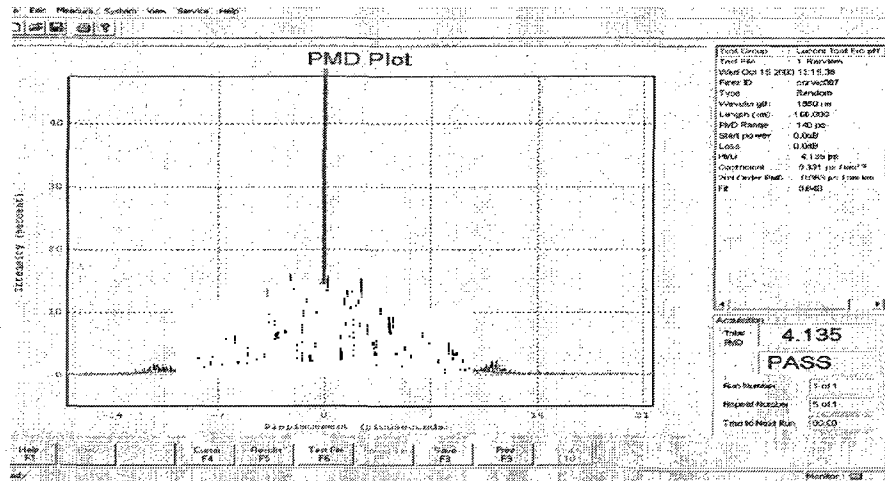


Figure 4- 13 Field Measurement of PMD

The PSP model provides a method to analytically describe the stochastic behavior of PMD, producing a smooth and continuous random distribution of differential group delay. The literature survey indicates Gaussian or Maxwellian envelope estimation for the differential group delay distribution $\Delta\tau$ in time domain [2, 6, 22 and 25].

In practice, a fiber span may accurately be viewed as a concatenation of a large number of discrete effects. The total PMD is thus a function of the interaction of these discrete/individual effects, and it is not clear that the mean value of a continuous

distribution will thoroughly characterize the actual ensemble of concatenated polarization-scrambled paths, especially when applied to the simulation of different signal formats and novel compensation techniques.

Furthermore, the stochastic nature of this impairment necessitates the characterization of PMD over a large range of values to accurately estimate the distribution. An exhaustive Monte Carlo simulation of a large population of PMD values sufficient for the accurate prediction of low bit-error rates is both difficult and time-consuming. The extrema (end regions or “tails”) of such continuous distributions (Maxwellian or Gaussian) define the values of the impairment responsible for the worst-case performance degradation of the network. Proper characterization of the distribution is therefore critical. Also, the asymptotic nature of the distribution may necessitate the design of a system that is tolerant to large variations of impairment. This, in turn, makes design of successful compensation techniques very challenging. The existing statistical system models for PMD do not have the ability to account for the random changes in birefringence induced in the fiber by the non-homogenous nature of the impairment over distance and they do not provide the ability to account for the pulse broadening accurately in such conditions. Consequently, they do not allow for dynamic analysis of the change in the output differential group delay distribution at the end of the fiber. The existing models do not have the ability to introduce and analyze anomalies such as differing sections of fibers or randomly occurring deviations. These limitations necessitate the need and provide the motivation for our new model to better represent the effect of PMD on communication system performance.

Summary

This chapter provided a review of polarization in optics and propagation of polarized modes in optical waveguides. The theory of Polarization Mode Dispersion, its first order and second order effects and its length dependence were discussed. Limitations of the existing statistical model of the PMD based on the Principal States of Polarization were identified. These limitations behoove us to develop a new approach for a new model which would adequately characterize the PMD impairment and its effect on the performance of optical networks which is discussed in the next chapter.

CHAPTER – 5

MODEL AND SIMULATION OF POLARIZATION MODE DISPERSION

Introduction

The previous chapter discussed the theory of Polarization Mode Dispersion, its first order and second order effects, and its length dependence and the limitations in the existing statistical models which are based on the theory of Principal States of Polarization. This chapter describes a new cumulative model which is able to capture the complete ensemble of discrete components of the output differential group delay distribution. It also describes the mathematical implementation of this model in MATLAB and C++ code. The first stage of this implementation generates delays of individual beat length segments based on a Gaussian distribution. The second stage generates the output differential group delay distribution based on the new approach using the output from the first stage. The final stage uses the resultant output DGD distribution from stage two in a system model and generates performance penalties that completely characterize the impact of this impairment on the performance of the optical systems.

5.1 Impact of PMD on Optical Systems

Digital light-wave systems require undistorted transmission of optical pulses over long lengths of fiber. Dispersive effects such as PMD cause a received pulse to be broadened or distorted in the time domain, depending upon the amount of differential delay and the relative amplitude of the delayed signal. In general, signal distortion that results from differential group delay and/or velocity is referred to as dispersion. The time-varying nature of PMD makes it difficult to calculate an adequate system design margin to ensure satisfactory performance of optical communication systems. Therefore, power margins are assigned to the PMD impairment that stipulate a maximum allowable outage probability ' P_{OUT} ', which is defined as the probability that the penalty due to the PMD exceeds the assigned power margin. The power penalty ϵ (dB) incurred by a Non Return to Zero (NRZ) optical signal modulated system is [18]:

$$\epsilon(dB) = \frac{A \Delta \tau^2 \cdot \gamma \cdot (1 - \gamma)}{T^2} \dots\dots[5.1]$$

where:

A = dimensionless parameter dependent on optical pulse shape and receiver sensitivity.

γ = Power splitting ratio between the two components.

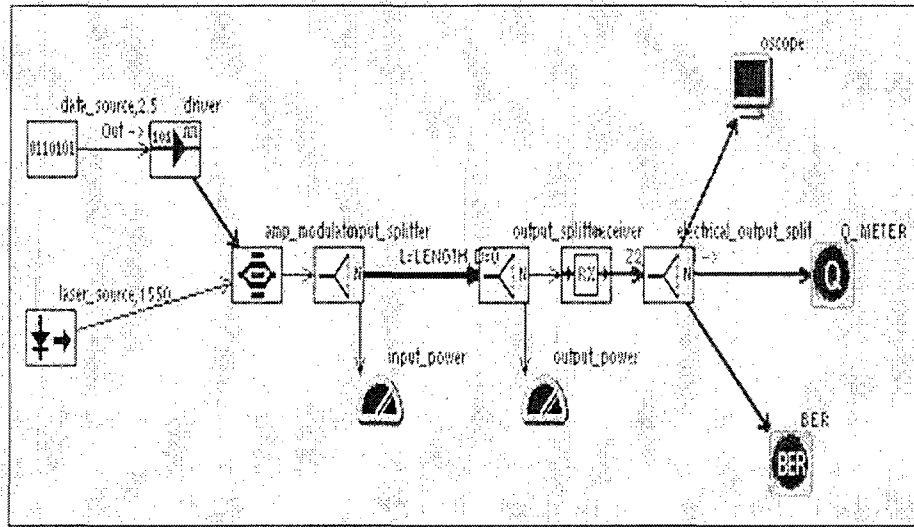
T = full width half maximum of pulse duration

$\Delta \tau$ = Differential Group Delay

Unavailability or system outage not exceeding thirty minutes per year (maximum) [18] due to PMD is generally required by network operators. Common design practices limit the power penalty ' ϵ ' incurred PMD to 1 dB in order to satisfy this availability guideline. These threshold calculations using the existing PMD model are based on the assumption of a continuous distribution of PMD in the time domain. A long-term penalty of 1 dB or less requires that the average differential delay time between the principal states of polarization remains less than 0.14 of the bit period. Thus, optical networks carrying data at a higher rate are more susceptible to PMD than networks carrying data at lower rates.

5.1.1 Impact of PMD on Network Data Rates

To demonstrate the impact of the PMD impairment on an optical network's ability to carry high speed data rates, a network configuration [Figure 5-1] is setup using the Optsim optical software simulation tool. In our network configuration, a continuous wave laser source at 1550nm is fed to an external modulator. The modulator is driven by a pseudo random binary sequence (PRBS) generator whose data rate can be varied from 2.5 Gbps to 40 Gbps. Thus, the output of the modulator is a continuous beam of light which is switched on and off at the data rate of driver. This modulated optical signal is launched into a span of Standard Single Mode Fiber (SSMF) of length 100 km. Optical power meters monitor the signal power level before and at the end of the span. A receiver detects the received signal at the end of the span and the detected signal is fed to an electrical oscilloscope, Q-meter and a bit error rate analyzer to record the corresponding values of bit error rate, Q(dB) and the shape of the eye.



Unit: OC48-BASE

Figure 5- 1 Network Configuration to Measure Impact of PMD on Network Data Rates

The software allows the PMD of the fiber to be varied by varying its PMD coefficient parameter. In order to evaluate the true impact of PMD on the network performance all other effects that could contribute towards signal degradation, such as chromatic dispersion and non-linear fiber effects e.g. four wave mixing are isolated or removed. The impact of PMD on the network performance is mapped on the basis of the change in value of bit error rate, Q and the shape of the eye (eye closure).

In the first round of simulations, the data rate is the fixed parameter and the mean PMD in picoseconds (ps) is the variable parameter. Thus, for a specific data rate, the mean PMD is varied over a wide range of values and the network performance in terms of the bit error rate is recorded. This process is repeated for each data rate (2.5 Gbps, 10 Gbps, and 40 Gbps). For a data rate of 2.5 Gbps with a pulse time period (T) of 400 ps

the mean PMD is varied from 0 to 100 ps. For a 10 Gbps data rate with a pulse time period of 100 ps the mean PMD is varied from 0 to 70 ps. For a 40 Gbps data rate with a pulse time period of 25 ps the mean PMD is varied from 0 to 50 ps. The maximum values of variation of mean PMD and the steps of their variation are different at each data rate so as to better capture the transition in system performance in terms of degradation of the bit error rate. Results from this exercise are shown in Figure 5-2. It is seen that at a data rate of 2.5 Gbps although the mean PMD is varied till 100 ps, which corresponds to 25% of its bit period there is no degradation in the bit error rate. At a data rate of 10 Gbps, the bit error rate starts to degrade when 35 ps of mean PMD (35% of bit period) is introduced in the fiber span. At a data rate of 40 Gbps, the bit error rate starts to degrade when a 5 ps mean PMD (20% of the bit period) is introduced in the fiber span.

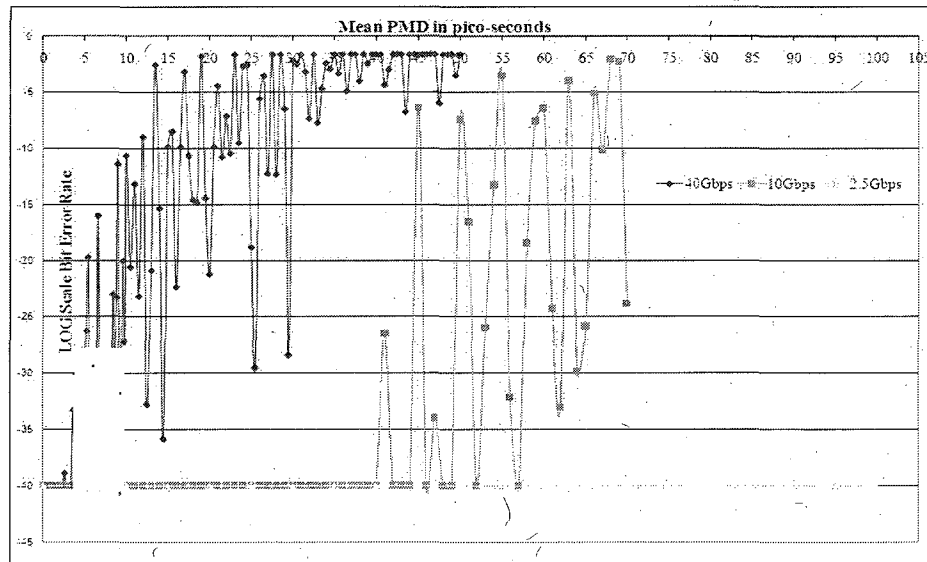


Figure 5-2 Mean PMD in Pico-Seconds v/s Bit Error Rate

Stage two of our simulations captures the statistical variance of PMD which, in turn, results in random variation in network performance. Owing to the random intrinsic and extrinsic effects that cause change in symmetry of the waveguide and contribute to random mode coupling of the orthogonal modes of propagation within the waveguide, the dispersion group delay (or PMD) is generally assumed to follow a Maxwellian distribution. This implies that over a sufficient observation period an optical network may see an instantaneous peak PMD value approximately three times the value of the mean distribution. This would imply a significant variation in bit error rate performance corresponding to the instantaneous value of PMD presented to the network at any particular instant in time. To capture this variation, specific mean PMD values are identified from previous stages of simulations. These identified points of transition in network performance are then introduced in the fiber and the simulation is carried out over a large range of random seeds to simulate the statistical variation of PMD. For a fixed data rate, the mean PMD is fixed at a particular value and the random seed of the PMD function is varied over 100 iterations and statistics for the variation in bit error rate are collected. Figures 5-3, 5-4 and 5-5 show the plots of this variation at respective data rates of 2.5 Gbps, 10 Gbps and 40 Gbps. For a 2.5 Gbps data rate, Figure 5-3 shows no variation in the bit error rate, thus implying that at low data rates (time period $T \ll$ PMD impairment), the statistical variation of the PMD does not affect the performance of the receiver and hence no statistical behavior of PMD is observed at this data rate. Figure 5-4 presents the random variation of bit error rate for a 10 Gbps data rate at a specific mean PMD value over 100 random seed runs; the statistical results are tabulated below in Table 5-1.

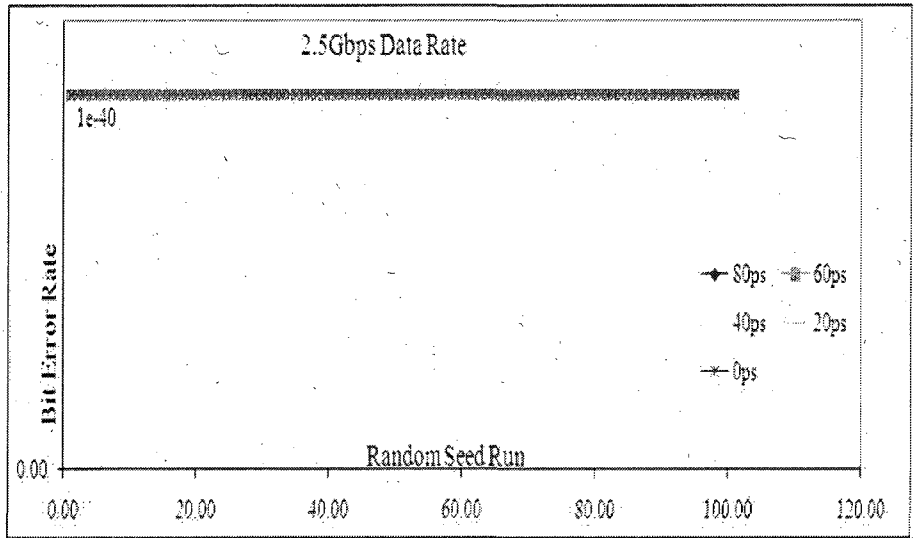


Figure 5- 3 Bit Error Rate Variation at 2.5 Gbps

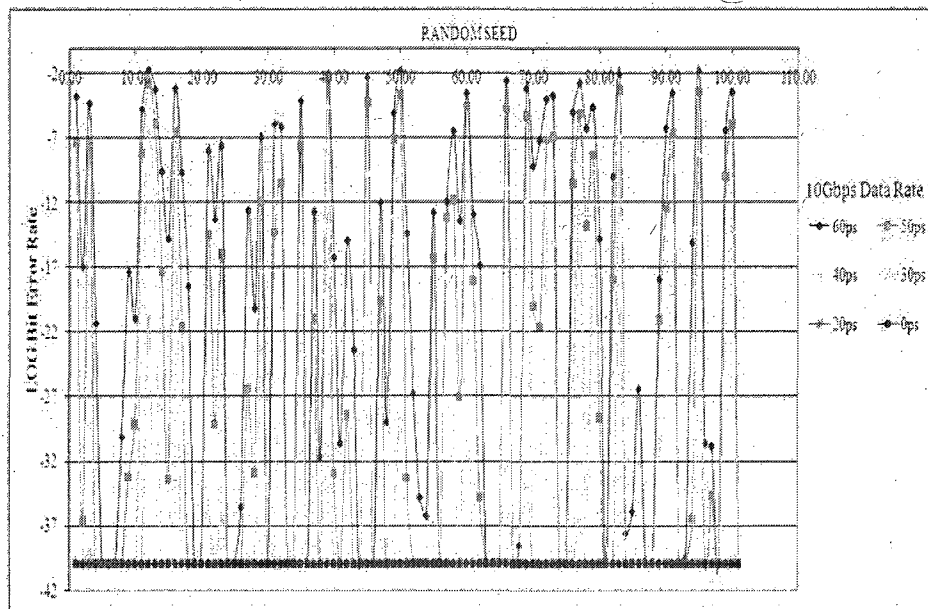


Figure 5- 4 Bit Error Rate Variation at 10 Gbps

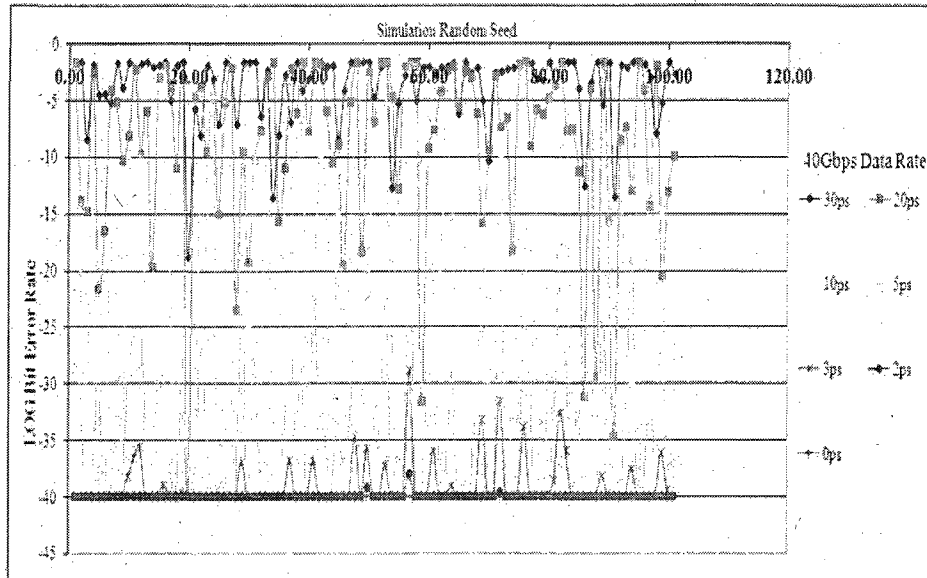


Figure 5- 5 Bit Error Rate Variation at 40 Gbps

Mean PMD ps	0	20	30	40	50	60
MIN	1.00E-40	1.00E-40	1.00E-40	1.00E-40	1.00E-40	1.00E-40
MAX	1.00E-40	1.00E-40	1.11E-13	3.77E-05	3.77E-03	1.99E-02
MEAN	1.00E-40	1.00E-40	1.09E-15	3.79E-07	6.46E-05	8.30E-04
STDEV	0	0.00E+00	1.10E-14	3.75E-06	4.08E-04	3.26E-03
VAR	0	0.00E+00	1.21E-28	1.41E-11	1.66E-07	1.06E-05

Table 5- 1 Statistical Variations Over 100 Runs in Bit Error Rate at 10 Gbps Data Rate

Table 5-1 shows no degradation in bit error rate performance until the mean PMD is close to 30% of the bit period (30ps). At around 30ps, the statistical nature of the PMD impairment is observed. Over 100 random seed simulation runs at a mean PMD of 30ps, the best recorded bit error rate is $1e-40$ indicating the lowest instantaneous peak PMD value while the worst bit error rate is $1e-13$ indicating the worst case PMD value. Over 100 random seed simulation runs at a mean PMD of 50ps, the minimum and maximum bit error rate recorded is $1e-40$ and $1e-3$ respectively with a mean bit error rate of $6e-5$. At 60ps mean PMD, the minimum and maximum bit error rates recorded are $1e-40$ and $1e-2$ respectively with a mean bit error rate of $8e-4$.

Figure 5-5 captures the random variation of bit error rate for 40Gbps data rates at a specific mean PMD value over 100 random seed runs. The statistical results are tabulated below in Table 5-2.

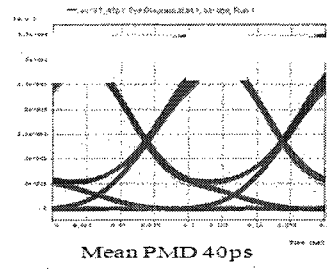
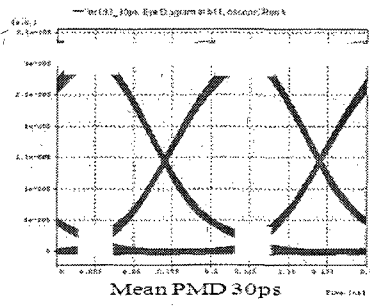
Mean PMD	0ps	2ps	3ps	5ps	10ps	20ps	30ps
Min BER	1.00E-40	1.00E-40	1.00E-40	1.00E-40	1.00E-40	1.00E-40	1.59E-19
Max BER	1.00E-40	9.96E-39	1.36E-29	3.16E-17	4.55E-04	2.28E-02	2.28E-02
Mean BER	1.00E-40	2.04E-40	1.34E-31	3.14E-19	5.02E-06	4.00E-03	9.63E-03
Stdev	0	9.82E-40	1.35E-30	3.14E-18	4.53E-05	7.81E-03	9.65E-03
Variance	0	9.65E-79	1.82E-60	9.88E-36	2.06E-09	6.10E-05	9.31E-05

Table 5- 2 Bit Error Rate over 100 Runs: 40 Gbps Data Rate

The minimum and maximum values of bit error rate at a mean PMD of 3 ps were $1e-40$ and $1.3e-29$ respectively. The mean bit error rate was $1.3e-31$. At a mean PMD of 5 ps, the minimum and maximum bit error rate was $1e-40$ and $3e-17$ respectively and the mean

bit error rate was $3e-19$. At a mean PMD of 10 ps, the minimum and maximum bit error rate was $1e-40$ and $4e-4$ and the mean bit error rate was $5e-6$. At 20 ps, the minimum and maximum bit error rate was $1e-40$ and $2e-2$ respectively and the mean bit error rate was $4e-3$. At 30 ps, the minimum and maximum bit error rate was $1.5e-19$ and $2e-2$ respectively and the mean bit error rate was $9e-3$.

Figure 5-6 and Figure 5-7 show the degradation in the eye diagrams or the eye closure due to PMD impairment at 10 Gbps and 40 Gbps. For 10 Gbps data rates ($T=100ps$), very little distortion is visible at 30 ps mean PMD. The eye starts to deteriorate at 40 ps mean PMD, which corresponds to a little more than one third the pulse width. At mean PMD's of 50 ps and 60 ps (greater than half the pulse width) the eye is degraded to a large extent due to the domination of inter-symbol interference created by PMD. Similarly, for a 40 Gbps data rate (implying a pulse width of 25 ps), the eye pattern at a mean PMD of 3 ps is nearly free of distortion. For a mean PMD of 10 ps (greater than one third the pulse width) the eye pattern begins to degrade, and for mean PMDs of 20 and 30 ps (greater than the pulse width), the eye is totally distorted.



10Gbps Data Rate

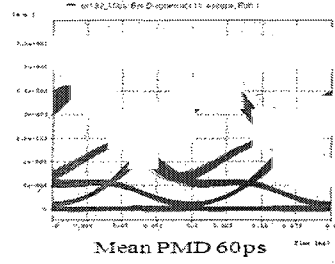
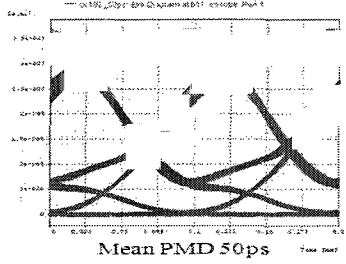


Figure 5- 6 Eye Diagrams at 10 Gbps Data Rate

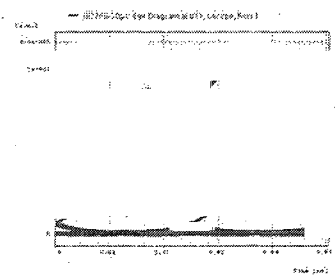
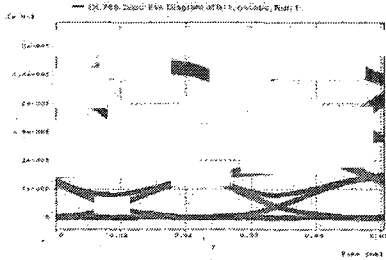
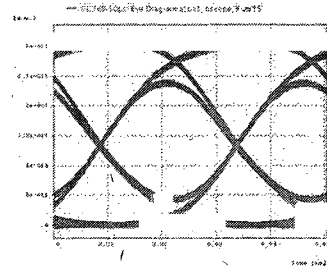
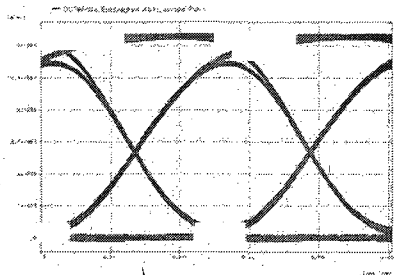


Figure 5- 7 Eye Diagrams at 40 Gbps Data Rate

Figure 5-8 shows the overall performance of the system, which is a plot of the mean PMD in picoseconds versus the mean bit error rate obtained from our simulation results. The plot shows that the mean bit error rate performance of the system remains unaffected at $1e-40$ at a 2.5 Gbps data rate. At a 10 Gbps data rate, the first transition point at which the bit error rate degrades below $1e-40$ is at a mean PMD of 20 ps (20% of bit period) and the performance becomes very poor at a mean PMD greater than 40 ps (40% of the bit period). At the 40 Gbps data rate, the first point of transition at which the bit error rate performance degrades is at a mean PMD of 3 ps (12% of the bit period). The performance becomes extremely poor for mean PMDs greater than 8 ps (32% of the bit period).

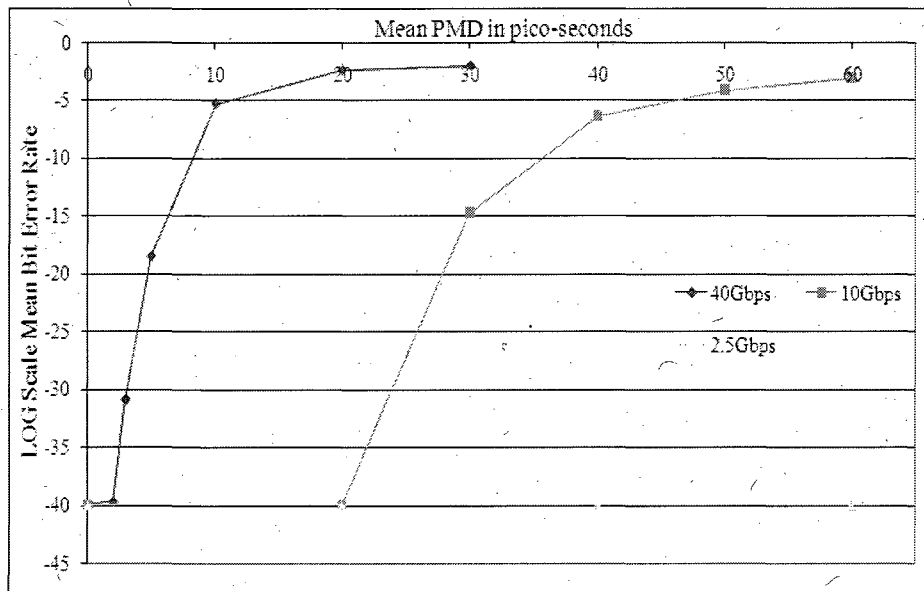


Figure 5- 8 Overall Performance System at 2.5 Gbps, 10 Gbps, 40 Gbps

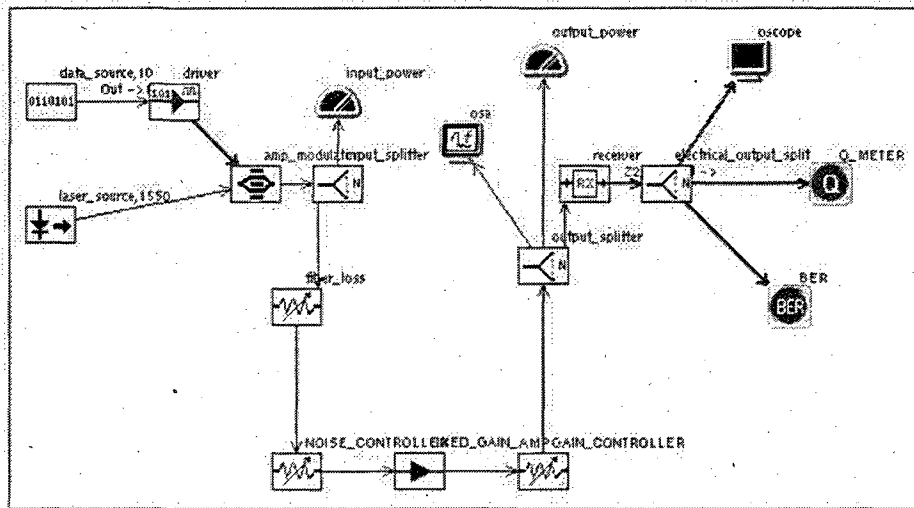
5.1.2 Performance Penalties due to PMD Impairment

In the previous section the results of our simulation of the effect of distributed PMD on a single span optical network configuration have been discussed. The results show that higher data rates have lower tolerance to PMD. Thus, the presence of PMD in optical fibers has the effect of limiting the ability of the network to transport data at higher rates. The next set of simulations use the transition points from the previous section to evaluate the impact of PMD on optical networks in terms of power penalties.

5.1.2.1 Receiver Characterization

The first step towards generating and comparing system performance degradation is to characterize the performance of the receiver employed in the architecture. This gives us the baseline performance of our network configuration without the addition of any PMD channel impairment. Receiver characterization is performed by degrading the signal arriving at the receiver by a controlled addition of noise. At each step of addition of noise, the values of the optical signal to noise ratio and bit error rate at the receiver are recorded. The plot of optical signal to noise ratio versus bit error rate maps the base line system performance and the procedure is called Receiver Characterization. Figure 5-9 shows the Optsim software simulation test-bed used to characterize the receiver. The transmitter section consists of a PRBS data source, a driver (10 Gbps) for the external modulator, an external modulator (for e.g. Mach Zehnder type) and a continuous wave laser source at 1550 nm. An attenuator of 20 dB is used to simulate an ideal fiber (without any dispersion impairments). For a noise source, a fixed gain (25 dB) Erbium Doped Fiber Amplifier (EDFA) is used. The noise generated by the EDFA is directly

proportional to the level of its optical input. Therefore, a noise-controller attenuator controls the input to the EDFA and thus controls the noise generated by the amplifier. The increase in noise is also accompanied by increased gain. Therefore, the gain-controller attenuator along with the noise-controller is used in such a way that any gain from the EDFA amplifier is excluded and only noise is introduced in the system. The receiver under consideration is a receiver, which has a specified bit error rate of $1E-09$ at a minimum received power level of -29 dBm. In all of our measurements the operating point of the receiver has been held steady at a receiver sensitivity of -17.8 dBm (which is well above -29 dBm). For each specific value of the noise-controller attenuator, the gain-controller attenuator is adjusted so that optical power received at the receiver is maintained at -17.8 dBm.



Unit: RECIEVER_BASE

Figure 5- 9 Receiver Characterization Test Bed

The values of OSNR of the channel and the optimal bit error rate are recorded and a plot of optimal OSNR versus BER is plotted as shown in Figure 5-10. This plot acts as our baseline performance metric against which is used to compare the system performance captured after addition of channel impairments, which in our case is PMD.

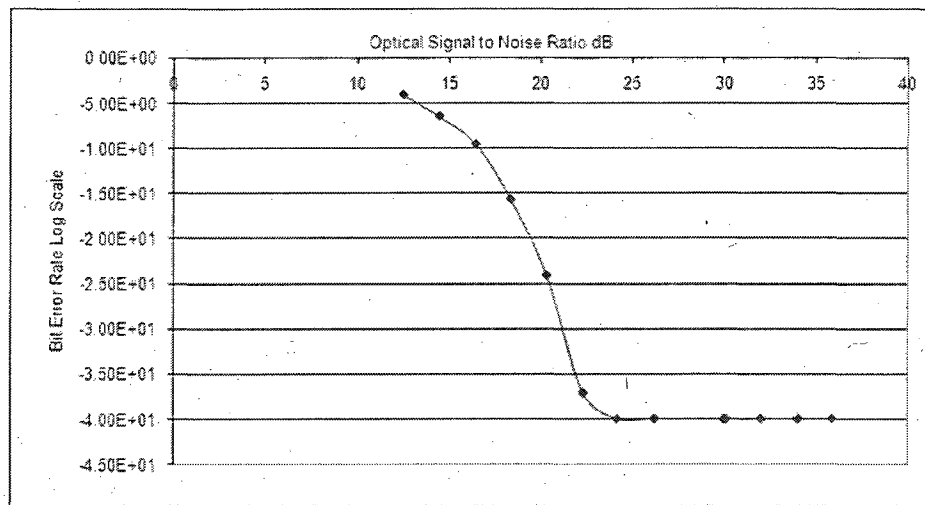


Figure 5- 10 Baseline Receiver Performance

5.1.2.2 Distributed PMD Test Configuration

The previous section mapped the performance of the receiver in the absence of any channel impairments; the next step is to evaluate the setup with the addition of PMD as a channel impairment in the test bed. This is done by replacing the fiber-loss attenuator from the receiver characterization setup with a real fiber of equivalent loss length (length 100 km, attenuation coefficient of 0.2 dB/km). This ensures that the operating point of the receiver remains unchanged at -17.8 dBm. Distributed PMD is introduced in the

system under test by changing the value of the mean DGD parameter in the fiber properties. The properties of all the remaining blocks in the simulation test bed remain unchanged. The mean PMD is set to 20 ps and noise is added in the system in the same steps of receiver characterization. At each step, the value of optical signal to noise ratio and bit error rate is recorded. For the case when a PMD with a mean value of 20 ps was introduced in the system, its corresponding plot of system performance is generated by plotting the optical signal to ratio against bit error rate. The above steps are repeated for different values of mean PMD (30ps, 40ps, and 50ps) the corresponding plots are shown in Figure 5-11. The results show that the performance plot with the mean PMD of 20ps closely matches with the baseline receiver performance. This confirms our previous conclusion that the transition point beyond which the system performance starts degrading in the presence of distributed PMD in our setup is close to 20 ps. The 30 ps plot shows a significant shift from the base line performance of the receiver. The plots for 35, 40 and 50 ps not only show a significant shift from the receiver baseline but also show large oscillating variations. This unstable behavior is not surprising as it can be attributed to the statistical nature of the distributed effect of the PMD. Owing to the unstable behavior of this effect, the generated plots cannot be used to determine the optical signal to noise ratio penalties for this architecture. To account for the statistical nature of this effect, five optical signal to noise ratio points from each plot are identified (corresponding to the specific value of PMD), which are located in the operating region of interest. For each optical signal to noise ratio point, the random seed parameter of the OptSim simulation tool is varied one hundred times to simulate different values of instantaneous PMD using a fixed mean value specified in the setup.

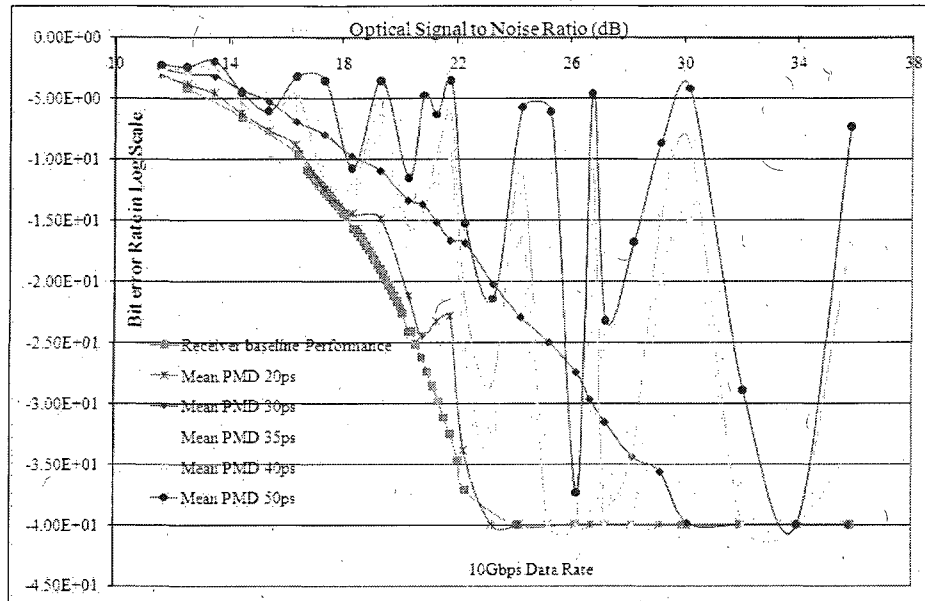


Figure 5- 11 System Performance with Distributed PMD

For each of these random seed runs the corresponding bit error rate is recorded and a mean bit error rate is calculated over the one hundred runs. Thus, for each value of chosen optical signal to noise ratio an average value of optimal bit error rate corresponding to specific value of mean PMD is obtained. A plot of these five OSNR points and their corresponding mean optimal bit error rates is generated. This plot is then optimized by applying a polynomial fit of the appropriate order (3,4,5) and the coefficients of the fit are obtained. Using these coefficients the remaining optical signal to noise ratio points are re-mapped and the corresponding mean optimal bit error rate is obtained. Figure 5-12 shows the fitted plots for various values of mean PMD. This approach of random seed variation along with polynomial fit optimization generates stable performance curves from which the optical signal to noise ratio penalties can be generated. For example, consider the design of a similar architecture network in which

the desired bit error rate is $5E-7$. The receiver characterization curve from Figure 5-12 indicates that in the absence of any channel impairments the required optical signal to noise ratio to maintain the desired bit error rate of $5E-7$ or better is at least 15 dB.

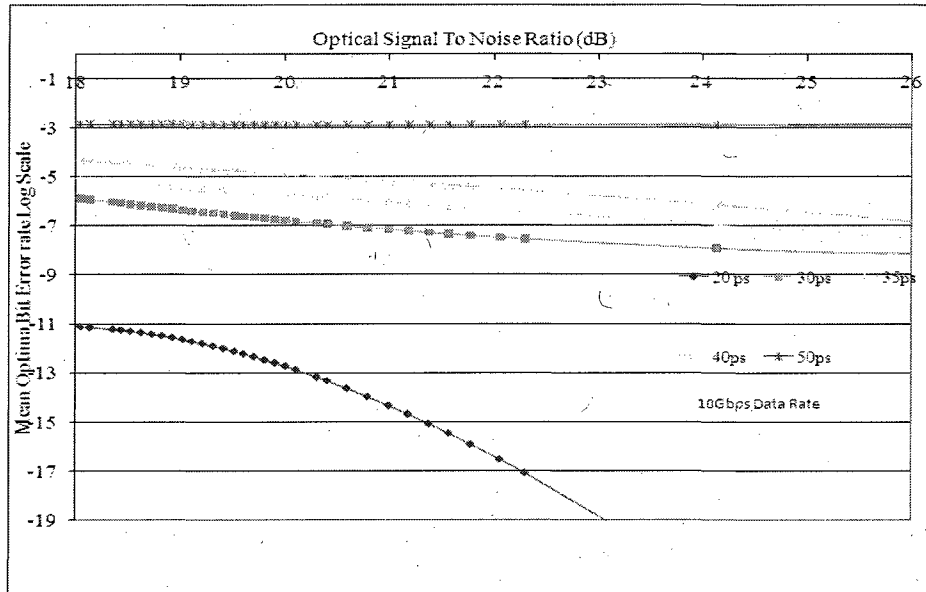


Figure 5- 12 OSNR versus Mean BER for Distributed Effect PMD

If PMD (as channel impairment) of 30 ps is introduced in the system, an optical signal to noise ratio of at least 18.82 dB would be needed to maintain the desired bit error rate of $5E-7$. Thus, an optical signal to noise ratio penalty of 3.82 dB is incurred due to the addition of this channel impairment. If 35 ps of mean PMD is introduced, the required optical signal to noise ratio to maintain the existing bit error rate is 21.57 dB thus incurring a penalty of 6.5 dB from the base line performance. Similarly a penalty of approximately 9 dB is incurred for 50 ps of mean PMD introduced in the system. These penalty results are summarized in Table 5-3 below.

PMD	0 (Base Line)	30ps	35ps	40ps
Req. OSNR (dB)	15	18.82	21.57	24.15
Penalty (dB)		3.82	6.57	9.15

Table 5-3 Optical Signal to Noise Ratio Penalties for Bit Error Rate of 5e-7.

5.1.2.3 Generating Deterministic PMD

The deterministic effect of PMD may be generated by an event of differential strain or geometry along the waveguide. It is sustained because there is no interaction (mode coupling) between the two orthogonal modes. If the fiber is highly birefringent, there would be no mode coupling between the two orthogonal modes and the differential group delay would increase linearly with the length of propagation (hence characterized by a coefficient with units of ps/km). A simple way to generate this effect in the lab would be to split the optical signal and pass the two signals through arms of different lengths of polarization maintaining fibers and then recombine them. Thus, the two modes with a fixed differential delay would add in such a way so as to distort the resultant pulse. The receiver, which is an intensity detector, would detect this resultant distorted pulse and may incorrectly decipher it as a one or a zero. Using the OptSim simulation tool, a similar effect has been generated by splitting the optical signal into two arms. An optical delay block (from OptSim block libraries) is introduced in the upper arm to provide the desired delay (in picoseconds). Attenuators α_1 and α_2 are used to control the signal strength (mode energy) in each arm as shown in Figure 5-13. In the test-bed, this

deterministic PMD setup is now introduced as the channel impairment instead of the optical fiber. A fiber-loss attenuator (20dB) is introduced in the setup to compensate for the fiber loss and to maintain the operating point of the receiver at -17.8 dBm [Figure 5-14]. Delays of 20, 30, 35, 40 and 50 ps are introduced into the setup and similar procedure (as in the case of distributed PMD) is followed to generate OSNR versus Optimal BER curves. Figure 5-15 – 19 compare the performance curves for a deterministic PMD and a distributed PMD for each value of PMD respectively. Figure 5-15 compares the performance penalty plot for distributed and deterministic effects of PMD at 20 ps. The two plots are observed to be very close to each other.

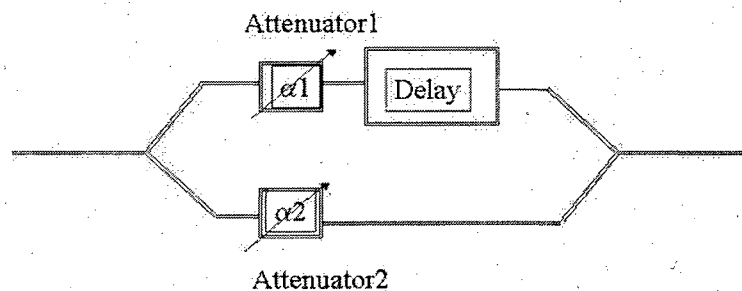
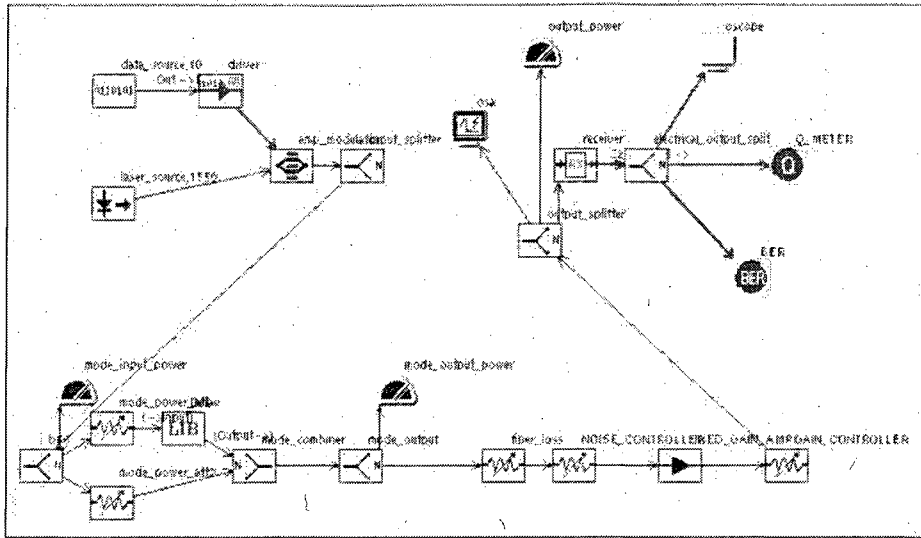


Figure 5- 13 Generating Deterministic PMD Using OptSim Simulation Test Bed



Unit: det_20ps

Figure 5- 14 Deterministic PMD Setup

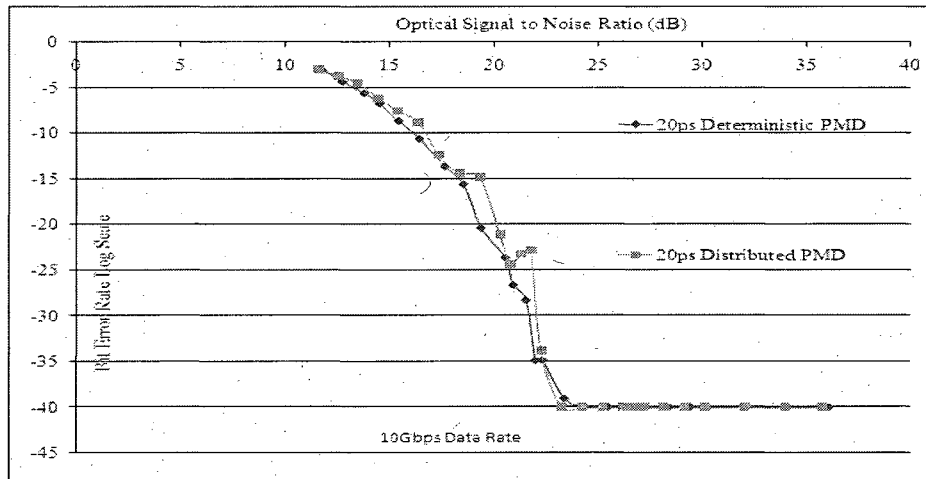


Figure 5- 15 Deterministic Versus Distributed Effect 20ps

Figure 5-16 shows that the distributed PMD curve at 30 ps is significantly displaced from the receiver baseline performance, but the plot for the 30 ps deterministic effect is very close to the receiver baseline performance, thus indicating that minimal performance degradation is introduced by a deterministic 30 ps PMD as compared to distributed 30 ps PMD.

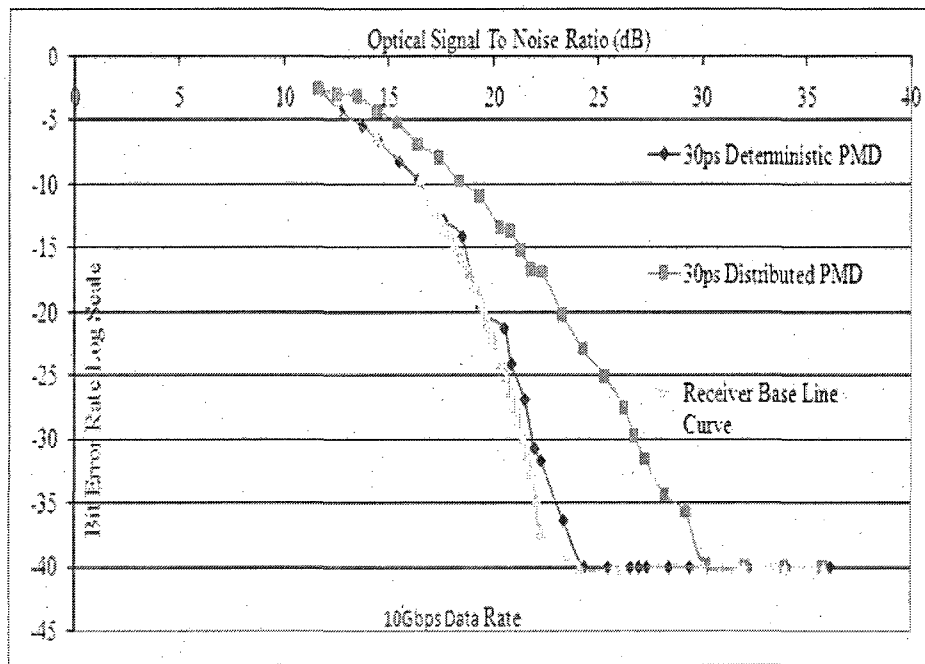


Figure 5- 16 Deterministic Versus Distributed Effect 30 ps

At 35 ps [Figure 5-17], the deterministic plot shows a stronger shift from the receiver baseline performance as compared to the 30 ps deterministic plot. The performance plot for 35 ps distributed effect is unstable due to the temporal nature of the distributed PMD impairment and therefore a stable performance plot is obtained by seed variation and

polynomial fitting. It is observed that the 35 ps deterministic plot follows the higher performance points from the unstable 35 ps distributed effect plot.

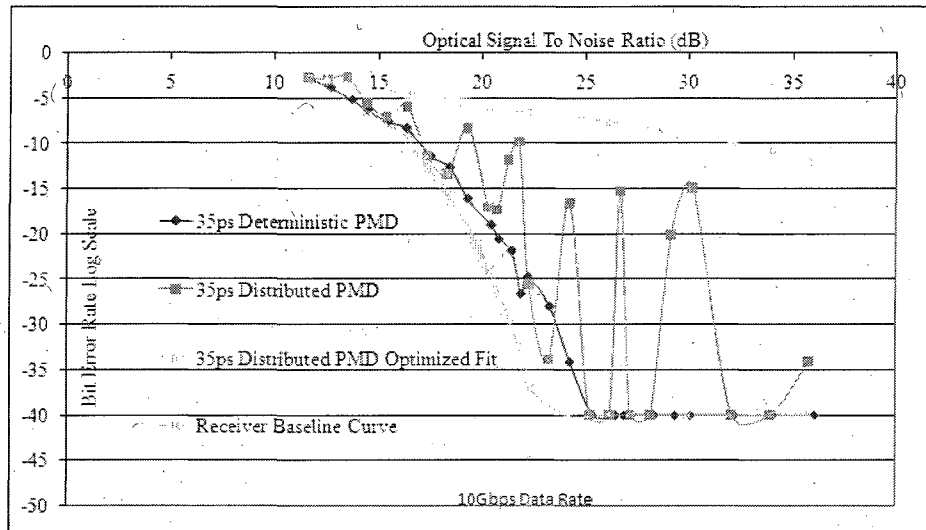


Figure 5- 17 Deterministic Versus Distributed Effect 35ps

Figure 5-18 and 19 show the plots for 40 ps and 50 ps which show similar trend as seen in the above case of a 35 ps PMD impairment. The deterministic curve shifts away from receiver baseline performance curve as the deterministic PMD increases from 20 ps to 50 ps. The results from 35 ps, 40 ps, 50 ps show that the deterministic plots tend to follow the better performance points of the unstable distributed effect plots whereas the plots obtained from the random seed variations and polynomial fitting tend to follow the worse case points.

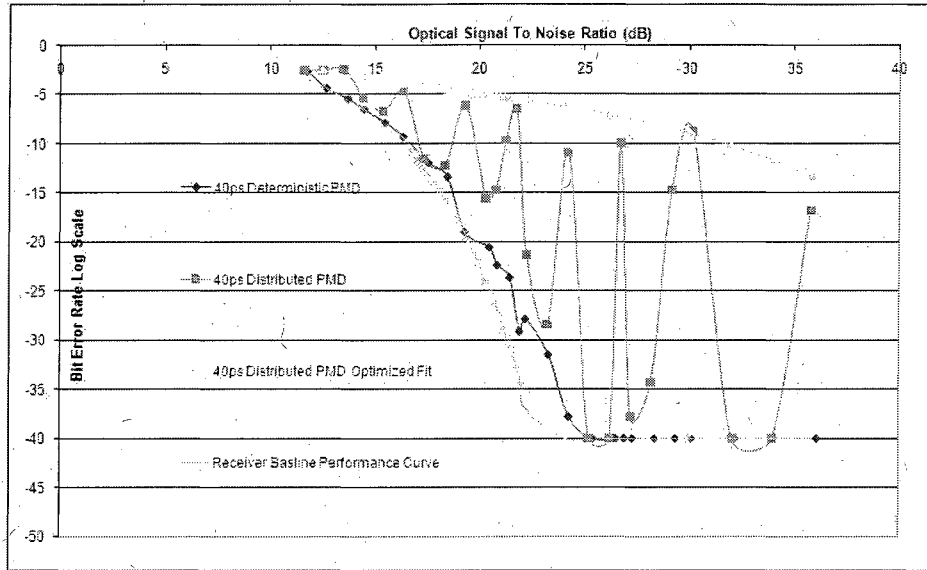


Figure 5- 18 Deterministic Versus Distributed Effect 40 ps

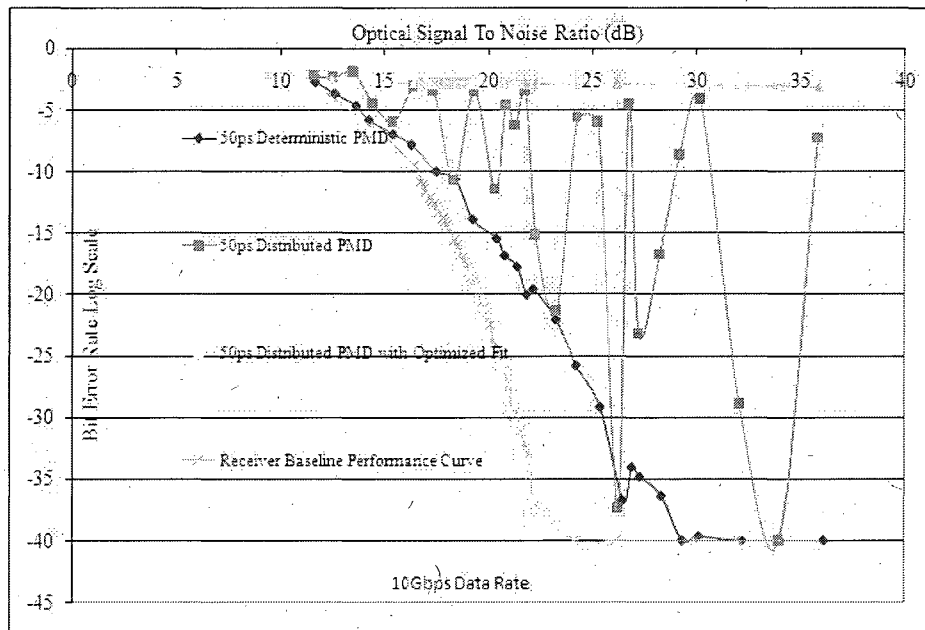


Figure 5- 19 Deterministic Versus Distributed Effect 50 ps

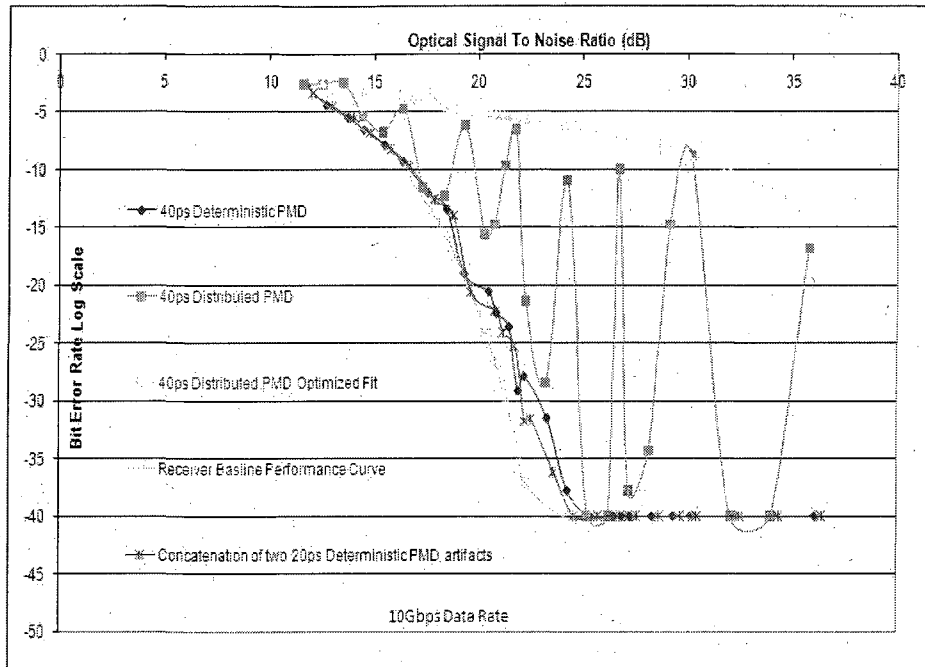


Figure 5- 21 Concatenation of 20 ps & 20 ps Deterministic Artifacts

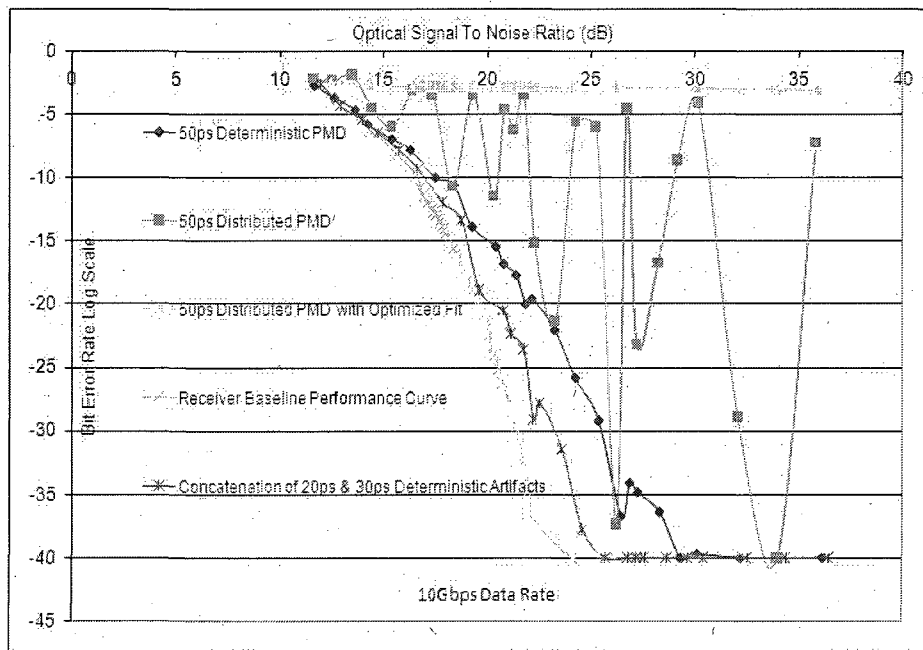


Figure 5- 22 Concatenation Of 20 ps & 30 ps Deterministic Artifacts

The intent of this section was to highlight the impact of PMD on optical networks. Our first set of simulation results showed that networks carrying higher data rate are more susceptible to the PMD impairment. Therefore, the presence of PMD in any optical network tends to limit its ability for faster rates of transmission. The simulation results also highlighted the temporal nature of PMD and required polynomial fit optimization to generate stable penalty plots. The simulation results showed the impact of PMD on the eye closure at different data rates, and it was observed that the degradation of the eye pattern became worse for higher values of the PMD impairment. The methodology to map the baseline performance of the receiver and to generate optical signal to noise ratio penalty curves was discussed. At the 10 Gbps data rate, optical signal to noise ratio penalty curves for distributed effect of PMD were generated for various values of mean PMD (20, 30, 35, 40 and 50ps). It was observed that the curves obtained for mean PMD's greater than 30 ps were varying due to the statistical nature of the PMD impairment. A seed variation and polynomial fit method was employed to generate stable curves from which OSNR penalties could be determined for a desired value of bit error rate. Comparison of the deterministic and distributed effects showed that the performance degradation (and thus the penalties) due to a deterministic effect is significantly lower than that due to an equivalent value of distributed effect. In the next section the existing statistical model of PMD is analyzed and its features and its limitations are discussed.

5.2 The New Statistical Model for PMD

Random statistical behavior of polarization in a long non-homogenous fiber may be examined in terms of the concatenation of small homogenous sections over which the input and output states of polarization are preserved. These incremental lengths are characterized by a beat length, which is the length over which the birefringence remains fixed. This is the distance over which relevant waveguide characteristics such as, waveguide propagation geometry, shape of the core, and external pressure, stress, and strain are constant. The polarization states at the input and output of the beat length remain the same. Since the birefringence over this distance is constant, there is no energy transfer between the two orthogonal modes and the separation $\Delta\tau$ between them is solely a function of the fixed group velocities between the Slow and the Fast axes and the length of propagation ' L_b '. Therefore $\Delta\tau$ increases linearly with distance [Figure 5-23]. Long beat length fibers can be obtained by a uniform drawing of the core and cladding during the manufacturing process. Intrinsic birefringence would be constant over the length of the draw and the polarization axes at the input and the output of such fibers would be maintained. The coefficient of polarization mode dispersion would be linearly proportional to the distance of propagation, and thus, large values of PMD could be obtained. In order to avoid this linear build-up of the group delay, present day fiber manufacturing processes incorporate various techniques to reduce the beat length to very small values, by spinning and turning the spool of fiber as it is drawn from the pre-form [26].

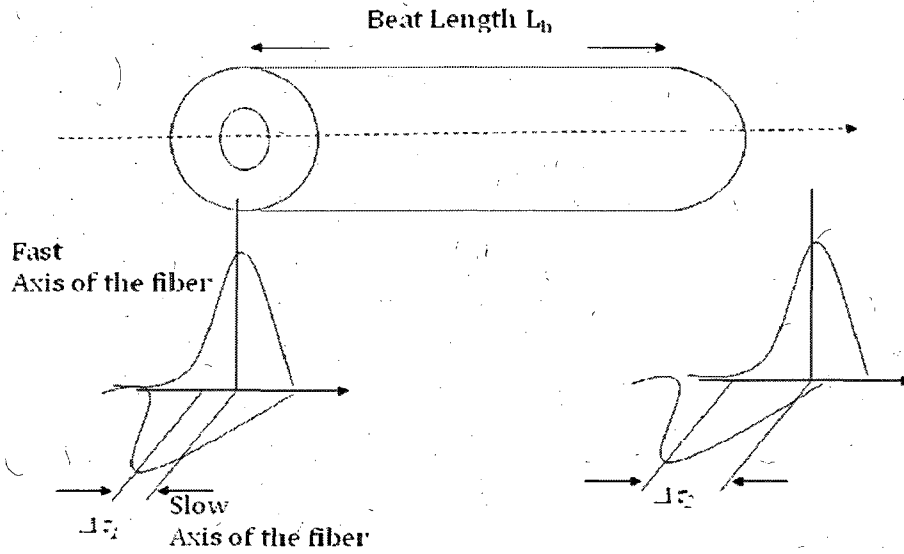


Figure 5- 23 Fixed Birefringence of Beat length Segment

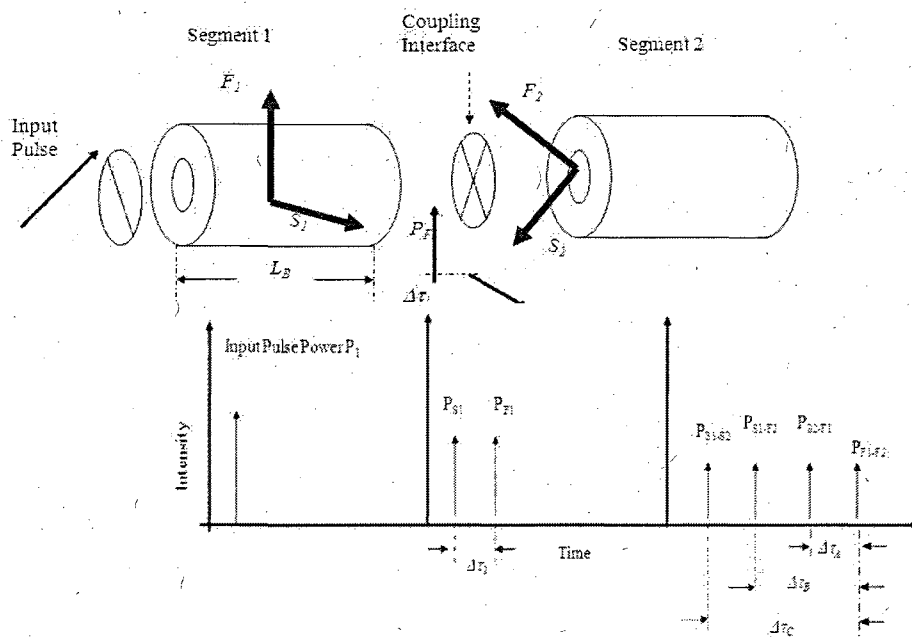


Figure 5-24 Concatenation of Two Beat Length Segments

Fibers thus obtained could be viewed as fused segments of small beat length sections of fibers, each having randomly oriented polarization axes and characteristic/distinct birefringence due to variations in fiber drawing and spinning processes and localized stress during spooling and cabling. This results in significant reduction in the accumulation of the group delay due to the non-linear interaction of spatial modes at each interface of the beat length sections. Thus, at the concatenation interface of the two beat segments, Fast and Slow modes from one beat length segment would 'couple' into the fast and slow modes of the next section. Figure 5-24 describes this process in detail. F_1 and S_1 denote the fast and slow axes of polarization of beat length segment 1. This homogenous section of fiber is characterized by its distinct birefringence, which defines the group velocities in the fast and slow axes respectively. A randomly polarized signal applied to the input of this section may transmit energy into both spatial polarization modes defined by the fast and the slow axes of the section (F_1 and S_1). The output of this same section is comprised of two separate signals (P_{F1} and P_{S1}) aligned with F_1 and S_1 , with differential group delay $\Delta\tau_1$. These two separate signals are coupled into Segment 2, with its own distinct birefringence and orientation of axes of polarization (F_2 and S_2) at the interface of the two segments. Power from the first signal P_{F1} couples into the fast and slow axes F_2 and S_2 to generate two more signals denoted by P_{F1-F2} and P_{F1-S2} . Power from the second S_1 couples into the fast and slow axes F_2 and S_2 of Segment 2 to form two more components denoted by P_{S1-F2} and P_{S1-S2} . The intensities of these newly formed signals depend on the interaction between the input modes P_{F1} and P_{S1} and the polarization modes F_2 and S_2 of beat segment 2. The group delays ($\Delta\tau_A$, $\Delta\tau_B$, $\Delta\tau_C$) depend upon the group velocities of the corresponding fast and slow axes of segment 2. Thus the

number of differentially delayed signals at the output of segment 2 grew to four from two at the output of segment 1. The concatenation of a large number of these beat segments, each with a random orientation of its polarization axes and distinct internal birefringence, results in the doubling of the number of differentially delayed signals at the output of each sequential beat segment as shown in Figure 5-25. The output at the end of the fiber would be an accumulation of differentially delayed signals with random power intensities. Variant external factors, such as, temperature, pressure, stress/strain, cabling, introduce random variations in the birefringence and this results in further randomization of the output distribution.

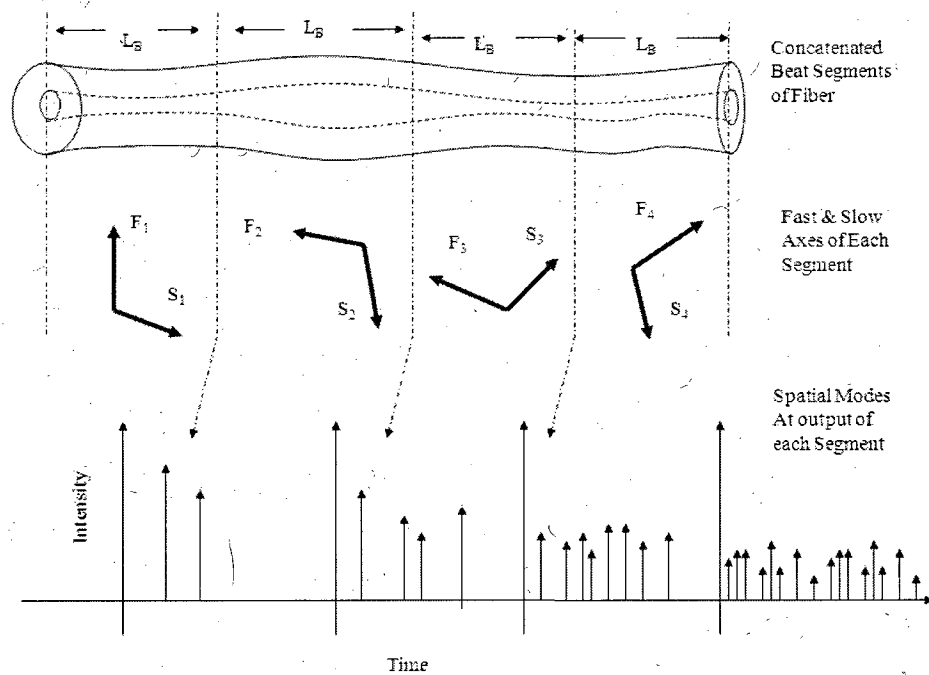


Figure 5-25 Concatenation of Multiple Beat Length Segments

A mathematical approach expressing the growth of number of discrete polarization modes and the associated delays for each mode at the end of concatenation of finite segments is discussed below. The input signal to segment-1 [Figure 5-24] could be expressed in terms of a carrier wave whose amplitude is varied about a mean value, linearly with the baseband modulation signal $m(t)$ [38]:

$$s(t) = A(t)e^{j2\pi f_c t} \quad \dots\dots[5.2]$$

$$A(t) = A_c(1 + k_a m(t))$$

where,

A_c is the amplitude of the carrier wave.

$m(t)$ is the NRZ encoded On Off Keyed modulating baseband signal.

k_a is the amplitude sensitivity of the modulator.

In the absence of any mode distortions across the length of a fiber section, the transmitted signal would be attenuated and would be delayed by the path length. The baseband signal $r(t)$ at the receiver can be expressed as:

$$r(t) = Loss_{path} \cdot A(t - t_{path}) \cdot e^{-j2\pi f_c (t - t_{path})} \quad \dots\dots[5.3]$$

If the input signal $s(t)$ is incident on a birefringent section of fiber (segment-1), it will get coupled with the fast and the slow modes of segment one. The output at the end of segment-1 would be composed of two components whose amplitude would be a function of the coupling coefficient between the input signal and each of the two

polarization axis and its phase would be a function of the individual delays across the fast and the slow axes of propagation. The received baseband signal $r(\text{segment1})$ can then be expressed as:

$$\begin{aligned} r(\text{segment1}) = & Loss_{1fast} \cdot A(t - t_{1fast}) \cdot e^{-j2\pi f_c t_{1fast}} \\ & + Loss_{1slow} \cdot A(t - t_{1slow}) \cdot e^{-j2\pi f_c t_{1slow}} \end{aligned} \quad \dots\dots[5.4]$$

where,

$Loss_{1fast}$ and $Loss_{1slow}$ are the loss functions associated with the fast and the slow axes of segment-1.

t_{1fast} and t_{1slow} are the propagation times across the fast and slow axes of segment-1.

The output components from segment-1 will act as the input signal to segment-2 which has its own random orientation of the polarization axis and its unique delay of propagation. The received baseband signal $r(\text{segment2})$ at the end of segment-2 could be expressed as:

$$\begin{aligned} r(\text{segment2}) = & Loss_{1fast} \cdot Loss_{2fast} \cdot A(t - (t_{1fast} + t_{2fast})) \cdot e^{-j2\pi f_c (t_{1fast} + t_{2fast})} \\ & + Loss_{2fast} \cdot Loss_{1slow} \cdot A(t - (t_{1slow} + t_{2fast})) \cdot e^{-j2\pi f_c (t_{1slow} + t_{2fast})} \\ & + Loss_{2slow} \cdot Loss_{1fast} \cdot A(t - (t_{1fast} + t_{2slow})) \cdot e^{-j2\pi f_c (t_{1fast} + t_{2slow})} \\ & + Loss_{1slow} \cdot Loss_{2slow} \cdot A(t - (t_{1slow} + t_{2slow})) \cdot e^{-j2\pi f_c (t_{1slow} + t_{2slow})} \end{aligned} \quad \dots\dots[5.5]$$

where,

$Loss_{2fast}$ and $Loss_{2slow}$ are the loss functions associated with the fast and the slow axes of segment-2.

t_{2fast} and t_{2slow} are the propagation times across the fast and slow axes of segment-2.

It can be observed from the above expression that the output at the end of segment-2 contains twice the number of components from the previous segment. The amplitude of each component is a function of the coupling between the input signal and the polarization axis of the next segment which the signal couples into. The increasing phase shift in each output component is a function of the propagation time through the current birefringent segment and the preceding segments. When these components propagate through a large number of concatenated beat length segments, each with its unique propagation delay and random orientation of polarization axes, the output at the end of such a fiber section will contain a large number of components whose amplitude is a function of the coupling coefficient across each beat length segment. The phase shift will grow with each concatenation and will be a function of the unique propagation delays of all the beat length segments that the signal has traversed.

Our new approach has distinct advantages over the existing statistical models. Firstly, it allows for controlled incremental growth of the output delay distribution. The model has the capability to change individual delays of beat length segments and captures their impact on the overall output distribution. Therefore, it allows for characterizing both the incremental and the cumulative nature of the resultant distribution more effectively. Our new model is able to express the true discrete nature of the differential group delay distribution which helps in accurate characterization of outlying behaviors which are responsible for the worst case degradation of the network performance. Integration of such a PMD model in an optical communication system model with reasonable

performance requirements and relevant transmission parameters allows for proper evaluation of the impact of PMD on various transmission schemes.

5.3 Numerical Implementation Of The New Model

In this section, the numerical implementation of our new model for generating the differential group delay distribution that results from concatenation of incremental sections of single mode fiber is described. The numerical implementation has been programmed using MATLAB and C++ and the original code has been provided in the Appendix. There are three stages in this implementation. The first stage involves the generation of beat length segments with individual delays. The second stage sequentially concatenates these delays of the individual beat length segments and generates the output DGD distribution. The third stage of the numerical implementation uses this output delay distribution from the second stage in an optical systems model to calculate performance penalties associated with the introduction of PMD impairment.

5.3.1 Implementation of the Delay Distribution

The physical fiber parameter that has the most significant impact on differential group delay is the beat length of the fiber ' L_b '. As described in the earlier section, beat length is the smallest increment of the fiber over which all physical conditions are constant and therefore the states of polarization are maintained. The first step in our algorithm is to generate unique differential group delays for ' n ' number of beat length segments. This is done using a Gaussian function with zero mean and very small variance. The resultant of this step is that ' n ' beat length delays for each of the beat length segments are generated. The zero mean ensures that these individual delays are

very small and the randomization of the variance (within fixed small bounds) ensures that each delay of each beat segment is randomly unique. The maximum value for the number of segments is 1024. This is because both the MATLAB and C++ compilers used have a limitation of 2^{1024} on the maximum value of the number of delay components. The sum of these 'n' individual delays defines the maximum worse case value of the delay component which will be a part of the output distribution. The next critical parameter for appropriately capturing the distribution is the bucket or the bin size of the simulation. The size of the bucket or bin used to capture the output distribution components is analogous to the measurement resolution or the size of the filter which is used in the physical setup in capturing and interpolating the output delay distribution components. If the bin size is too large, the delay distribution will be compressed and close to the origin. The total numbers of buckets or bins which are used to capture the distribution depend on the sum of the delays and the bin size as shown below:

$$\text{Number of Bins} = \text{Sum of 'n' delays} / \text{bin size} \quad \dots\dots[5.6]$$

Thus, the three critical setup parameters of our simulation are the mean of the Gaussian distribution, the variance of the Gaussian distribution and the bin size of the simulation. The mean and the variance of the Gaussian distribution are responsible for the magnitude of the individual beat length delays and the bin size determines the capture resolution of the distribution. The following example helps us walk through the steps of the code to generate delay distribution.

Consider 3 concatenated beat length segments (Segment-1,2,3) each with unique differential delay ($d_1=5$ ps, $d_2=9$ ps, $d_3=6$ ps). The bin size is assumed to be 2 ps. Therefore,

$$\text{Sum of delays} = 20 \text{ ps}$$

Total number of bins = sum of delays/bin size = $19/2 = 10$ (considering the ceiling of this computation). Thus the output distribution will have 10 buckets each separated by 2ps.

Let us assume the output matrix is given by:

$$\text{Output} = \{1,0,0,0,0,0,0,0,0,0\} \dots\dots[5.7]$$

The input to segment one is a randomly oriented linearly polarized pulse of light. This illuminates the fast and the slow axes of the Segment-1. The output of the fast axes at the end of segment1 represents the fastest element of the output distribution array. The initial distribution will have this element populating the first bin. The output at the slow axis at the end of Segment-1 is delayed with respect to the fast axis output by delay value $d_1=5$ ps. The output distribution at the end of each segment is dependent on the number of steps by which the output distribution of the previous stage is to be shifted. The number of steps is decided by dividing the delay of the individual segment by the bin size.

$$\text{Number of Steps} = \text{delay of Segment-1 } d_1 / \text{bin size} \dots\dots[5.8]$$

$$\text{Number of Steps} = 5/2 = 2 \text{ (considering the floor of this computation).}$$

The existing output distribution is to be shifted by 2 buckets to generate the new output distribution. Therefore, the output distribution at the end of the first beat length segment will be:

$$\text{Output at end of Segment-1} = \{1,0,1,0,0,0,0,0\}$$

The output from Segment-1 will be the input for Segment-2 with delay $d_2=9$ ps. The shifting of its input to generate the output at the end of Segment-2 is decided by;

$$\text{Number of steps} = \text{delay of Segment-2 } d_2 / \text{bin size} \quad \dots\dots[5.9]$$

$$\text{Number of steps} = 9/2 = 4 \text{ (Considering the floor of the computation)}$$

Therefore, the input to Segment-2 will be shifted by 4 buckets to get the output at the end of Segment-2;

$$\text{Output from Segment-2} = \{1,0,1,0,1,0,1,0,0,0\}$$

This would act as input to Segment-3 with delay $d_3 = 6$ ps.

$$\text{Number of Steps} = \text{delay of Segment-3 } d_3 / \text{bin size} \quad \dots\dots[5.10]$$

$$\text{Number of Steps} = 6/2 = 3 \text{ (Considering the floor of the computation)}$$

Therefore, the input to Segment-3 will be shifted by 3 buckets to get the output at the end of Segment-3.

$$\text{Output from Segment-3} = \{1,0,1,1,1,1,1,0,1\} \quad \dots\dots[5.11]$$

Therefore, at the end of the three segments the delay distribution can be explained as follows: there is one delay component in the 0-2 ps bin, there are no delay components in

the 2-4 ps bin, there is one delay component each in the 4-6 ps, 6-8 ps, 8-10 ps, 10-12 ps, 12-14 ps, 14-16 ps bin, there are no delay components in the 16-18 ps bin and there is one delay component in the 18-20 ps bin. it should be observed that number of output delay components at the end of each segment is binary (2^n). Therefore, at the end of the third segment the output has 8 delay components. The above process is the way in which the output delay distribution is sequentially grown for each concatenated segment where the output distribution of the $n-1^{th}$ segment acts as the input to the n^{th} segment. The output delay distribution at the end of n^{th} segment will have 2^n components and will depend upon the input distribution and the individual delay of that particular n^{th} segment. Generalizing this for a large number of segments;

$O_j = j^{th}$ delay component of the output distribution after 'i' stages

$S_k =$ Output distribution matrix after 'i-1' segments

Where,

'i' is such that $1 \leq i \leq$ number of delays

'j' is such that $1 \leq j \leq 2^{\text{number of delays}}$

Then,

$$O_j = S_k \otimes h_k \quad \text{.....[5.12]}$$

Where,

$h_k = \{1,0,\dots,0,1\}$ where the number of zeroes is determined by 'num_steps(i)'

$$num_steps(i) = delay(i) / bin\ size \quad \dots\dots[5.13]$$

$$O = \{o_1, o_2, \dots, o_{num_delays}\} \quad \dots\dots[5.14]$$

The final output delay distribution ‘O’ [Equation 5.14] at the end of n^{th} segment will be a matrix comprising of 2^n elements of distribution components whose magnitude is a resultant of the interaction of delay components of all beat length segments comprising the fiber span.

Matlab code has been used to generate the unique individual delays of the ‘n’ beat length segments. The output of this code is a comma separated file which holds the delay values of the ‘n’ beat length segments. This file which holds the individual delays of the ‘n’ beat length segments is used as input to the C++ code which implements the delay distribution model. The delay distribution is captured in an output matrix which contains the number of delay components occurring in each bin. It is assumed that the amplitude of each of these delay components at the output is equal i.e., the optical power is equally split among all the new modes that get excited at the interface between two adjacent beat length segments. There is no interaction between these modes as they propagate within each beat length segment. This output DGD distribution matrix is used as the input to the second stage of the C++ code where the penalties and statistics associated with the PMD impairment on optical networks are derived.

5.3.2 Implementation of the DGD Model in an Optical System

In this section the output DGD distribution generated in the previous stage is used to evaluate the impact of PMD impairment on optical network performance in terms of Q

penalty. In an optical network transport system, a randomly polarized pulse of light from the transmitter section is incident on the input interface of the single mode optical fiber. This excites two orthogonally polarized modes and light travels across the beat length segment along the two polarized modes. At the coupling interface of each adjacent beat length, these modes are coupled into the subsequent beat length segment and subjected to a binary growth in the number of components across the propagation along the beat lengths. At the end of the fiber, the output DGD distribution incident on the receiver contains a large number of replicas of the original pulse each slightly shifted or delayed from the original pulse. The impact of such a delay distribution incident on the receiver can best be visualized with the help of a Sinc response of these delay pulses in the time domain. The Sinc response of an original pulse without any delay having a certain fixed amplitude at $t=0$ and having zero crossings at time period T is shown in Figure 5-26. Sinc plots of each subsequent delay component can then be visualized as slightly shifted from the original. This Sinc plot may have its peak amplitude slightly shifted from $t=0$ and therefore its value at each sampling time period T of the original pulse will be a non-zero value. Figure 5-27 shows a sample chart showing Sinc plots of all delayed replicas of the original signal. The larger the delay spread across the DGD distribution, the wider is the spread of the Sinc plots and the higher is the amplitude content at samples of time period T .

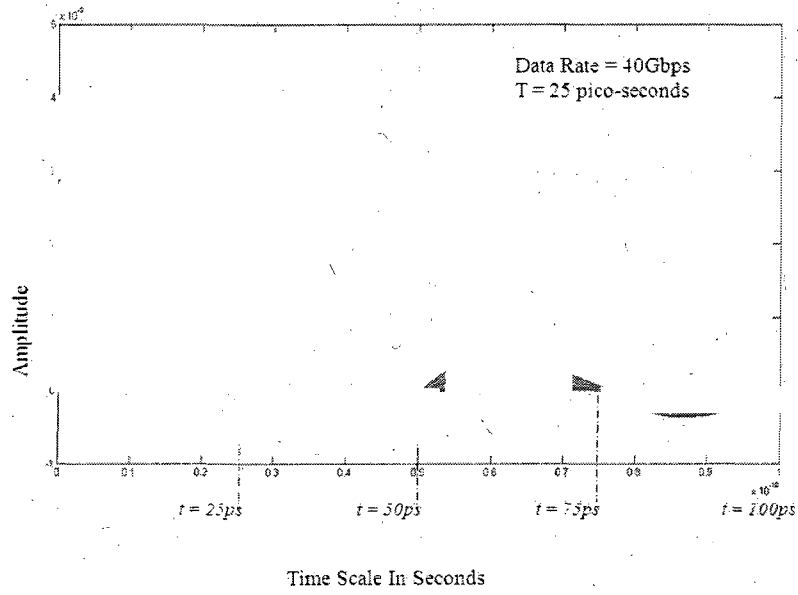


Figure 5-26 Sample Sinc Response Showing the Effect of Delays

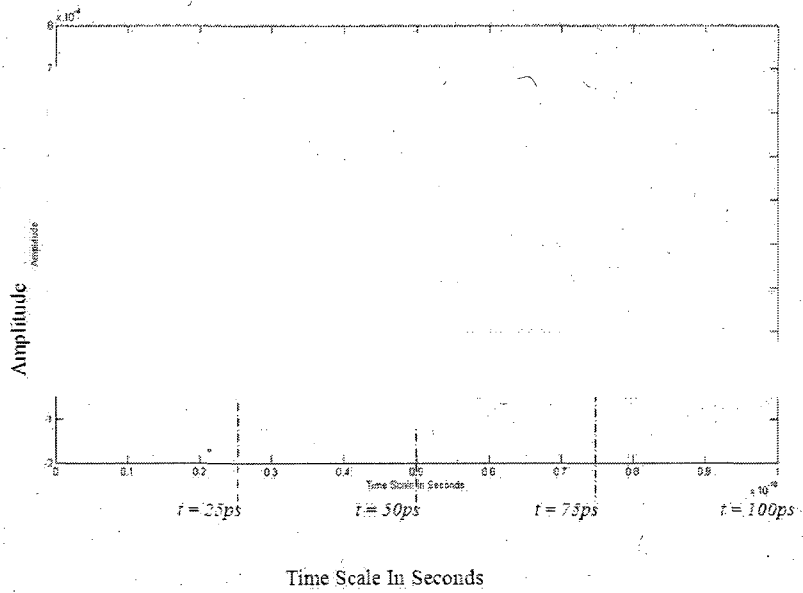


Figure 5-27 Effect of DGD on the Zero Crossing Points

The output DGD distribution matrix consists of elements which indicate the frequency or the number of signal replicas occurring in each sequential delay bucket. The summation of all components in the output DGD matrix gives the total number of signal replicas being received at the receiver. All the delay components being received at the receiver are assumed to have equal amplitude. Identifying the delay bucket gives us the associated delay of the signal replicas under consideration. The ratio of the number of signal replicas in that bucket to the total number of signal replicas across all buckets gives the normalized amplitude for that particular delay. For a specific data rate of transmission (10 Gbps $T = 100$ ps, 40 Gbps $T = 25$ ps, 100 Gbps $T = 10$ ps) the Sinc plot for each delay value is generated. For the purpose of estimating Q penalty, the amplitude content of the Sinc plot at $t = 0, t = T, t = 2T, t = 3T, t = 4T$ is collected. Therefore, at a 40 Gbps rate of data transmission, the amplitude content from the Sinc plot is collected at $t = 0, t = 25ps, t = 50ps, t = 75ps, t = 100ps$. From this data statistics like maximum amplitude, average amplitude, minimum amplitude, median and standard deviation at all five sampling instances ($t = 0, t = 25ps, t = 50ps, t = 75ps, t = 100ps$) are collected. Table 5-4 on the following pages gives an example of the statistics that are captured from our simulation results. In this case, the data rate is 40Gbps (Time period $T = 25ps$), the simulation bin size is 0.0025ps and the number of beat segments is 1000. The table shows the simulation results captured at four different simulation variances (0.001ps, 0.01ps, 0.05ps and 0.1ps). The root mean square value of the output DGD distribution is calculated and recorded for each simulation run. The normalized RMS DGD is shown as a fraction of the pulse time period. The first part of Table 5.4 indicates the maximum or

the largest amplitude component at sample time ' t ' =0, 25ps, 50ps, 75ps and 100ps. For each simulation run, Peak or maximum conventional ISI is calculated as:

$$\text{Max conventional ISI} = \frac{\sum \text{Max components at } t=25,50,75,100\text{ps}}{\text{Max component at } t=0} \dots\dots[5.15]$$

where, ISI is defined as the ratio of sum of the signal fractions found at successive time periods ($T=25\text{ps}$, $2T=50\text{ps}$, $3T=75\text{ps}$, $4T=100\text{ps}$) to the value of signal level at the expected time $t = 0$.

Simulation Variance	1e-3ps	1e-2ps	5e-2ps	1e-1ps
RMS (DGD) ps	0.9175	2.8625	6.535	9.22
NORM RMS DGD	0.0367	0.1145	0.2614	0.3688
MAX (largest amplitude component at t=0ps)	0.004019854	0.001284354	0.00055886	0.000395502
MAX (largest amplitude component at t=25ps)	4.85123E-05	5.10648E-05	5.4623E-05	5.67799E-05
MAX (largest amplitude component at t=50ps)	1.41623E-06	4.5249E-07	1.96892E-07	1.39339E-07
MAX (largest amplitude component at t=75ps)	1.53085E-05	1.60804E-05	1.62596E-05	1.60995E-05
MAX (largest amplitude component at t=25ps)	1.51669E-06	4.84587E-07	2.10858E-07	1.49223E-07
Sum of max at t=25,50,75,100ps	6.67537E-05	6.80823E-05	7.12904E-05	7.3168E-05
Max Conventional ISI	0.016606004	0.053008958	0.127563883	0.185000093
MEAN (average value of all components at t=0ps)	0.000184757	6.01033E-05	2.66738E-05	1.84591E-05
MEAN (average value of all components at t=25ps)	2.9316E-06	3.19042E-06	3.58835E-06	3.74475E-06
MEAN (average value of all components at t=50ps)	-1.40957E-06	-1.51631E-06	-1.60168E-06	-1.5764E-06
MEAN (average value of all components at t=75ps)	9.10809E-07	9.89077E-07	1.03005E-06	1.00063E-06
MEAN (average value of all components at t=25ps)	-6.62999E-07	-7.30781E-07	-7.57913E-07	-7.3237E-07
Sum of Mean at t=25,50,75,100ps	1.76984E-06	1.93241E-06	2.25881E-06	2.43661E-06
Mean Conventional ISI	0.009579299	0.032151497	0.084682543	0.132001001
Mean Pulse Spreading Loss		9.754051313	16.8103025	20.0078217
MEDIAN (midpoint value of all components at t=0ps)	4.83296E-48	2.38381E-46	4.2806E-113	2.8476E-165
MEDIAN (midpoint value of all components at t=25ps)	1.27211E-48	1.02838E-45	8.20965E-43	6.63961E-85
MEDIAN (midpoint value of all components at t=50ps)	-3.80357E-49	-1.36815E-46	1.4508E-112	4.9531E-165
MEDIAN (midpoint value of all components at t=75ps)	1.70718E-49	6.66246E-47	4.8729E-112	2.82409E-84
MEDIAN (midpoint value of all components at t=25ps)	-8.84365E-50	-4.11585E-47	-6.7741E-113	2.3404E-164
Sum of Median at t=25,50,75,100ps	9.74039E-49	9.17029E-46	8.20965E-43	3.48805E-84
Median Conventional ISI	0.201541107	3.846913527	1.91785E+70	1.22492E+81
STDEV (Statistical Spread of all components at t=0ps)	0.000700884	0.000225844	9.91769E-05	6.94937E-05
STDEV (Statistical Spread of all components at t=25ps)	9.76553E-06	1.04358E-05	1.14191E-05	1.18904E-05
STDEV (Statistical Spread of all components at t=50ps)	4.71838E-06	4.98975E-06	5.17773E-06	5.14352E-06
STDEV (Statistical Spread of all components at t=75ps)	3.06254E-06	3.26306E-06	3.34438E-06	3.28503E-06
STDEV (Statistical Spread of all components at t=25ps)	2.24023E-06	2.41526E-06	2.46633E-06	2.41129E-06
MIN (Smallest amplitude components at t=0ps)	0	-4.76449E-71	-4.9547E-17	-2.23933E-11
MIN (Smallest amplitude components at t=25ps)	-1.21529E-06	-3.88289E-07	-1.68956E-07	-1.19569E-07
MIN (Smallest amplitude components at t=50ps)	-2.35229E-05	-2.45389E-05	-2.50818E-05	-2.50786E-05
MIN (Smallest amplitude components at t=75ps)	-1.48321E-06	-4.73889E-07	-2.06203E-07	-1.45929E-07
MIN (Smallest amplitude components at t=25ps)	-1.12246E-05	-1.19188E-05	-1.2013E-05	-1.18462E-05

Table 5-4 Statistical Data from Output Simulation Results

The next part of the table records the mean or the average value of the amplitude components at sample time 't' =0, 25ps, 50ps, 75ps and 100ps. For each simulation run mean conventional ISI is calculated as;

$$\text{Mean conventional ISI} = \frac{\sum \text{Mean components at } t=25,50,75,100\text{ps}}{\text{Mean component at } t=0} \dots\dots[5.16]$$

For the mean pulse spreading loss the mean value of amplitude components at $t=0$ for the simulation run at 0.001ps is treated as the base line value. The mean pulse spreading loss in dB is then calculated:

$$\begin{aligned} \text{Mean pulse spreading loss (0.01ps variance)} = \\ 20*\text{Log} \left[\frac{\text{Mean value } t=0 \text{ (0.001ps variance)}}{\text{Mean value } t=0 \text{ (0.01ps variance)}} \right] \dots\dots[5.17] \end{aligned}$$

$$\begin{aligned} \text{Mean pulse spreading loss (0.05ps variance)} = \\ 20*\text{Log} \left[\frac{\text{Mean value } t=0 \text{ (0.001ps variance)}}{\text{Mean value } t=0 \text{ (0.05ps variance)}} \right] \dots\dots[5.18] \end{aligned}$$

Where the pulse spreading in dB is defined the ratio of the value of reference measurement signal at $t = 0$ to the value of the signal at $t = 0$ after the PMD impairment has been introduced.

The median of the amplitude components at sample time 't' =0, 25ps, 50ps, 75ps and 100ps is recorded for each simulation run and the median conventional ISI is calculated for each simulation run as:

$$\text{Median conventional ISI} = \frac{\sum \text{Median components at } t=25,50,75,100\text{ps}}{\text{Median component at } t=0} \dots\dots[5.19]$$

Minimum amplitude components and the Standard deviation is also recorded at sample time 't' =0, 25ps, 50ps, 75ps and 100ps for each simulation run.

For each simulation run, the maximum composite signal value is evaluated in terms of peak and root mean square (RMS) closure as:

$$\text{Peak Closure} = \left[\frac{\text{Maximum Value at } t=0}{\sum \text{Maximum Values at } t=25,50,75,100\text{ps}} \right] \dots\dots[5.20]$$

$$\text{RMS Closure} = \left[\frac{\text{Maximum Value at } t=0}{\sqrt{\sum (\text{Maximum Values at } t=25,50,75,100\text{ps})^2}} \right]$$

Here, the eye closure is defined as the ratio of the value of signal level at the expected time $t = 0$ to the sum of signal fractions found at successive time periods ($T=25\text{ps}$, $2T=50\text{ps}$, $3T=75\text{ps}$, $4T=100\text{ps}$).

The mean composite signal value for each simulation run is evaluated in terms of peak and RMS closure as:

$$\text{Peak Closure} = \left[\frac{\text{Mean Value at } t=0}{\sum \text{Mean Values at } t=25,50,75,100\text{ps}} \right] \dots\dots[5.21]$$

$$\text{RMS Closure} = \left[\frac{\text{Mean Value at } t=0}{\sqrt{\sum (\text{Mean Values at } t=25,50,75,100\text{ps})^2}} \right]$$

The median composite signal value for each simulation run is evaluated in terms of peak and RMS closure as:

$$\text{Peak Closure} = \left[\frac{\text{Median Value at } t=0}{\sum \text{Median Values at } t=25,50,75,100\text{ps}} \right] \dots\dots[5.22]$$

$$\text{RMS Closure} = \left[\frac{\text{Median Value at } t=0}{\sqrt{\sum (\text{Median Values at } t=25,50,75,100\text{ps})^2}} \right]$$

Mean composite signal value with standard deviation (σ) is evaluated in terms of peak and RMS closure as:

$$\text{Peak Closure} = \left[\frac{(\text{Mean} + \text{Stdev Value at } t=0)}{\sum (\text{Median} + \text{Stdev}) \text{ Values at } t=25,50,75,100\text{ps}} \right] \dots\dots[5.23]$$

$$\text{RMS Closure} = \left[\frac{(\text{Mean} + \text{Stdev Value at } t=0)}{\sqrt{\sum (\text{Mean} + \text{Stdev})^2 \text{ at } t=25,50,75,100\text{ps}}} \right]$$

Mean composite signal value with 3σ is evaluated in terms of peak and RMS closure as:

$$\text{Peak Closure} = \left[\frac{(\text{Mean} + 3 * \text{Stdev Value at } t=0)}{\sum (\text{Median} + 3 * \text{Stdev}) \text{ Values at } t=25,50,75,100\text{ps}} \right] \dots\dots[5.24]$$

$$\text{RMS Closure} = \left[\frac{(\text{Mean} + 3 * \text{Stdev Value at } t=0)}{\sqrt{\sum (\text{Mean} + 3 * \text{Stdev})^2 \text{ at } t=25,50,75,100\text{ps}}} \right]$$

Mean composite signal value with 5σ is evaluated in terms of peak and RMS closure as:

$$\text{Peak Closure} = \left[\frac{(\text{Mean} + 5 * \text{Stdev Value at } t=0)}{\sum (\text{Median} + 5 * \text{Stdev}) \text{ Values at } t=25,50,75,100\text{ps}} \right] \dots\dots[5.25]$$

$$\text{RMS Closure} = \left[\frac{(\text{Mean} + 5 * \text{Stdev Value at } t=0)}{\sqrt{\sum (\text{Mean} + 5 * \text{Stdev})^2 \text{ at } t=25,50,75,100\text{ps}}} \right]$$

Q penalty is calculated in two steps. In the first step the statistical degradation of the signal in dB is calculated for each simulation run:

$$\text{Signal Degradation (dB)} = 20 * \text{Log} \left\{ \frac{[\text{Mean at } t=0 - \sum \text{Mean at } t=25,50,75,100\text{ps}]}{[(\text{Stdev at } t=0)^2 - \sum (\text{Stdev at } t=25,50,75,100\text{ps})^2]} \right\} \dots\dots[5.26]$$

where, the degradation of the signal due to the PMD impairment is defined as the ratio of difference between the mean value of the signal at $t = 0$ and the sum of mean values of the signal at other time intervals ($T=25\text{ps}$, $2T=50\text{ps}$, $3T=75\text{ps}$, $4T=100\text{ps}$) to the difference between the square of standard deviations at $t = 0$ and sum of squares of standard deviation at other time intervals ($T=25\text{ps}$, $2T=50\text{ps}$, $3T=75\text{ps}$, $4T=100\text{ps}$).

In Table 5-1 the signal degradation calculated at simulation variance of 0.001ps is considered as the reference measurement and the Q penalty for each of the subsequent simulations runs is calculated as:

$$\begin{aligned} \text{Qpenalty}_{\text{at } 0.01\text{ps variance}} \text{ (dB)} = & (\text{Signal degradation})_{\text{at } 0.001\text{ps variance}} - (\text{Signal degradation})_{\text{at } 0.001\text{ps variance}} \dots\dots[5.27] \\ & + (\text{Mean Pulse Spread Loss})_{\text{at } 0.01\text{ps variance}} \end{aligned}$$

Summary

The impact of PMD impairment on the network performance was analyzed using the Optsim software simulation test bed. It was observed that networks carrying data at higher rates of transmission are more susceptible to the PMD impairment. The effect of PMD on eye closure at different data rates was captured along with performance penalties for distributed and deterministic effects of the PMD impairment. A new model to characterize the DGD distribution of the PMD impairment is defined. The ability of this model to overcome the limitations of the existing statistical models by its ability to grow the DGD distribution in discrete steps and to capture the complete ensemble of discrete components of the output differential group delay distribution is demonstrated. The new model has the ability to change the delays associated with individual beat length segments and evaluate their impact on the output DGD distribution. The mathematical implementation of this model using MATLAB and C++ is discussed. In the first stage of implementation, delays for individual beat length segments are generated. In the following stage, the individual delays of the beat length segments are used to sequentially grow the output delay distribution. In the final stage, the output DGD distribution is used to generate performance penalties that quantify the impact of the PMD impairment on the performance of optical communication systems. In the following chapter, the test cases and results from our simulations which aid in characterizing this channel impairment are discussed.

CHAPTER – 6

SIMULATION RESULTS

Introduction

In the previous chapter, our approach to a new statistical PMD model and its advantages over existing statistical models were discussed. The mathematical implementation of such a model to generate the output DGD distribution and to measure the impact of the impairment on network performance in terms of Q penalty was illustrated. In this chapter results from our various simulations that characterize the PMD impairment are shown. The first stage illustrates the effect of change in bin size on our simulation results; the second stage of simulation shows the sequential growth of the DGD distribution. The third stage of simulation results shows the output DGD distribution for types of fibers with differing amounts of accumulated DGD and in the fourth stage the ability of our model to characterize fiber impairments in the form of mixed fiber sections and PMD artifacts is illustrated. The last stage evaluates the impact of the PMD impairment on optical networks in terms of Q penalty and our simulation results are compared against published results.

6.1 Configuration of Simulation Bin Size

The sampling bin size is a critical simulation parameter since an incorrect value will result in inadequate capture of the output DGD distribution. In this section the relationship between the simulations's sampling bin size and the output DGD distribution is illustrated. In these simulations the number of beat length segments is fixed at $n = 1000$ and the optical transmission data rate is 40Gbps. In the first set of simulations, the individual beat segment delays for the 1000 beat segments are generated using a truncated Gaussian distribution with a zero mean and variance of 0.01ps. Figure 6-1 compares the plots of output DGD distributions for different bin sizes (0.2ps, 0.1ps, 0.01ps, and 0.0025ps). All the four output DGD plots are normalized with respect to the maximum frequency component observed in each case respectively; hence all the plots originate on the Y-axis at the same value of 1. This is done to enable plotting the different curves within a single chart. It is observed that the output DGD distribution spreads or widens as the bin size is decreased from 0.2ps to 0.1ps to 0.001ps. This is because as the sampling width increases, the output delay components get grouped in larger coarse bins and this tends to compress the shape of the output plot. The net effect of having a very large sampling bin size is to reduce the capture resolution of the simulation. The output DGD distribution curves with bin size at 0.001ps and 0.0025ps are very close to each other and any further reduction of the bin size generates output DGD curves which overlap with the plot of 0.0025ps bin size. Any further sharpening of the capture resolution by reducing the bin size has minimal effect on the captured output DGD distribution. Figure 6-2 shows a plot of the performance penalty (data rate 40Gbps) at different bin sizes for different types of fibers. Results are tabulated in Table 6-1.

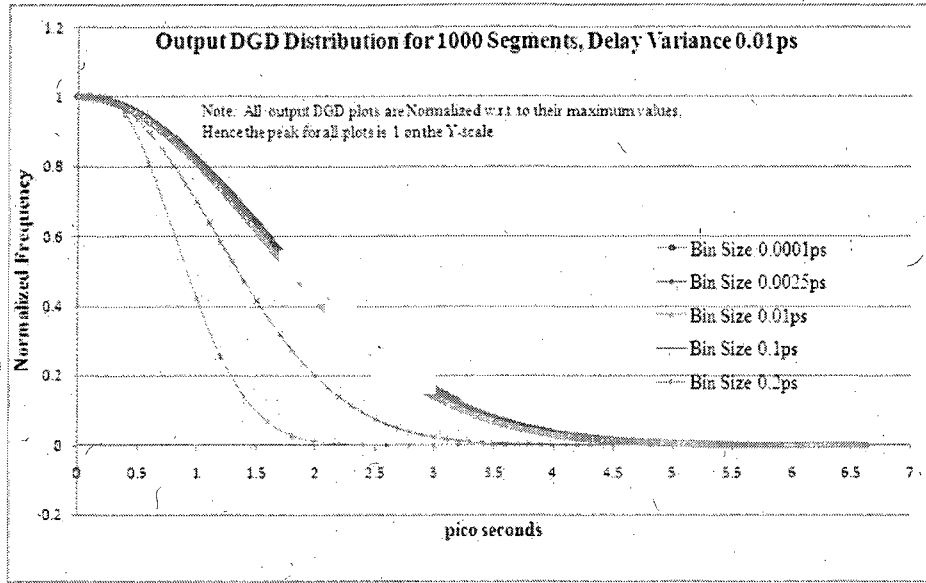


Figure 6- 1 Effect of Sampling Bin Size on Output DGD Distribution curves

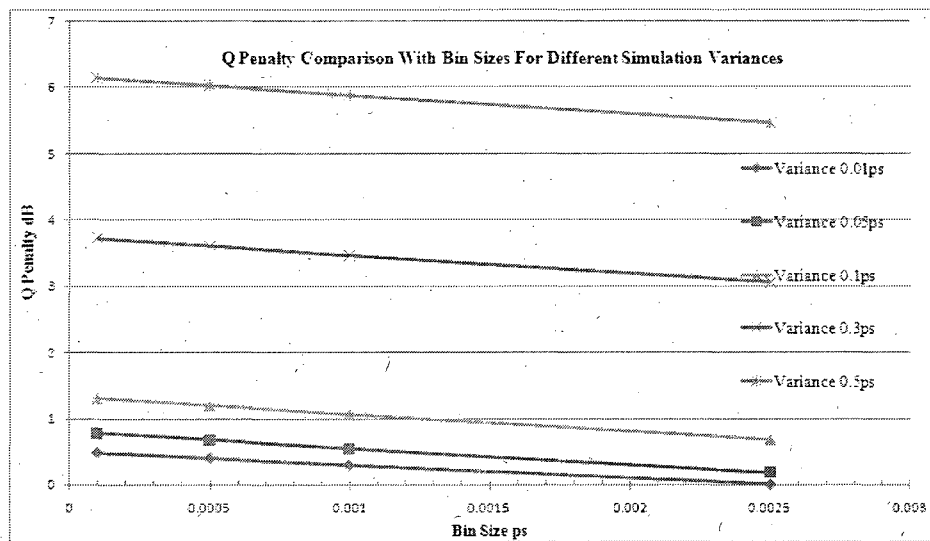


Figure 6- 2 Q Penalty vs. Bin Size for Types of Fibers with Different Delay Variance

Data Rate 40Gbps
Time Period = 25ps

Variance	1e-2ps	5e-2ps	1e-1ps	3e-1ps	5e-1ps
Norm RMS DGD @0.0025ps Bin Size	0.11512	0.262108	0.369332	0.65198	8.70E-01
Bin Size ps	Q penalty (dB)	Q penalty (dB)	Q penalty (dB)	Q penalty (dB)	Q penalty (dB)
0.0001	0.48	0.78	1.30	3.72	6.14
0.0005	0.40	0.68	1.20	3.61	6.03
0.001	0.29	0.54	1.06	3.46	5.88
0.0025	0.01	0.18	0.68	3.06	5.47
Max	0.48	0.78	1.30	3.72	6.14
Average	0.30	0.54	1.06	3.46	5.88
Median	0.35	0.61	1.13	3.54	5.95
Stdev	0.20	0.26	0.27	0.29	0.30
Min	0.01	0.18	0.68	3.06	5.47

Table 6- 1 Q Penalty Statistics for Different Fiber Types at Various Bin Sizes

A truncated normal distribution with a zero mean and a specified value of variance is used to create individual delays for a number of beat segments of the fiber from which the output DGD distribution is generated. This allows us to simulate different fiber types which are characterized by the shape of the output DGD distribution and the accumulated PMD impairment. For example, conventional single mode fibers have a small value of accumulated PMD and can be simulated from the delays produced from a normal distribution with a zero mean and a small value of variance. Fibers with a moderate accumulation of the PMD impairment (spun dispersion shifted fibers) can be simulated by generating delays of beat segments using a normal distribution with a zero mean and a medium value of variance. Fibers with a large accumulation of PMD impairment can be simulated by using a normal delay distribution with a zero mean and a large value of variance.

It is observed that the Q penalty at a specific bin size increases as the delay variance of the fiber increases. Table 6-1 shows that at a bin size of 0.0025ps, the Q penalty for a fiber with a delay variance of 0.01 ps is 0.48 dB and for a fiber with a delay variance of 0.1 ps the Q penalty is 1.3dB. When the delay variance is increased to 0.5 ps, the Q penalty is observed to increase to 6.1dB. This is appropriate since the increased delay variance of the fiber translates into a wider DGD distribution and a larger value of the PMD impairment, which results in larger signal degradation measured in terms of the Q penalty. Therefore, the plots for subsequently higher values of variance appear higher as they enclose larger values of Q penalty. The standard deviation of the Q penalty across different bin sizes for each fiber type is observed to be less than 0.3 dB.

6.2 Configuration of Concatenated Homogenous Channel

In this section the growth of the incremental model by concatenating a large number of beat length segments and independently varying a normally distributed group delay of beat length segments to represent the statistical behavior of a real fiber span is illustrated. The impact of this incremental growth on the performance of optical networks in terms of Q Penalty is also discussed. Our sampling bin size for the simulations in this section is fixed at 0.0025 ps. Individual delays for a fiber section with 100 beat length segments are generated using a normal distribution with a zero mean and a small variance of 0.001 ps. The output DGD distribution is simulated for the fiber section and the root mean square value of the distribution is recorded along with the associated Q penalty. A plot of this output DGD distribution is captured in Figure 6-3. The number of beat

segments is increased to $n = 200$ for the same fiber type, i.e. one whose beat segment delays are calculated from a normally distributed function with zero mean and a small variance of 0.001 ps. The output distribution is generated and the RMS DGD and the associated Q Penalty are recorded. These steps are repeated for $n = 400, 800, 1000$ beat segments. The output DGD distribution of these increasing fiber lengths ($n = 100, 200, 400, 800, 1000$ beat segments) is compared in Figure 6-3 which is a plot of delay in picoseconds on the x-axis versus normalized frequency of delay components on the y-axis. It may be noted that all the plots initially start from a unit point on the y-axis. This is because all the plots are normalized against its respective maximum frequency component. This enables us to compare different plots within the same chart. It is observed that the output DGD distribution broadens with increase in fiber length for a fixed type of single mode fiber as the number of segments are increased from $n = 100$ to 1000 beat segments.

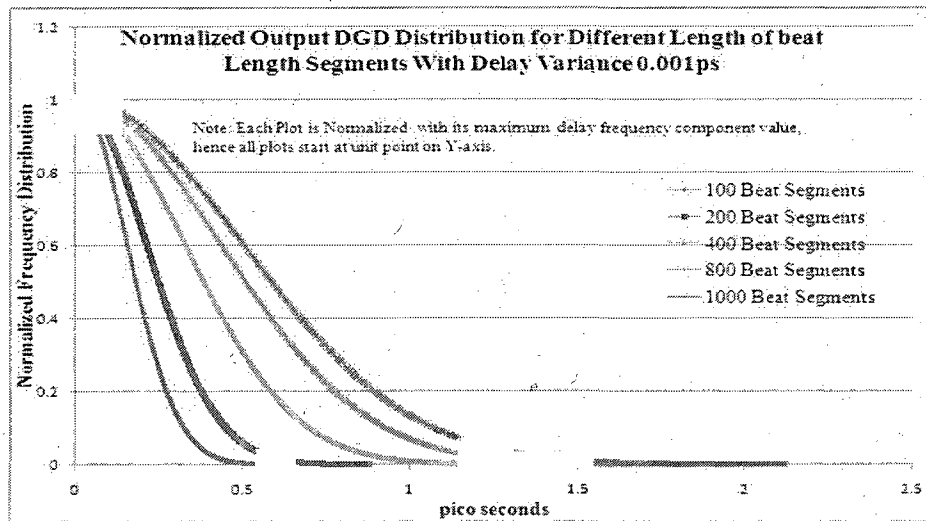


Figure 6- 3 Plots of Output DGD Distribution for different Lengths of Same Fiber Type (Variance 0.001 ps)

Table 6-2 below shows the root mean square value of the DGD and its relationship with the length of the fiber. The table also gives the values of the PMD grown by concatenating multiples of 100 beat segments, which are calculated using the square root dependence of PMD on length [5]:

$$\text{PMD of the new link (ps)} = \sqrt{(\text{PMD of Link-1})^2 + (\text{PMD of Link-2})^2} \text{ ps} \quad \dots\dots[6.1]$$

Therefore, if the PMD of a 100 beat segment link is 0.2275ps, the approximate value of PMD for a section with a concatenation of two such links, each of 100 beat segments (n = 200 beat segments) is:

$$\text{PMD of the new Link (ps)} = \sqrt{(0.2275)^2 + (0.2275)^2} \text{ ps} = 0.32\text{ps} \quad \dots\dots[6.2]$$

Delay Variance 0.001ps Data Rate 40Gbps						
Number of Segments	100	200	400	600	800	1000
RMS DGD ps	0.23	0.34	0.56	0.69	0.79	0.92
Calculated Value (Sq Root Dependence) ps		0.32	0.46	0.56	0.64	0.72

Table 6- 2 Growth of RMS DGD (ps) with Length of Fiber (Delay Variance 0.001ps)

Figure 6-4 shows the plot indicating the growth of RMS DGD with increase in length of the fiber. The plot has the number of beat segments on the x-axis and the RMS DGD in pico-seconds on the y-axis. The plot also includes a comparison of the actual RMS DGD obtained from our simulation results against theoretically calculated values.

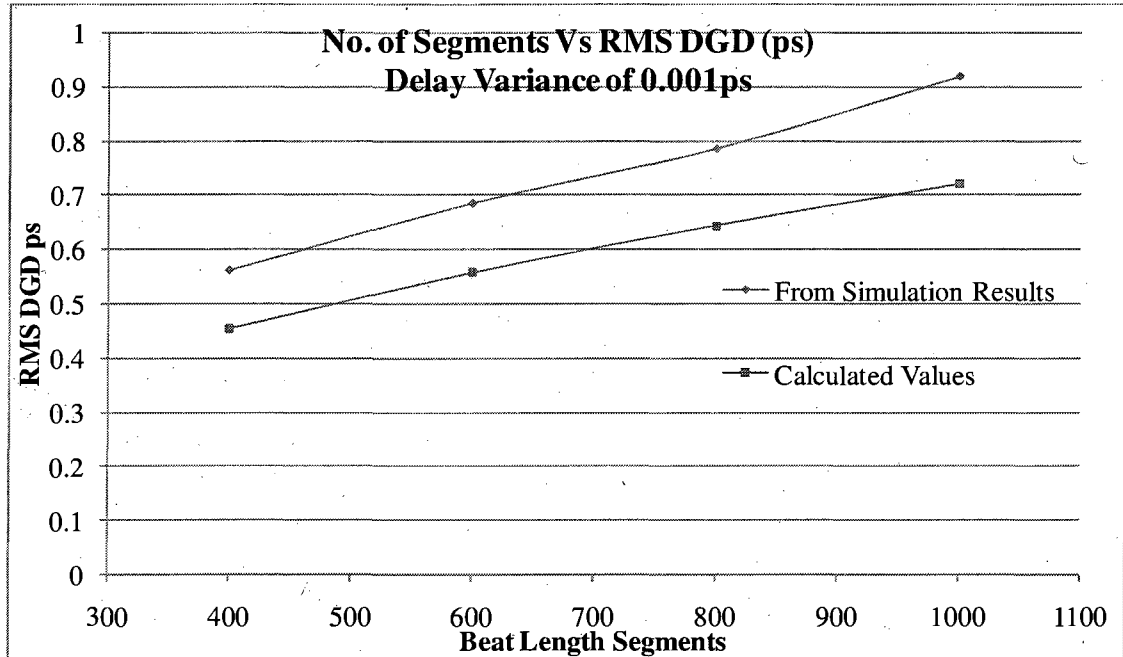


Figure 6- 4 Beat Length Segments versus RMS DGD for Fixed Fiber Type (Variance 0.001 ps)

Figure 6-4 and Table 6-2 validate the trend that the PMD impairment increases with increase in the length of the fiber. The trend of RMS DGD values observed from our simulation results is similar to the trend in our calculated values. Our compiler limitation on the maximum value of the number of delay components prevents us from simulating an extremely large number of beat segments (fiber lengths). This prevents us from completely mapping the trend of the PMD impairment for large lengths of optical fibers.

The impact of the increase in PMD impairment with the length of fiber on performance of optical networks is shown in Figure 6-5 as a plot of the beat length segments versus Q penalty. The penalties are captured considering the performance at $n = 200$ beat segments as the baseline performance. Hence, the penalty plots start at $n = 400$

beat segments. The results are listed in Table 6-3 below. It is observed that the Q penalty increases with increase in fiber length.

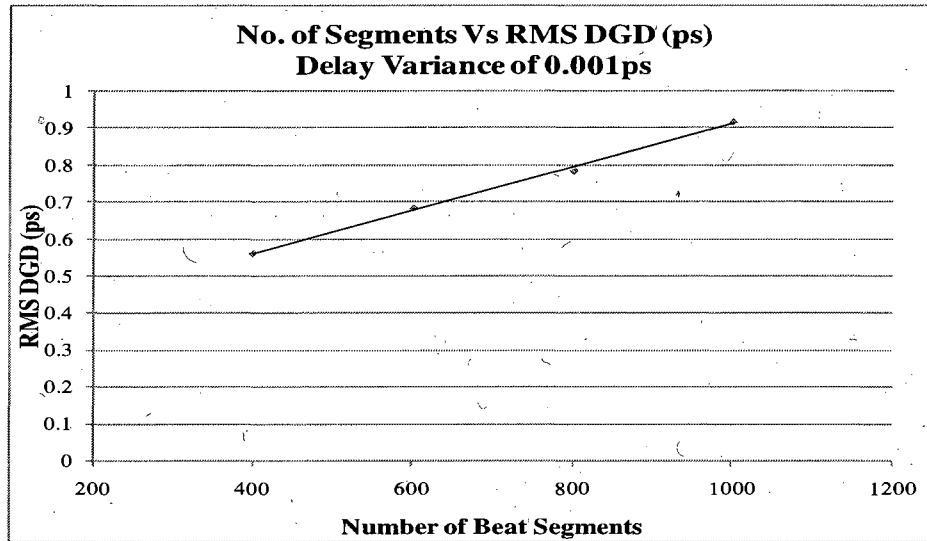


Figure 6- 5 Beat Length Segments versus Q Penalty dB for Fixed Fiber Type (Variance 0.001 ps)

Delay Variance 0.001ps

Data Rate 40Gbps

Number OF Beat Segments	200	400	600	800	1000
RMS DGD	0.34	0.56	0.69	0.79	0.92
Conventional Q penalty dB	Reference	3.33	4.62	5.46	6.60

Table 6- 3 Growth of Q Penalty with Length for Fixed Fiber Type (Variance 0.001 ps)

To validate our results and observed trends the above exercise is repeated for a different type of fiber i.e. one whose beat length delays are calculated from a normal distribution with zero mean and a large variance of 0.5ps. The length of the fiber is increased by increasing the number of beat length segments and a plot of the output DGD distribution is captured in each case as shown in Figure 6-6.

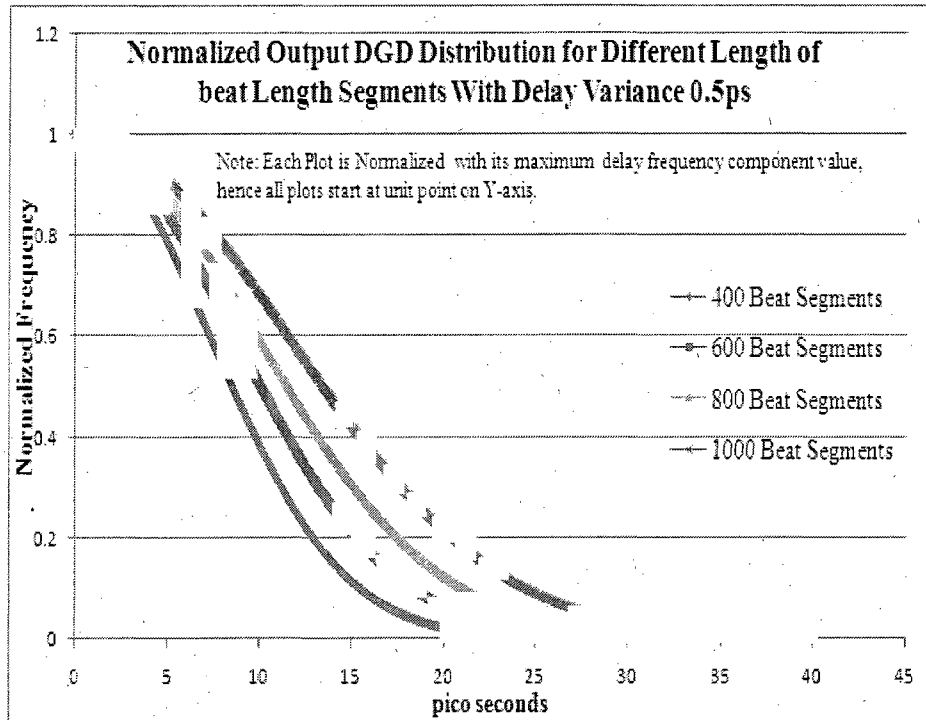


Figure 6- 6 Plots of Output DGD Distribution for different Lengths of Same Fiber Type (Variance 0.5ps)

It is observed that the output DGD distribution broadens with increase in fiber length. Table 6-4 shows the RMD DGD obtained from simulation results for various beat length segments. It also shows the theoretical values obtained using the square root of length dependence by concatenating multiples of 100 segments.

Delay Variance 0.5ps
Data Rate 40Gbps

Number of Segments	100	200	400	600	800	1000
RMS DGD ps	6.09	7.37	12.21	14.98	17.57	20.86
Calculated Value (Sq Root Dependence) ps		8.61	12.18	14.91	17.22	19.25

Table 6- 4 Growth of RMS DGD (ps) with Length of Fiber (Delay Variance 0.5ps)

Figure 6-7 plots the beat length segments with the RMS DGD and also compares this with the theoretical values. It is observed that the RMS DGD increases with the increase in fiber length. The RMS DGD from simulations and the theoretical values are in agreement, which validates the growth of PMD impairment with length using our model.

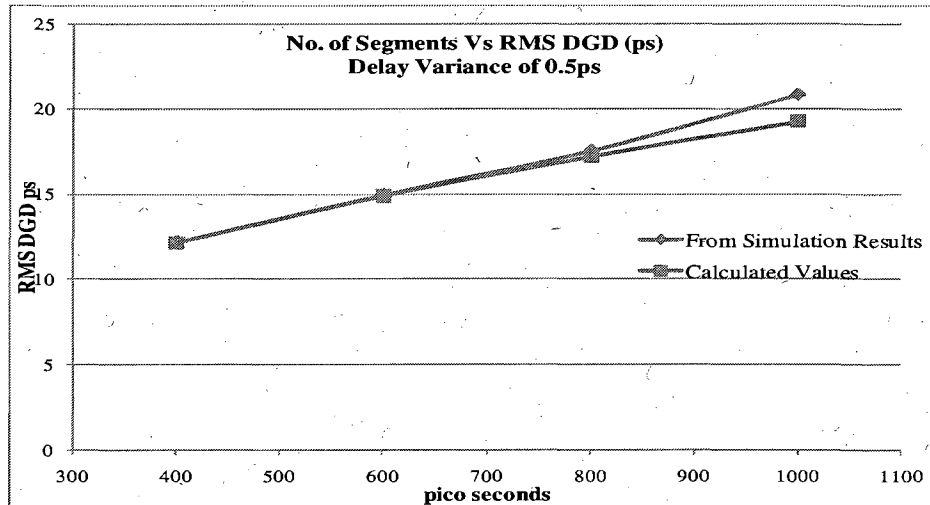


Figure 6- 7 Beat Length Segments versus RMS DGD for Fixed Fiber Type (Variance 0.5ps)

Figure 6-8 and Table 6-5 show the relationship between Q penalty and the length of fiber.

It is observed that the Q Penalty increases with increase in the length of fiber.

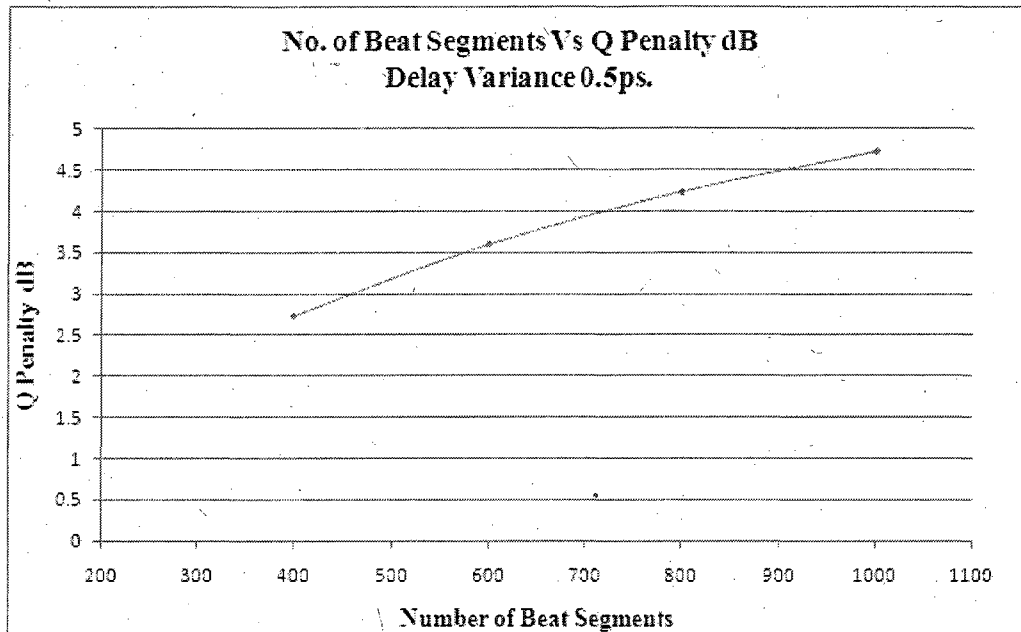


Figure 6- 8 Beat Length Segments versus Q Penalty dB for Fixed Fiber Type (Variance 0.5 ps)

Delay Variance 0.001ps

Data Rate 40Gbps

Number OF Beat Segments	200	400	600	800	1000
RMS DGD	7.37	12.21	14.98	17.57	20.86
Conventional Q penalty dB	Reference	2.72	3.59	4.23	4.72

Table 6- 5 Growth of Q Penalty with Length for Fixed Fiber Type (Variance 0.5 ps)

Figures 6-9 – 11 show the field measurements of the output DGD distribution for three fiber spools with different lengths .Figure 6-9 shows the measured output distribution for

a fiber spool of length 7 km; the measure of the PMD impairment is recorded as 0.09 ps with the coefficient of PMD recorded as 0.05 ps/sqr.root.km. Figure 6-10 shows the output distribution for a fiber spool of length 77 km with measured value of the PMD impairment as 0.39 ps and with the coefficient of PMD recorded as 0.045 ps/sqr.root.km. Figure 6-11 shows the output distribution for 124 km of fiber spool with measured PMD at 0.47 ps and a recorded PMD coefficient of 0.043 ps/sqr.root.km. The plots have been magnified to show the details. It is observed that the width of the distribution increases with increase in length of the fiber as indicated in our simulation results. It is also interesting to observe in Figure 6-10 that the Gaussian fit of the field measurement technique is not able to account for the small set of discrete delay components observed 5 ps away from the central peak and that it reports the resultant measure of the impairment to be 0.395 ps. This further validates the advantage of our discrete approach towards capturing the DGD distribution.

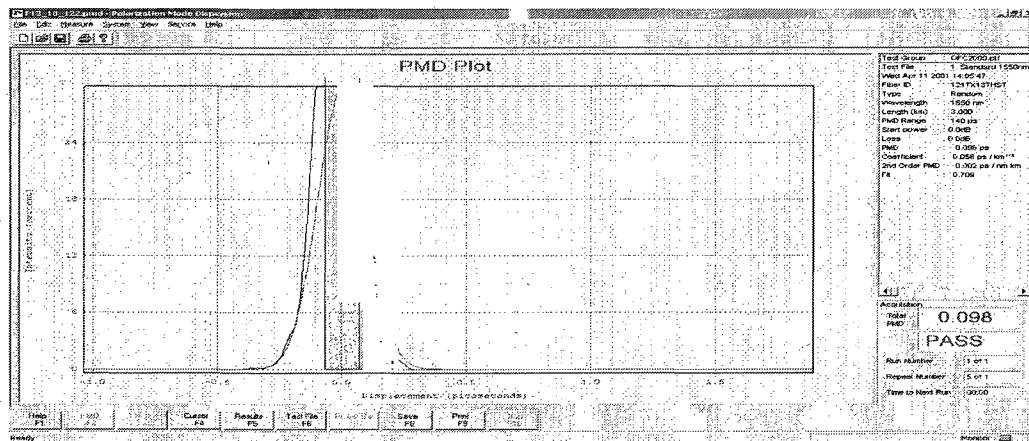


Figure 6- 9 Field Measurement 7Kms Fiber Spool

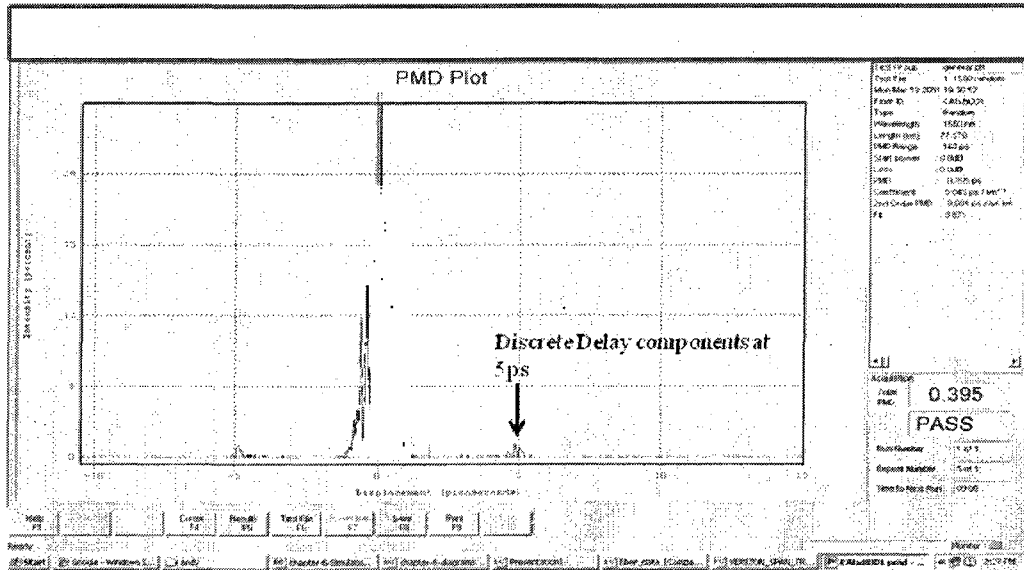


Figure 6- 10 Field Measurement 77Kms Fiber Spool

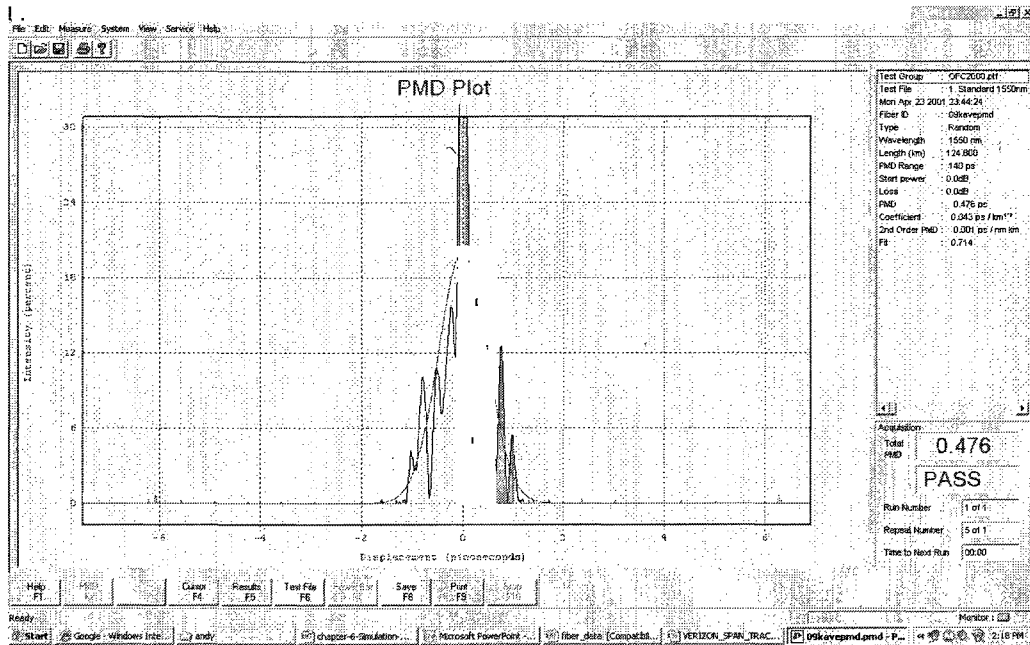


Figure 6- 11 Field Measurement 124Kms Fiber Spool

6.3 Configuration of Incremental Channel

In this section the relationship between the mean and the variance of the normal delay distribution for PMD and the output DGD distribution is demonstrated. The mean and variance of the normal delay distribution define the beat segment delay and this, in turn, directly relates to the fiber type. A typical contemporary single mode fiber (e.g. conventional single mode fiber) will have zero mean and a very small variance which implies very small values of beat segment delays. This in turn, will result in minimum distributed PMD over large lengths of the fiber and a minimal value of performance penalty at high data rates of transmission. A typical legacy fiber (e.g. spun Dispersion Shifted Fiber) will have zero mean and moderate variance which will result in moderate performance penalty at high data rates and minimal penalty at low data rates of transmission. Lastly, a marginal fiber (e.g. non-spun Dispersion Shifted Fiber) will have zero mean and a large variance resulting in failure to support high data rates and will have a high penalty for low data rates of transmission. In the first part of this section the effect of mean and variance of the normal delay distribution on the output DGD distribution is illustrated and in the second part its impact on the optical network performance in terms of Q penalty is shown. Results from our simulation will be compared with published data.

In the following simulations the number of beat segments ' n ' is fixed at 1024, the sampling bin size at 0.0025ps and the data rate transmission at 40Gbps ($T=25$ ps). In the first case individual delays for 1024 beat segments are generated using a normal distribution with zero mean and a small variance value of 0.001ps. This is analogous to

simulating a conventional single mode fiber with zero mean and a very small variance. The delay values obtained from this normal distribution are used to generate the output DGD distribution and the associated Q penalty is then recorded. In the next step individual delays for 1024 beat segments are generated using a normal distribution with zero mean and a moderate variance of 0.01 ps. This is analogous to simulating a spun Dispersion Shifted fiber with zero mean and moderate variance. The delay values obtained from the normal distribution are used to generate the output DGD distribution and the associated Q penalty is then recorded. The above procedure is repeated for delays obtained from a normal distribution with zero mean and a variance of 0.3 ps and also for delays obtained from a normal distribution with zero mean and a variance of 0.5 ps. Figure 6-12 compares the output DGD distribution plots for fibers with different delay variance (0.001 ps, 0.01 ps, 0.1 ps and 0.5 ps).

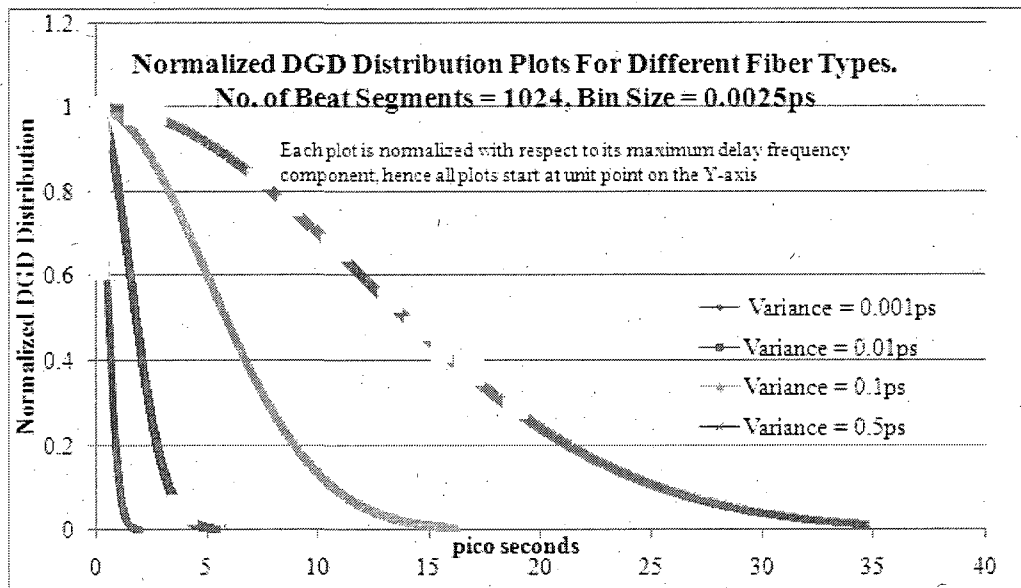


Figure 6- 12 Output DGD Distribution for Different Fiber Types

For a very small value of delay variance (0.001 ps), the output delay distribution is very narrow and the root mean square value of the distribution is 0.91 ps (3% of the bit period). For a delay variance of 0.01 ps, the output DGD plot is wider than that of delay 0.001 ps variance and the RMS DGD value of the distribution is 2.86 ps (11% of the bit period). The output DGD plots for a delay variance of 0.1 ps continue to show the trend of an increasing width for the distribution with an RMS DGD of 9.2 ps (36% of bit period). The output DGD distribution at 0.5 ps delay variance has the largest width with an RMS DGD value of 21.7 ps (86% of the bit period) and confirms the trend that the output DGD distribution spreads and has a larger width for larger values of delay variance. Figure 6-13 and Table 6-6 show the performance penalty associated with different delay variances.

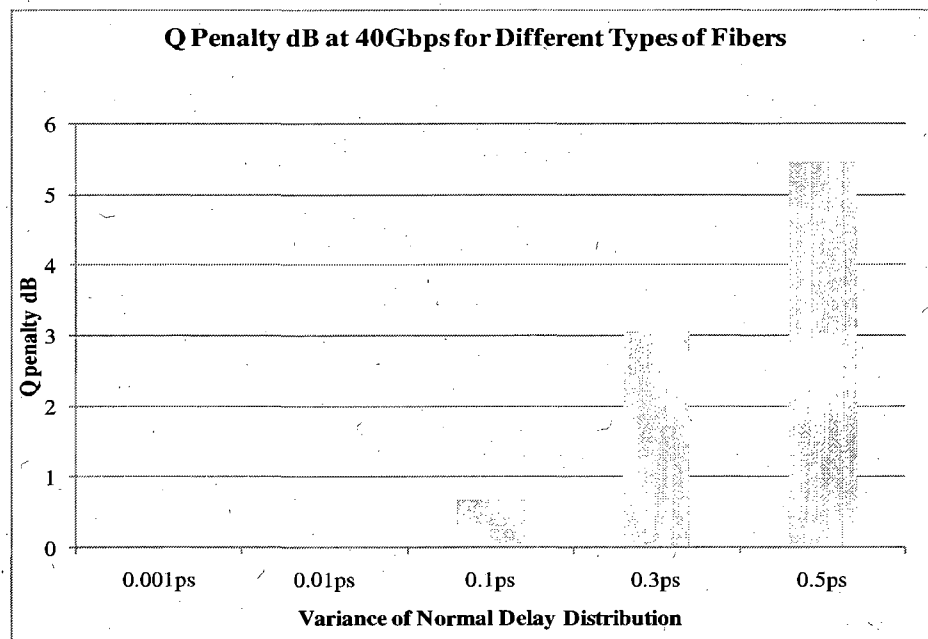


Figure 6- 13 Q Penalty for Different Fiber Types

Variance Of Normal Delay Distribution with Zero Mean	RMS DGD (ps)	Q Penalty (dB)
0.001ps	0.92	0.00
0.01ps	2.86	0.01
0.1ps	9.22	0.68
0.3ps	16.27	3.06
0.5ps	21.72	5.47

Table 6- 6 Q Penalty for Different Fiber Types

It is observed that the RMS DGD increases with increase in the variance of the normal delay distribution with zero mean. The performance at 0.001ps variance is considered as the base line towards Q penalty calculations. It is observed that the performance penalty increases with increase in delay variance. Thus, a fiber with a low delay variance of 0.01ps will have a small value of accumulated RMS DGD of 2.8ps and a small performance penalty of 0.01dB. A fiber with a large delay variance of 0.5ps will have significant accumulation of RMS DGD at 21.7ps and will have a very large performance penalty of 5.4dB.

6.4 Configuration of Concatenated Heterogeneous Channel

In this section the ability of our model to simulate the mixing of segments having different statistical behavior is illustrated. In real world field deployments of optical networks, mixing of different fiber types might occur in two specific cases:

- i) **Mix of Distributed effect:** In such cases, sections of fibers with different delay variances are mixed together. This might happen in the case of

submarine fiber where an old section is replaced with a new type of fiber or in the case of optical network deployments where information on installed fiber data is not available.

- ii) **Mix of Distributed and Deterministic Effect:** In such cases, one or more artifacts of PMD are introduced in a section of the fiber. This introduction of artifacts is possible in the case of manufacturing defects in the fiber where an air gap in the core or cladding may be introduced or in the case of mixing polarization maintaining fiber with conventional fibers.

The results show that our model is able to simulate these real world situations and accurately characterize the PMD impairment.

6.4.1 Mix of Distributed Effect

The simulation bin size for all simulations in this section is fixed at 0.0025 ps. In the first case, a mix of equal lengths of a fiber section is considered, one of which has very low accumulated PMD and the other has very high accumulated PMD. The fiber section with low PMD accumulation is simulated by generating the individual delays of its beat length segments from a normal distribution with zero mean and a very low variance of 0.0001 ps. The fiber section with a high accumulation of PMD is simulated by generating the individual beat delays of its beat length segments from a normal distribution with zero mean and a high variance of 0.1 ps. A mixed fiber type of 1000 segments is simulated by mixing 500 segments with a delay variance of 0.0001 ps and 500 segments with a delay variance of 0.1 ps. Figure 6-14 compares the output

distribution plot for this mixed case with the output DGD distributions of 1000 segments of fibers with delay variance 0.0001 ps and 0.1 ps respectively.

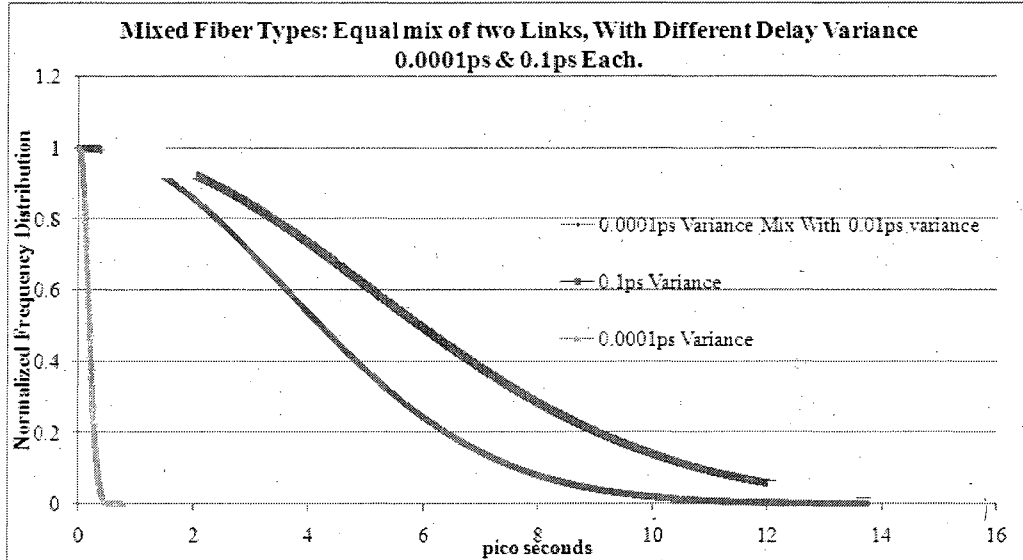


Table 6- 14 Equal Parts Homogenous Mix with Variance 0.0001ps & 0.1ps

It is observed that the output DGD distribution of the fiber with a delay variance of 0.0001ps is much narrower than the output DGD distribution of a fiber with a delay variance of 0.1ps. The output DGD distribution of the mixed fiber type occurs in between the two distributions but is heavily shifted towards the fiber type with a higher delay variance, implying that in the case of equal lengths of mixed types of fiber, the fiber type with the higher delay variance will tend to dominate the resultant output DGD distribution. Table 6-7 shows the root mean square value of the output DGD distribution for the different fiber types.

Variance ps	RMS DGD ps
0.0001	0.27
Equal Mix	6.22
0.1	9.22

Table 6- 7 RMS DGD for Case 1 of Fiber Mix

The RMS DGD value for 1000 segments with a delay variance of 0.0001ps is 0.27ps while the RMS DGD value for a fiber with a delay variance of 0.1ps is 9.22ps. The RMS DGD for the equal mix fiber type (500 Segments each) shows a RMS DGD value of 6.22ps. Figure 6-15 compares the output distribution plot for 1000 segments of fiber with a low delay variance of 0.0001ps, 1000 segments of fiber with a high delay variance of 0.01ps and a mixed fiber type formed by concatenating 500 segments with a delay variance of 0.0001ps and 500 segments with a delay variance of 0.01ps.

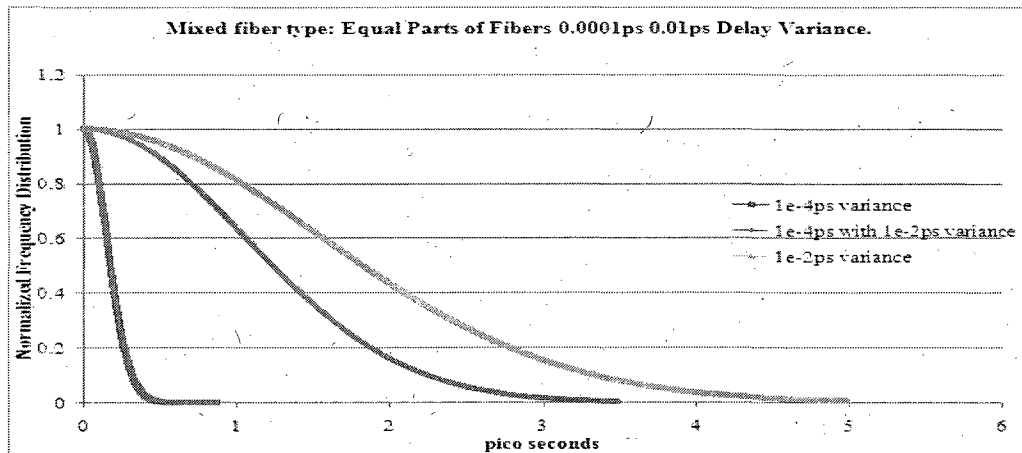


Figure 6- 15 Equal Parts Homogenous Mix with Variance 0.0001ps & 0.01ps

It is observed that the output distribution of the equal mix fiber type is closer to the output DGD distribution of the fiber with a higher delay variance of 0.01ps. Table 6-8 shows the root mean square DGD values of the output DGD for each fiber type.

Variance ps	RMS DGD ps
0.0001	0.27
Equal Mix	1.85
0.01	2.86

Table 6- 8 RMS DGD for Case 2 of Fiber Mix

In the third case of our simulation, 1000 segments of two types of fiber are considered, where one fiber type is formed with a delay variance of 0.0001ps (normal distribution with zero mean and a low variance of 0.0001ps), while the other one is formed with a delay variance of 0.001ps (normal distribution with zero mean and a moderate variance of 0.001ps). Three different cases of mixed fiber types are created by changing the mix of these two fiber types. First, a mixed fiber, type 80% of whose link is composed of fiber with a delay variance of 0.0001ps and 20% of whose fiber is composed with delay variance of 0.001ps, is created. Next, a mixed fiber type in which we have an equal percentage of both fiber types i.e. 50% of the fiber with a delay variance of 0.0001ps and 50% of the fiber with a delay variance of 0.001ps is created. Lastly, a mixed fiber type, 20% of whose link is composed of fiber with a delay variance of 0.0001ps and 80% of whose link is composed of fiber with a delay variance of 0.001ps, is created. Figure 6-16 compares the output DGD distribution of the above cases. The leftmost and the narrowest

plot shows the output DGD distribution for the pure case of fiber with low delay variance (1000 segments with delay variance of 0.0001 ps).

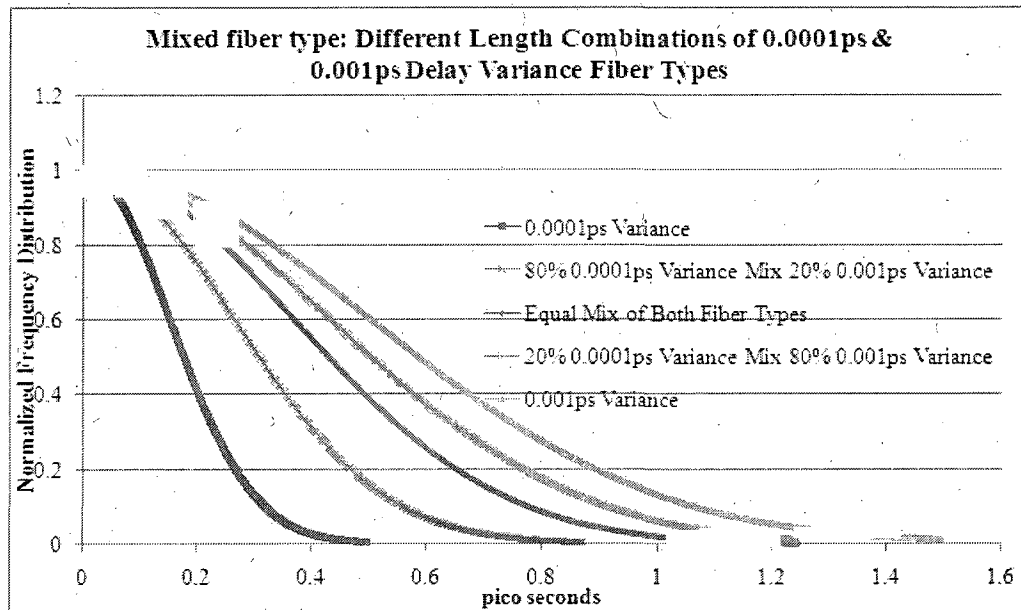


Figure 6- 16 Different Length Combinations of Homogenous Mix with Variance 0.0001 ps & 0.001 ps

The root mean square value of the DGD distribution is 0.27ps (refer Table 6-9). The next plot on its right side shows the case of mixing 20% of fiber with a delay variance of 0.001ps. The output DGD distribution becomes wider than that of fiber with a delay variance of 0.0001ps with a calculated RMS DGD of 0.47ps. As more fiber with a delay variance 0.01ps is mixed the output delay distribution becomes wider as shown by the plot of 50% mix (RMS DGD = 0.66ps) and the plot of 80% mix (RMS DGD = 0.78ps). The figure also shows the output DGD plot for 1000 segments with a delay variance of 0.01ps which has the widest distribution and an RMS DGD equal to 0.91ps.

Variance ps	RMS DGD ps
100% 0.0001ps	0.27
80% 0.0001ps Variance Mixed with 20% of 0.001ps Variance	0.47
Equal Mix (50% Each)	0.66
20% 0.0001ps Variance Mixed with 80% of 0.001ps Variance	0.78
100% 0.001ps	0.91

Table 6-9 RMS DGD for Case 3 of Fiber Mix

The three cases discussed in this section show that the output delay distribution of mixed fiber types differs in shape to the output distribution of a pure conventional fiber section. The evolution of the output DGD when a pure fiber with a low delay variance is mixed with different proportions of fiber with a moderate value of delay variance has been shown. In the case of fiber with an equal mix of two different fiber types it is observed that the output DGD distribution is dominated by the fiber type with the higher delay variance.

6.4.2 Mix of Distributed and Deterministic Effect

This section illustrates the ability of our model to simulate mixing of the deterministic effect of PMD by introducing a PMD artifact in a fiber section. The sampling bin size for all simulations in this section is 0.0025ps. There are four sub sections:

- i) Introduction of different values of the PMD artifact in the fiber section and showing the output DGD distribution in each case.

- ii) Introduction of a fixed value of the PMD artifact and capturing the output DGD distribution for different lengths of the fiber.
- iii) Introduction of a fixed value of PMD artifact and plotting the output DGD distribution for different types of fibers by varying the delay variance of the fiber.
- iv) Introduction of multiple artifacts and plotting the output DGD distribution for different types of fibers by varying the delay variance of the fiber.

6.4.2.1 Introduction of a PMD Artifact in Fiber Section

A normal distribution with zero mean and a small variance of 0.0001ps is used to generate individual delays for 1000 beat segments. For the PMD artifact, the delay of one beat segment is changed to equal the value of the PMD artifact. This beat segment is concatenated with the remaining fiber section and the output DGD distribution is generated. The output DGD distribution of such a fiber will show the distribution peaking at the value of the artifact that was introduced. For e.g. Figure 6-17 shows the output DGD distribution of a fiber section with a delay variance of 0.0001 ps and a PMD artifact of 0.5 ps. It is observed that output DGD shows a small peak 0.5 ps away from the central peak (or origin of the axes). We increase the value of artifact to 1ps and the results are as shown in Figure 6-18. The output DGD distribution shows a distinct peak 1ps away from the central peak. Figures 6-19 – 21 show the output DGD distribution with PMD artifacts of 4 ps, 8 ps and 12 ps. In each case the output DGD distribution shows a distinct peak away from the central peak by a value equal to the value of the PMD artifact.

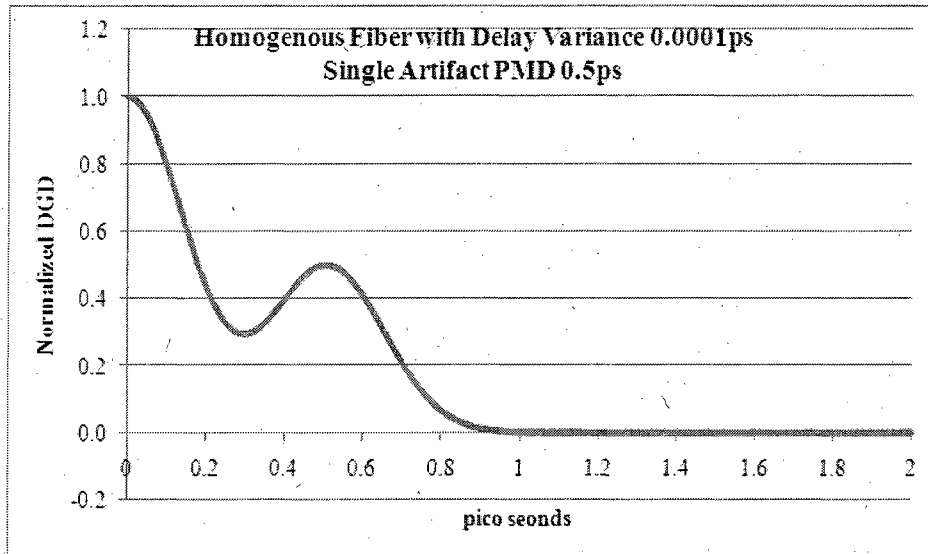


Figure 6- 17 Homogenous Fiber Delay variance 0.0001 ps With Single PMD Artifact 0.5 ps. Simulation Bin Size = 0.0025 ps

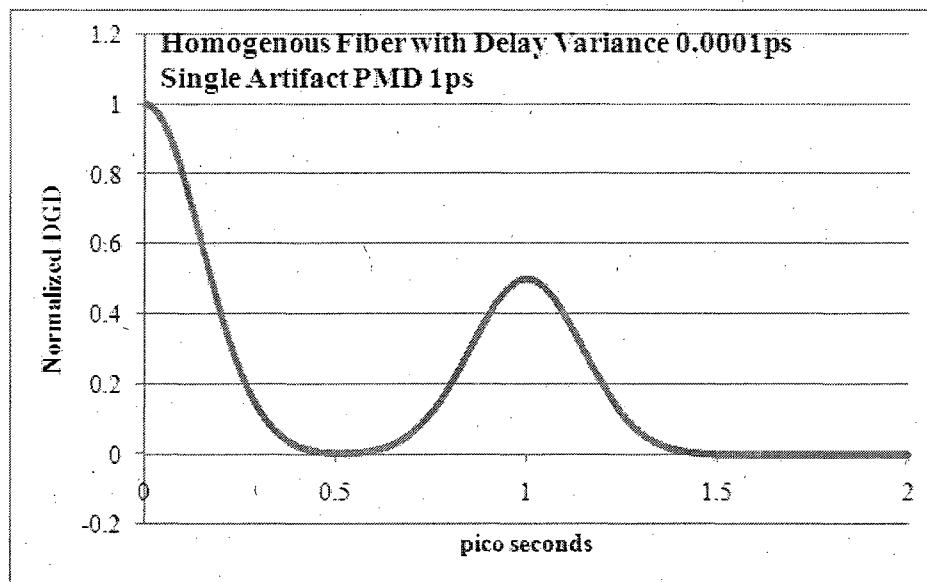


Figure 6- 18 Homogenous Fiber Delay variance 0.0001 ps With Single PMD Artifact 1 ps. Simulation Bin Size = 0.0025 ps

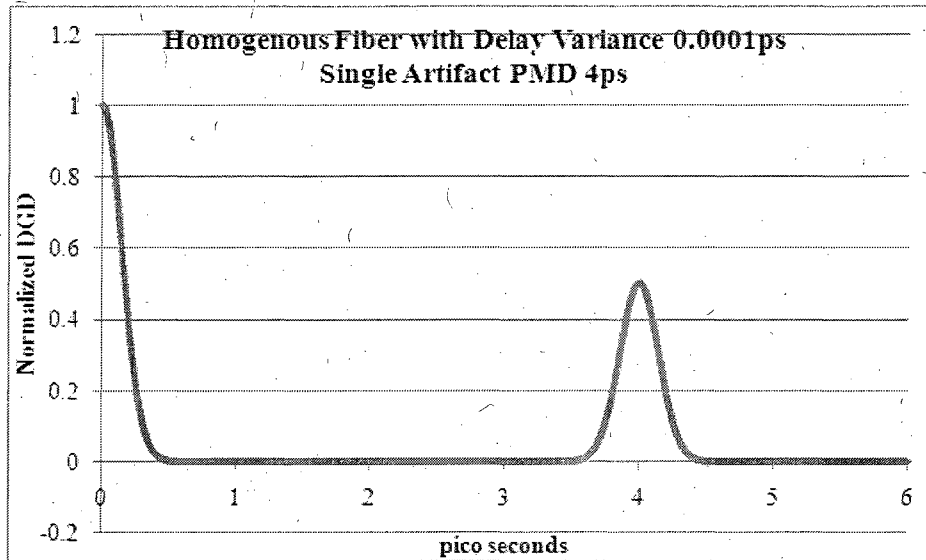


Figure 6- 19 Homogenous Fiber Delay variance 0.0001 ps With Single PMD Artifact 4 ps. Simulation Bin Size = 0.0025 ps

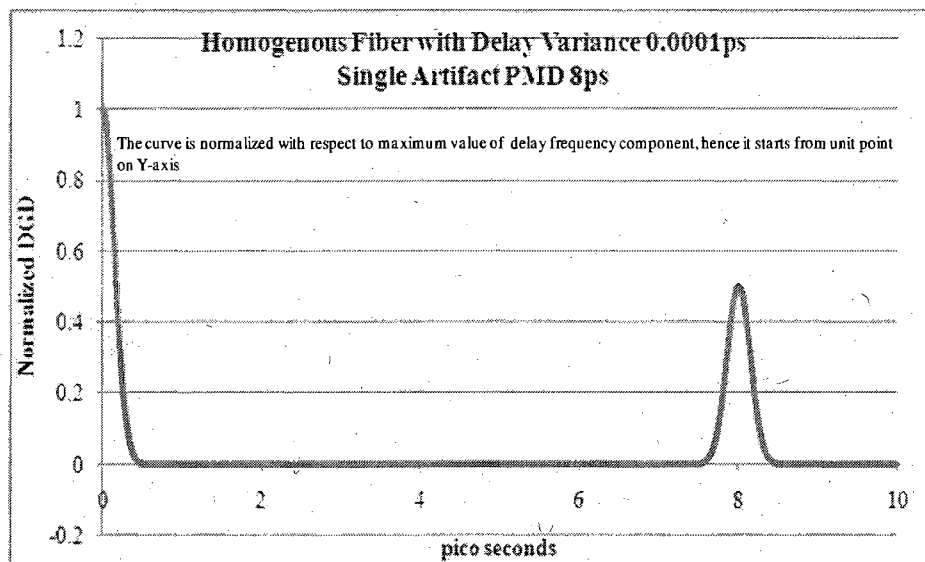


Figure 6- 20 Homogenous Fiber Delay variance 0.0001 ps With Single PMD Artifact 8 ps. Simulation Bin Size = 0.0025 ps

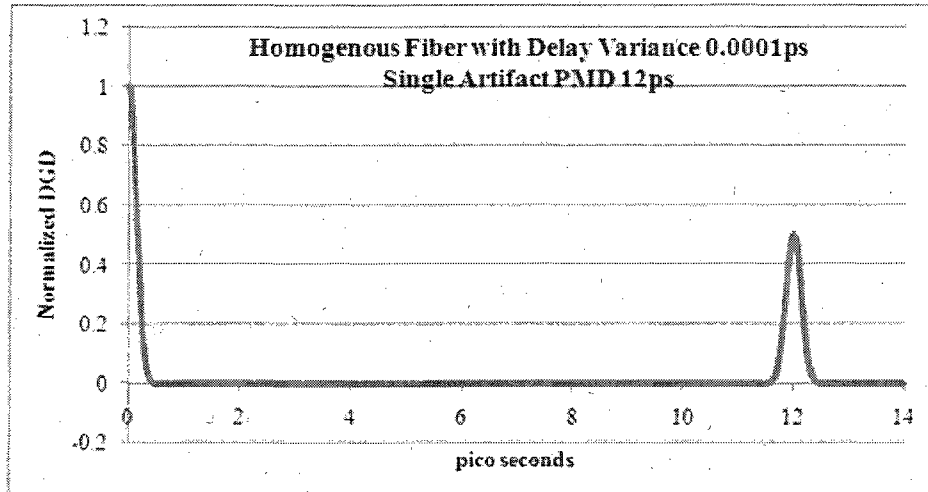


Figure 6- 21 Homogenous Fiber Delay variance 0.0001 ps With Single PMD Artifact 12 ps. Simulation Bin Size = 0.0025 ps

6.4.2.2 PMD Artifact with Different Lengths of Fiber

In this set of simulations the PMD artifact value is fixed at 5 ps, the delay variance for the fiber section is 0.0001 ps i.e. the individual delays of the beat segments are generated from a normal distribution with zero mean and small variance value of 0.0001 ps. The PMD artifact is introduced in a fiber section made with 100 beat segments and the output DGD distribution is captured as shown in Figure 6-22. The plot shows a distinct peak 5 ps away from the central peak. The number of beat segments is increased to 200, 400, 600, 800, 1000 along with the PMD artifact and the output DGD distribution is compared in Figure 6-22. It is observed that as the number of beat segments is increased (increasing the length of the fiber section) the width of the output DGD distribution starts to become wide. If the length of the fiber section is increased significantly, the output DGD will become broad enough to engulf the peak of the PMD artifact at 5 ps.

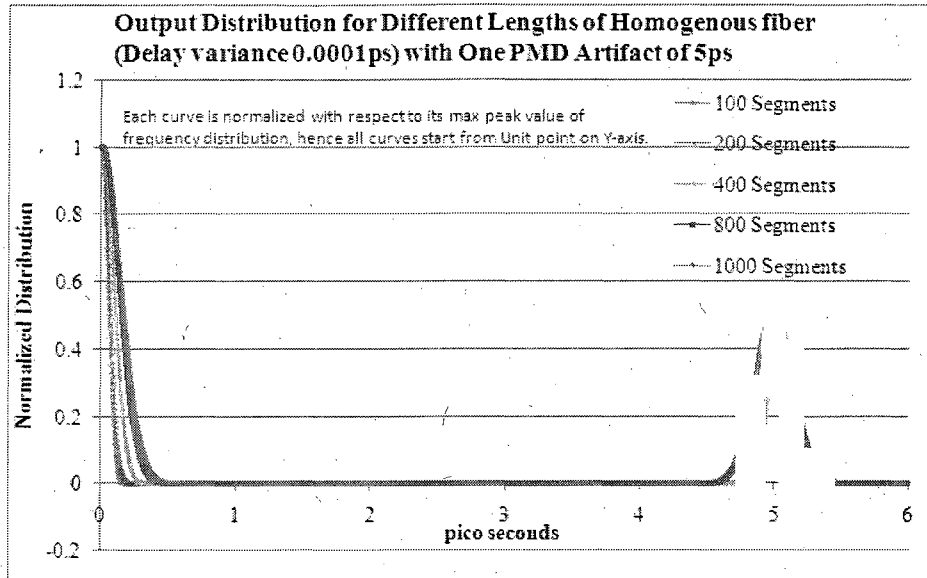


Figure 6- 22 5 ps PMD Artifact with Varying Lengths of Homogenous Fiber (Delay Variance 0.0001 ps), Sampling Bin Size 0.0025 ps

Figure 6-23 and Table 6-10 show a comparison of the relative Q penalty for increasing lengths of fiber with the performance at 100 segments being considered as the base line or reference for penalty calculations.

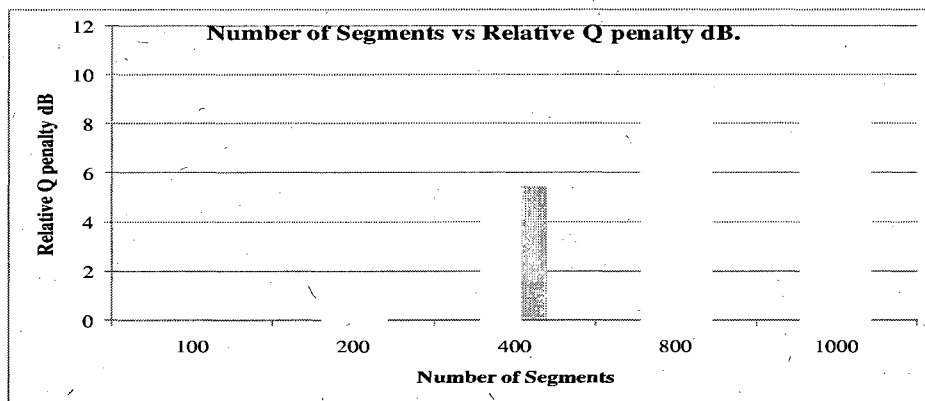


Figure 6- 23 Q Penalty for 5 ps PMD Artifact with Varying Lengths of Homogenous Fiber (Delay Variance 0.0001 ps)

A steady increase in the Q penalty with increase in fiber length is observed. Table 6-10 tabulates these values along with the calculated root mean square value of the DGD distribution.

Number of Segments	RMS DGD ps	Q Penalty (dB)
100	0.1	Base Line
200	0.12	1.62
400	0.18	5.47
800	0.25	8.53
1000	0.29	9.57

Table 6- 10 Q Penalty for Different Lengths: Fiber Section with 5ps PMD Artifact

The Q penalty at 200 segments calculated against the performance at 100 segments is 1.62 dB and more than doubles to 5.47 dB when the length increases to 400 segments. The Q penalty at 1000 beat segments is 9.57 dB.

6.4.2.3 PMD Artifact with Different Fiber Types

In this set of simulations a PMD artifact of 5 ps is introduced in a fixed length of fiber (1000 beat segments). A normal distribution of a zero mean and a small variance of 0.0001 ps is used to create the individual delays of beat segments from which the output DGD distribution is generated. The output DGD is narrow and has a peak at a distance of 5 ps away from the central peak. The delay variance is increased to 0.01 ps, 0.1 ps and 0.5 ps and output DGD distribution is captured for all the cases [Figure 6-24].

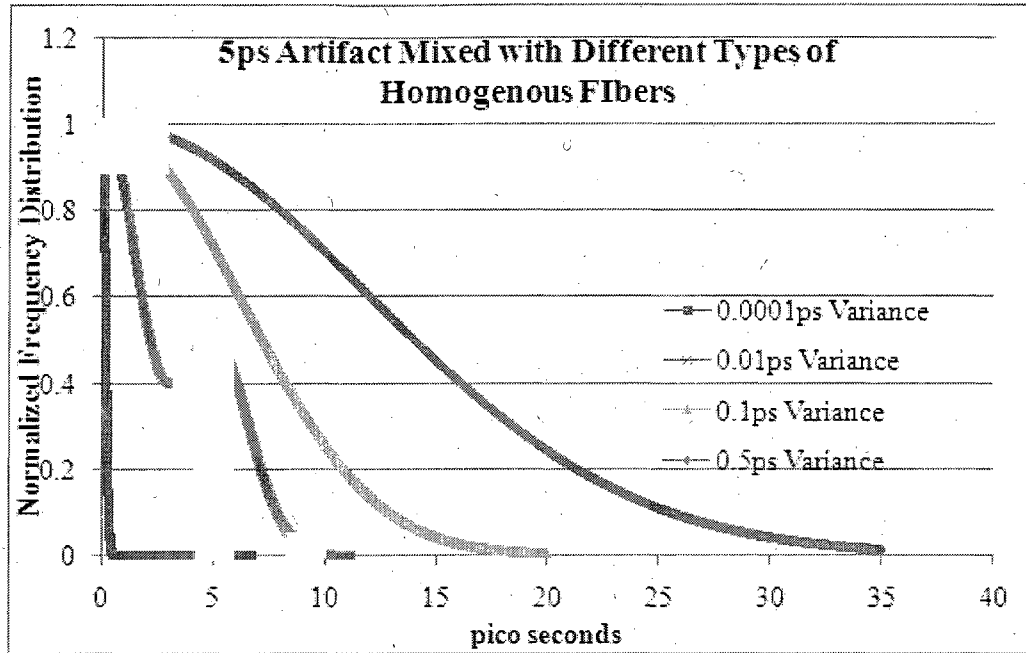


Figure 6- 24 5 ps PMD Artifact Mixed with Different Types of Homogenous Fibers. Simulation Bin Size = 0.0025 ps

It is observed that the plot for a delay variance of 0.01 ps captures the output distribution just before the peak created by the PMD artifact of 5 ps is engulfed in the overall distribution. The output DGD distribution plots for a delay variance of 0.1 and 0.5 ps do not reveal the peak of the PMD artifact at all. As the delay variance of the normal distribution is increased, the output DGD distribution widens as the individual delays of the beat segments are larger in value and this generates a larger spread of the output DGD distribution. When the individual delay values of the beat segments are sufficiently large, the output DGD distribution thus generated is wide enough to assimilate the PMD artifact.

6.4.2.4 Multiple Artifacts in the Fiber Section

In these sets of simulations two PMD artifacts are introduced in a fixed length (1000 segments) fiber section by changing the delay values of two beat segments to match the value of the two artifacts. These two beat segments are concatenated with remaining fiber section made of beat segments whose delay values have been derived from a normal distribution with zero mean and small variance of 0.0001 ps. The expected output with the two artifacts should have the distribution components at delay values of the artifacts along with the sum and difference of the delay values of the artifacts. For e.g. if two PMD artifacts of value 8 ps and 5 ps are introduced into a fiber section with a low delay variance, the output DGD distribution is expected to show distinct delay peaks at 3ps, 5 ps, 8 ps and 13 ps. Figure 6-25 shows a plot of the output DGD distribution which has 8 ps and 5 ps PMD artifacts concatenated with a section of fiber (1000 segments) whose delay variance is 0.0001 ps.

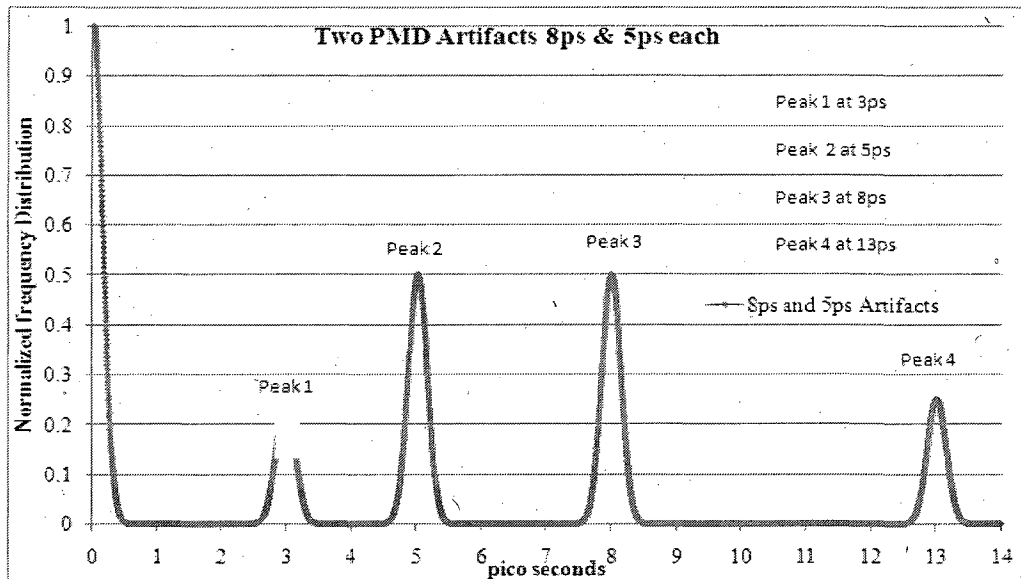


Figure 6- 25 Simulation Result Output DGD Distribution of Two Artifacts of 8 ps and 5 ps

It is observed that in addition to the central peak on the y-axis, the output has four peaks. The first peak occurs at 3 ps, the second at 5 ps, the third at 8 ps and the last one at 13 ps. Figure 6-26 is a snap shot of a field measurement with two artifacts of 8 ps and 5 ps respectively. The location of the peaks of the simulation and the field measurements match well.

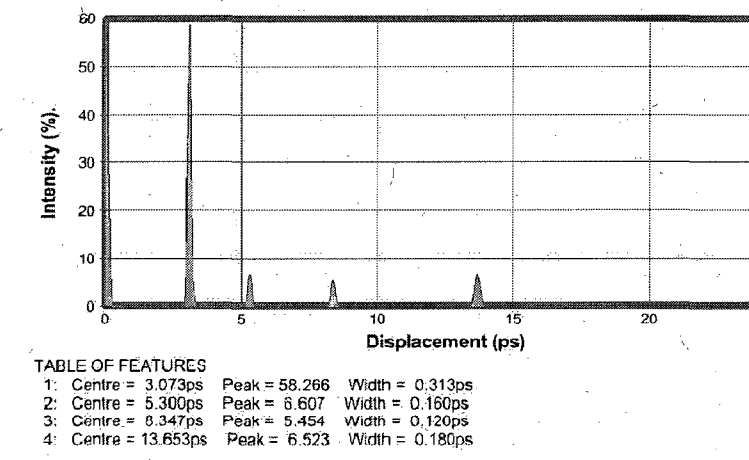


Figure 6- 26 Field Measurement Snapshot of Resultant output DGD Distribution with 8ps and 5ps Artifact

This experiment is repeated with two artifacts at 2 ps and 3 ps each. Figure 6-27 shows the output DGD distribution with four peaks beyond the central peak at the origin. The first peak is at 1ps, followed by a peak at 2 ps, 3 ps and lastly at 5 ps as expected. The figure also shows the effect of increasing the delay variance of the fiber section from 0.0001 ps to 0.01 ps. It is observed that the output DGD starts to widen as the delay variance is increased.

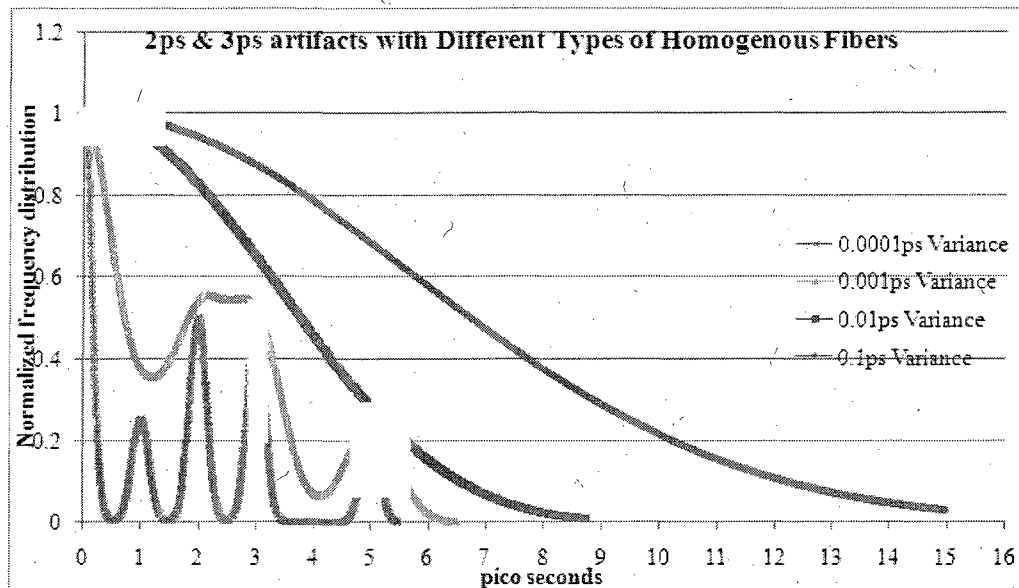


Figure 6- 27 Two PMD Artifacts of Value 2 ps & 3 ps with Different Fiber Types. Simulation Bin Size = 0.0025 ps

It is observed that the peak at 1 ps is completely absorbed by the output DGD while the peaks at 2 and 3 ps are close to being engulfed by the output DGD distribution. Increasing the delay variance of the fiber section to 0.01 ps and 0.1 ps completely engulfs all the peaks of the PMD artifacts.

The above exercise is repeated with two PMD artifacts of equal value of 2 ps each. When concatenated with a fiber section (1000 segments) of delay variance 0.0001 ps the output DGD distribution shows peaks at 0, 2 ps and 4 ps. Figure 6-28 shows the output DGD distribution for this case of two artifacts with an equal value of 2 ps concatenated with a fiber section that has a delay variance of 0.0001 ps.

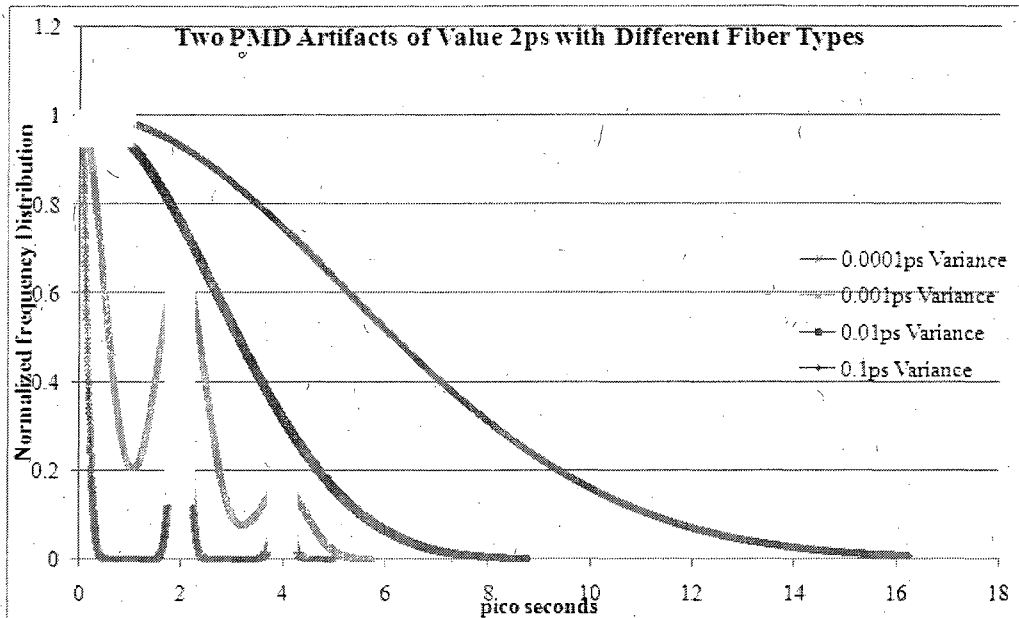


Figure 6- 28 Two PMD Artifacts of Value 2 ps & 2 ps with Different Fiber Types. Simulation Bin Size = 0.0025 ps

It is observed that in addition to the central peak, we see two peaks at 2 ps and 4 ps respectively. The figure also shows the effect of increasing the delay variance of the fiber section. The peaks of PMD artifacts tend to get assimilated into the output DGD distribution as it widens with an increase in delay of individual beat segments. This shows that our simulation is able to accurately characterize the deterministic effect of PMD and the mixing of this effect with a distributed effect in sections of fibers.

6.5 Impact of PMD Impairment on Network Performance

In this final section of the chapter, the ability of our model to evaluate and illustrate the impact of PMD impairment on the performance of optical networks in terms of Q penalty is illustrated. Various output DGD distributions are generated using different values of delay variance. Each output DGD distribution is characterized by its unique root mean square value of the DGD distribution and corresponding Q penalty respectively. The performance penalty curve is plotted with normalized RMS DGD (RMS DGD represented as a function of the bit period) on the x-axis versus Q Penalty on the y-axis.

Individual delays for a fiber section with 1000 beat segments are generated using a normal delay distribution with zero mean and a small variance of 0.001 ps. The output DGD distribution of this fiber section is simulated and the RMS DGD and the associated Q penalty at 10 Gbps, 40 Gbps and 100 Gbps are recorded. This process is repeated for increasing values of the delay variance. The RMS DGD and the Q penalty at the three data rates are recorded for each case. Figure 6-29 shows a plot of the normalized RMS DGD on the x-axis with the Q Penalty (dB) on the y-axis for data rate transmission of 10 Gbps ($T = 100$ ps).

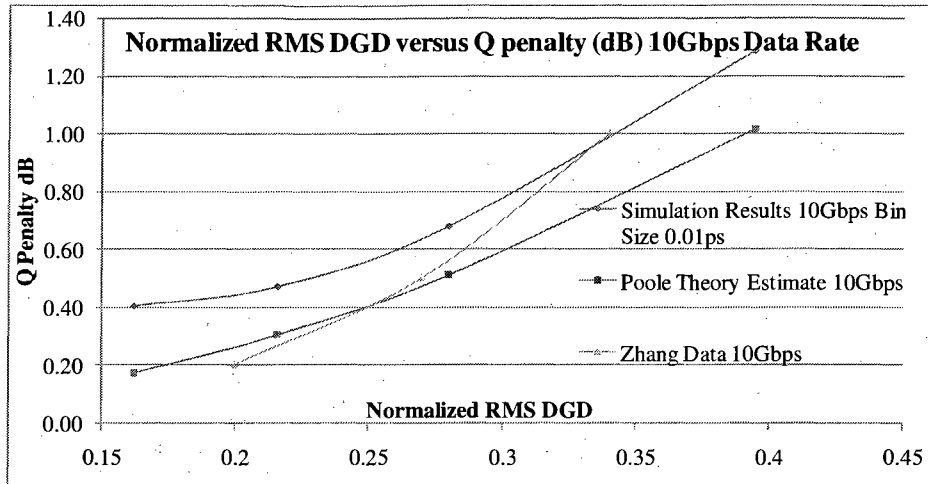


Figure 6- 29 Normalized RMS DGD versus Q penalty (dB) 10 Gbps Data Rate

Table 6-11 below tabulates the results from Figure 6-29. Normalized RMS DGD is the ratio of RMS DGD value to the time period of the pulse. Therefore,

$$\text{Normalized RMS DGD} = \frac{\text{RMS DGD (ps)}}{\text{Time Period (ps)}} \quad \dots\dots[6.3]$$

The Q Penalty is calculated with reference to the performance of the optical system at a base line delay variance of 0.1 ps.

10Gbps	T= 100ps	Simulation Results	
Bin Size	0.01ps		
Delay Variance (ps)	RMS DGD (ps)	Norm RMS DGD	Q Penalty dB
0.1	9.1	0.091	Base Line
0.3	16.2	0.162	0.40
0.5	21.6	0.216	0.47
1	28	0.28	0.68
2	39.5	0.395	1.28

Pooles Estimate	RMS DGD (ps)	Norm RMS DGD	Q Penalty dB
	16.2	0.162	0.17
	21.6	0.216	0.30
	28	0.28	0.51
	39.5	0.395	1.01

Zhangs Measured Data	RMS DGD (ps)	Norm RMS DGD	Q Penalty dB
	20	0.2	0.2
	27	0.27	0.5
	34	0.34	1

Table 6- 11 Q Penalty Results at 10 Gbps Data Rate

Results from our simulation at 10Gbps show that with the PMD impairment in the optical system close to 15% of the bit period, the Q penalty is very small at a value of 0.4 dB. Introducing a PMD impairment close to 30% of the bit period causes the penalty to rise to 0.7 dB. At 35% of the bit period (RMS DGD is ~35 ps) the performance penalty is approximately 1 dB. Over their analysis of fading in light-wave systems due to PMD, Poole and Tkach [8] came up with a generic estimate for penalty. Assuming a square pulse data stream consisting of pulses of full width T which is the reciprocal of the bit rate, the approximate performance penalty in dB is [8]:

$$\text{penalty (dB)} = 26 \frac{\Delta\tau^2 \cdot \gamma}{T^2} (1 - \gamma) \quad \dots\dots[6.4]$$

where γ is the relative power launched between the two principal states and is approximated to 0.5 under maximum penalty conditions.

Table 6-11 includes the estimated penalty by Poole et al [8] and their plot is compared against our simulation results in Figure 6-29. It is observed that our simulation results are within 0.3 dB of Poole's estimated penalty values [8]. Zhang, Xie *et al* [10] measured the PMD penalty on a real deployment-ready dense wavelength multiplexed system at a 10 Gbps data rate and their results are tabulated in Table 6-11. Figure 6-29 includes a plot comparing our simulation results with the measured data points from Zhang et al [10]. It is observed that our simulation results are within 0.3 dB of the measured data. This shows that our mapping of the PMD channel impairment at a 10 Gbps data rate is very close to the published results. Our software compiler limitation prevents us from simulating a larger number of beat segments for generating distributions for larger fiber lengths. Hence, we are not able to reproduce larger values of PMD impairments which will better map the performance penalty characterization at 10 Gbps data rate of transmission.

Figure 6-30 shows the penalty characterization at a data rate of 40 Gbps ($T = 25$ ps). The performance with a delay variance of 0.001 ps is considered as the base line for Q penalty calculations. A non linear trend in the increase of performance penalty with the increase in PMD impairment (Normalized RMS DGD) is observed. Table 6-12 tabulates the simulation results along with results from other authors. Results from our simulation show that at PMD impairment close to 25% of the bit period, the performance penalty is

0.18 dB. At close to 50% of the bit period, the performance penalty is approximately 2 dB. With PMD impairment at 65% of the bit period, the penalty is close to 3 dB. Figure 6-30 compares the plots of our simulation results with Poole's estimated penalties at 40 Gbps [8]. The plots are in agreement in terms of the closeness of the results and in terms of the shape of the plot.

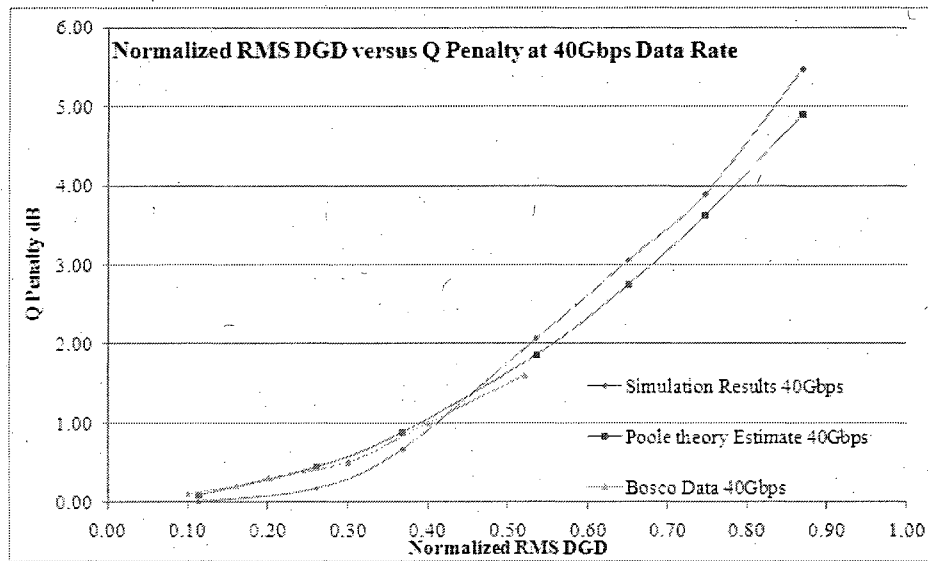


Figure 6- 30 Normalized RMS DGD versus Q penalty (dB) 40 Gbps Data Rate

40Gbps	T= 25ps	Simulation Results	
Bin Size	0.0025ps		
Delay Variance (ps)	RMS DGD (ps)	Norm RMS DGD	Q Penalty dB
0.001	0.91	0.04	Base Line
0.01	2.86	0.11	0.01
0.05	6.54	0.26	0.18
0.1	9.22	0.37	0.68
0.2	13.38	0.54	2.07
0.3	16.27	0.65	3.06
0.4	18.66	0.75	3.89
0.5	21.72	0.87	5.47

	RMS DGD (ps)	Norm RMS DGD	Q Penalty dB
Poole's Estimate	2.86	0.11	0.09
	6.54	0.26	0.44
	9.22	0.37	0.88
	13.38	0.54	1.86
	16.27	0.65	2.75
	18.66	0.75	3.62
	21.72	0.87	4.90

	RMS DGD (ps)	Norm RMS DGD	Q Penalty dB
Bosco's Estimate	2.5	0.1	0.1
	4	0.16	0.2
	5	0.2	0.3
	7.5	0.3	0.5
	10	0.4	1
	13	0.52	1.6

Table 6- 12 Q Penalty Results at 40 Gbps Data Rate

Figure 6-30 also shows the comparison between simulation results from Bosco et al [41] and our results. The plots again are in agreement with each other. This validates our

performance characterization with PMD impairments at a 40 Gbps data rate of transmission.

Figure 6-31 and Table 6-13 show the results for the performance penalty at a 100Gbps data rate of transmission ($T = 10$ ps).

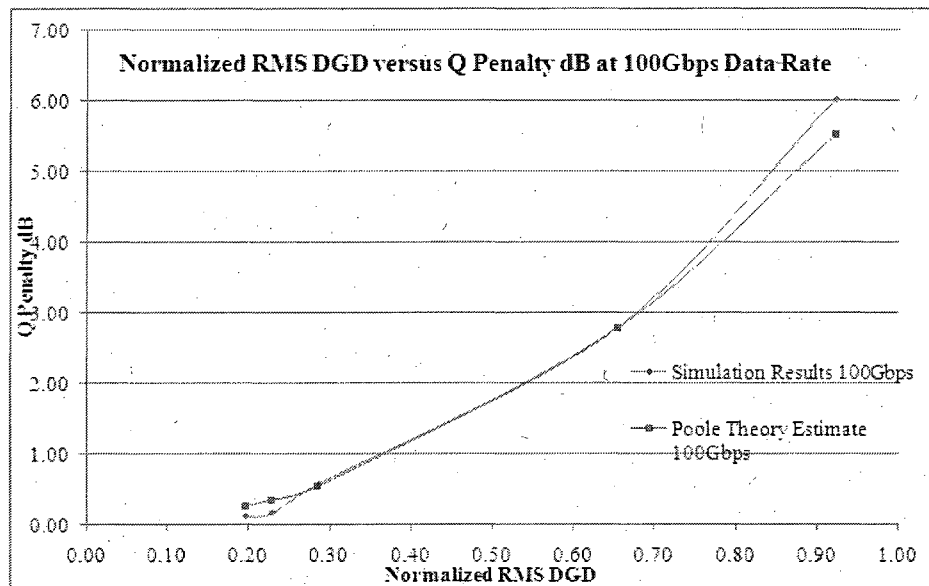


Figure 6- 31 Normalized RMS DGD versus Q penalty (dB) 100 Gbps Data Rate

Commercial networking products at this data rate are currently being planned and dense wavelength multiplexed optical metro and long haul optical networks at this data rate will mark the next generation in the evolution of optical network transmission. Published results at this data rate are not readily available as technology is currently evolving for commercial products at this data rate. Our model is able to evaluate the impact of PMD impairment on the performance of optical networks capable of carrying such fast data

rates. From our simulation results it is observed that with a PMD impairment of 2ps (20% of the bit period) the performance penalty is 0.11 dB. For a PMD impairment close to 30% of the bit period the performance penalty is 0.58 dB while Poole [8] estimates a penalty of 0.53dB. With a PMD impairment of 65% of the bit period the Q Penalty is 2.79 dB while Poole estimates a penalty of 2.78 dB. With a PMD impairment of 9.2 ps (92% of the bit period) our simulation results indicate a penalty of 6.03 dB while Poole estimates a penalty of 5.53 dB.

100Gbps	T= 10ps	Simulation Results	
Bin Size	0.0025ps		
Delay Variance (ps)	RMS DGD (ps)	Norm RMS DGD	Q Penalty dB
0.001	0.91	0.09	Base Line
0.0045	1.965	0.20	0.11
0.006	2.29	0.23	0.16
0.01	2.86	0.29	0.58
0.05	6.54	0.65	2.79
0.1	9.22	0.92	6.03
Poole's Estimate	RMS DGD (ps)	Norm RMS DGD	Q Penalty dB
		0.20	0.25
		0.23	0.34
		0.29	0.53
		0.65	2.78
		0.92	5.53

Table 6- 13 Q penalty results at 100 Gbps Data Rate

Figure 6-31 compares the plots from our simulation results with estimated penalty from Poole. Both the plots are very close to each other and are in agreement in terms of their closeness in values and the trend of growth.

Summary

In this chapter results from our various simulations which validate the success of our model in terms of being able to simulate the distributed and deterministic nature of the PMD impairment and in terms of being able to characterize the impact of this impairment on the performance of optical systems have been shown. The importance of the appropriate choice of a simulation sampling bin size and its impact on generating the complete output DGD Distribution has been discussed. The ability of our model to incrementally grow the discrete distribution which allows us to capture performance penalties as the fiber span is grown has been illustrated. Results from our simulation validated the square root dependence of distributed PMD impairment on length in a fiber with distributed DGD accumulation. The configuration of an incremental channel using our model wherein we could create a new type of output DGD distribution of fiber by changing the individual delays of beat length segments by changing the variance of the normal delay distribution has been illustrated. The configuration of a concatenated heterogeneous channel in which our model could simulate cases of different types of mixed fibers (different delay variances) or fiber sections mixed with deterministic PMD artifacts has been shown. The ability of our model to simulate multiple deterministic impairments in sections of fiber has been illustrated. Lastly, the results from our

simulation characterizing the impact of distributed PMD impairment on optical systems at different commercial data rates of 10 Gbs, 40 Gbps and 100 Gbps have been shown. The performance characterization of optical systems at these data rates showed our simulation results to be in agreement with published data and penalty trends. In summary, the observations discussed in this chapter show that our model is able to appropriately characterize the PMD impairment and its impact on optical systems. The next chapter will discuss our conclusions and recommendations for future work.

CHAPTER - 7

CONCLUSIONS AND RECOMMENDATIONS

Conclusions

An exhaustive systems model to characterize the effect of Polarization Mode Dispersion and to measure its impact on network configuration in terms of reach and quality of data transmission has been developed in this dissertation. This model overcomes many limitations in existing methodologies by:

- a) Providing an incremental approach to methodically grow the output DGD distribution of single mode optical fibers.
- b) Assisting in the identification and development of new and more effective PMD compensation techniques.
- c) Providing the flexibility to change individual beat segment delays and hence simulate mixed fibers and impairments, thus allowing the characterization of distributed and deterministic effects of PMD.

Our simulation model highlights the importance of measurement resolution or the sampling bin size which is responsible for collecting the delay components in appropriate delay buckets. Choice of too large a bin size will result in a compressed and inaccurate capture of the output DGD distribution.

Results from simulations demonstrating the incremental growth of our model show that the root mean square value of the output DGD distribution grows with a square root dependence on the length. This is in agreement with the understood trend of growth for the distributed effect of this PMD impairment as documented in the literature.

Our model has the ability to change the individual delays of beat segments and generate delays for a number of beat segments using a normal distribution. This allows us to simulate conventional single mode fiber types which are characterized by delays produced from a zero mean and a small value of variance resulting in a small value of accumulated PMD. Fibers with a moderate accumulation of the PMD impairment (spun dispersion shifted fibers) can be simulated by generating delays of beat segments using a normal distribution with zero mean and a medium value of variance. Fibers with a large accumulation of PMD impairment can be simulated by using a normal delay distribution with zero mean and a large value of variance. These two unique advantages, being able to incrementally grow the model and to simulate different types of fibers with different accumulated PMD impairment allows us to simulate and analyze the output distributions pertaining to real world network deployments wherein different types of fibers may be fused together. Our simulations have been able to illustrate the evolution of the output DGD distribution of such a case by changing the mixed proportions of two types of fiber with different delay variances. It was observed that in the case of an equal mix of two fiber types the output DGD distribution is largely influenced by the fiber type with a higher delay variance.

Our model allows for the simulation of deterministic PMD impairments in the fiber and is able to characterize the mix of deterministic and distributed DGD effects. Simulation results for the case of introduced PMD artifacts show that the resultant output DGD distribution contains a second peak separated from the central peak by a delay value equal to the value of the PMD artifact that was introduced. In the case of multiple PMD artifacts, the output distribution also includes the presence of peaks which are separated from the central peak by the sum and difference of the PMD artifact values as expected. Increasing the lengths or the delay variances of the distributed fiber section widens the output DGD distribution, and for large length of fiber or large delay variance the DGD distribution will completely assimilate the peaks of the PMD artifacts.

The systems model is able to accurately evaluate the impact of the PMD impairment on the performance of optical networks in terms of Q penalty. The Q penalty is calculated as a measure of the inter-symbol interference and impacts the eye closure and is directly linked with the receiver's ability to decipher a 1 bit or a 0 bit. The performance penalty comparisons at 10Gbps, 40Gbps and 100Gbps data rates of transmissions have been illustrated. The results from these simulations were plotted for different values of PMD impairment expressed as a fraction of its bit period. At 10Gbps data rates with a time period of 100ps, our simulation results are comparable with measured and predicted data from other sources. It should be pointed out that at a large time period of 100ps, large lengths of fiber need to be simulated to generate higher values of PMD impairment in order to better characterize its impact on network performance. At 40Gbps (time period of 25ps) and 100Gbps data rates of transmission, our performance penalties show very good agreement with published trends.

PMD is a critical channel impairment which restricts the ability of a network to transport data at high rates of transmission. Its statistical nature does not permit simple or cost effective compensation techniques. Analyses of the field measurements indicate that more than 3% of measured spans are found to exceed mean DGD per span by 10ps. This is equivalent to 40% of the bit period at 40Gbps and 100% of the bit period at 100Gbps data rates. Results from our simulations indicate a reduction in reach of an optical network by more than 5km when subjected to PMD impairment of value close to 40% of the symbol duration.

Recommendations

In this section, areas for future work have been proposed which could further contribute toward enhancing the performance of this model and would advance the development of economically viable compensation techniques and aid in accurate network designs and evaluation of their performance.

Future work will allow for simulation of longer fiber sections and thus produce output distributions with larger accumulated DGD. This will result in better mapping of the performance of optical networks at 10Gbps data rates as it will generate accumulated DGDs comparable to the bit period of 100ps.

Over the manufacturing process, optical fiber is drawn from molten silica and this may result in constant random twisting and turning of the fiber. Such random movement may generate small beat lengths with low values of birefringence. This process could be

responsible for the delay distribution the fiber segments. In our channel model unique beat segments delays are generated using a normal distribution. Future work can include the generation of the individual delays using different distributions to evaluate the impact on the output distribution. This can aid in design of better fibers which could be more tolerant to this channel impairment.

In our model, beat segments with different delays are concatenated with each other. Output modes of preceding beat segments couple with the input modes of the next beat segment and the output DGD distribution is grown incrementally. It is assumed that the power splitting ratio is equal at all interfaces of mode coupling, and consequently the resultant output DGD distribution of the fiber section is assumed to have all delay components with equal power. Future work could explore the power coupling or the interaction of power within different modes at beat segment interfaces and their resultant impact on the output distribution and the resulting performance penalties for the optical network.

In our model, a simple Non Return to Zero Optical transmission scheme to generate the optical pulses has been considered. Future work could expand on this and could explore the impact of different optical modulation schemes like Return to Zero, Optical Differential Phase Shift keying (DPSK) and Optical Differential Quadrature Phase Shift keying (DQPSK) to understand which transmission scheme would be more tolerant to PMD impairment at high data rates.

The ability of this model to capture the complete ensemble of discrete delay components enables the identification of worst case values of the impairment which have

the largest impact on the degradation of network performance. This can be applied to identify new approaches to characterize PMD compensation and to assist in the evaluation of more effective compensation techniques.

LIST OF REFERENCES

- [1] S.C Rashleigh, R Ulrich "Polarization Mode Dispersion in Single Mode Fibers" Optical Letters Vol 3, No.2 August 1978
- [2] C. D. Poole, R. E. Wagner, "Phenomenological approach to polarization dispersion in long single-mode fibres," Electron. Letters. 22, 1029-1030 1986
- [3] Craig D. Poole and C. R. Giles "Polarization-dependent Pulse Compression and Broadening due to Polarization Dispersion in Dispersion-Shifted fiber" Optics Letters, Vol. 13, Issue 2 Feb 1 1988
- [4] C.D. Poole, J.H. Winters and J.A Nagel "Dynamical Equation for Polarization Dispersion" Optics Letters Vol 16, No.2 March 15 1991
- [5] G.J Foschini and C.D. Poole "Statistical Theory of Polarization Mode Dispersion in Single Mode Fibers" Journal of Lightwave Technology Vol 9 No. 11 Nov 1991
- [6] N. Gisisn, B. Perny et.al "Experimental Investigation of the Statistical Properties of Polarization Mode Dispersion in Single Mode Fibers" IEEE Photonics Tech Letters Vol 5 no. 7 July 1993
- [7] GNNetest, "PMD440 Polarization Mode Dispersion Test System", Part# 32172, Rev.B, June 2000.
- [8] C.D. Poole D.A Fishman et.al "Fading In Lightwave System Due to Polarization Mode Dispersion" IEEE Photonics Tech Letters Vol 3 No. 1 Oct 1991
- [9] J. Zhou, M.J. O'Mahony "Optical Transmission System Penalties Due to Fiber Polarization Mode Dispersion" IEEE Photonics Tech Letters Vol 6 No. 10 Oct 1994
- [10] J. Zhang, C Xie et.al "Impact of Fiber Nonlinearity on PMD Penalty in DWDM Transmission Systems" IEEE Photonics Tech Letters, Vol. 17, NO. 2, Feb 2005
- [11] D Mahgerefteh, C. Menyuk "Effect of First Order PMD Compensation on Statistics of Pulse Broadening in a Fiber with Randomly Varying Birefringence" IEEE Photonics Tech Letters Vol.11 No.3 Mar 1999
- [12] H. Sunnerud, M. Karlsson et.al "Analytical Theory for PMD-Compensation" IEEE Photonics Technology Letters, VOL. 12, No. 1, Jan 2000

- [13] H. Sunnerud, C. Xier et.al "A Comparison Between Different PMD Compensation Techniques" Journal of Lightwave Technology, Vol. 20, Issue 3, 2002
- [14] B. Hakki "Polarization Mode Dispersion in a Single Mode Fiber" Journal of Lightwave Technology Vol 14 No.10 Oct 1996
- [15] H. Bulow "System Outage Probability Due to First and Second Order PMD" IEEE Photonics Tech Letters, Vol. 10, No. 5, May 1998
- [16] H. Kogelnik R.M. Jopson et.al "First Order PMD Outage for the Hinge Model" IEEE Photonics Tech Letters, Vol. 17, No. 6, June 2005
- [17] S. Savory, F. Payne et.al "Estimating Outages Due to Polarization Mode Dispersion Using Extreme Value Statistics" Journal of Lightwave Technology Vol. 24 No. 11 Nov 2006
- [18] C.D Poole & J Nagel "Polarization Effects in Lightwave Systems" Optical Fiber Communications IIIA.
- [19] G.P Agrawal "Fiber-Optic Communication Systems" Second Edition
- [20] TIA Fiber Optic Test Procedures-174
- [21] GNNetest, "PMD440 Polarization Mode Dispersion Test System", Part# 32172, Rev.B, June 2000
- [22] Daino B, Mater F et al, "Statistical treatment of Evolution Of The Principal States Of Polarization In The Single Mode Fibers", Electronic Letters , vol.22, pp.1029-1030, 1986
- [23] TSB-107 "Guideline for statistical specification of polarization mode dispersion on optical fibers". TAH, TIA SC-6.7, 1998.
- [24] Ciprut P, Gisin B et al, "Second Order Polarization Mode Dispersion: Impact on Analog and Digital Transmissions", Journal of Lightwave Technology, vol.16, No.5, May 1998
- [25] Nagel J. A., M. W. Chbat et.al. 2000. Long-term PMD mitigation at 10 Gb/s and time dynamics over high-PMD installed fiber. Proc. European Conference on Optical Communication, ECOC 2000. 2:31
- [26] Galtarossa, A., L. Palmieri, A. Pizzinat, G. Roba and D. Sarchi. 2001a. "Ultra low PMD fibers for Long-haul High-capacity Systems" Proc. Optical Fiber Communication Conference, OFC'01. Paper ThA8

- [27] C. Bianchi, A. Chitambar "Characterization of Optic Networks for High Bit Rate Time-Division-Multiplexed and Dense Wavelength-Division-Multiplexed Transport" NFOEC Orlando 2003
- [28] ITU-T Recommendation G.652, Characteristics of a Single Mode Fiber Optical cable, April 1997
- [29] ITU-T Recommendation G.653, Characteristics of Dispersion Shifted single mode fiber optical cable, April 1997.
- [30] ITU-T Recommendation G.655, Characteristics of non-zero Dispersion Shifted single mode fiber optical cable. October 1996
- [31] Gowar John, "Optical Communication Systems" Prentice Hall, 1984
- [32] A. Snyder, J. Love "Optical Waveguide Theory" Chapman and Hall 1983
- [33] A.B Buckman "Guided Wave Photonics" Saunders College 1992
- [34] G. Lachs "Fiber Optic Communications Systems, Analysis and Enhancements" McGraw Hill 1998
- [35] M. Cvijetic "Optical Transmission Systems Engineering" Artech House 2004
- [36] J. Palais "Fiber Optic Communications" Prentice Hall 1998
- [37] J. Proakis "Digital Communications" McGraw Hill 1995
- [38] S. Haykin "Communication Systems" Wiley 1983
- [39] F. Foghieri, R. Tkach "Fiber Nonlinearities and Their Impact on Transmission Systems" Optical Fiber Communications IIIA Chapter 8
- [40] G. Agrawal "Non Linear Fiber Optics" Academic Press 1995
- [41] G. Bosco A. Carena et.al "The Impact of Polarization Mode Dispersion: Optical Duo binary VS. NRZ Transmission" IEEE Photonics Tech Letters 2002
- [42] D. Halliday, R. Resnick "Physics Part II" Wiley 1977

APPENDIX

MATLAB CODE TO GENERATE BEAT SEGMENT DELAY

This MATLAB code generates delays for the individual beat length segments. The delays for n segments are generated using a Gaussian function with a specified value of mean and variance. The output of this program is used by the C++ code to generate the output DGD distribution of a fiber section composed of n beat segments.

```
% Clears the workspace before running the program
clear all

% Specifying the number of segments
bb=1
temp_delays = randn(n_old,1)
delays_counter=0
n_loop1=0
n_loop2=0
n_loop3=1996

temp_delays1 = randn(n_loop1,1)
temp_delays2 = randn(n_loop2,1)
temp_delays3 = randn(n_loop3,1)

delays_counter=0
delays_counter1=0
delays_counter2=0
delays_counter3=0

% Generating the delays of the beat length segments
for i1=1:n_loop1
    delays_old1(i1) = 0 + sqrt(1e-4)*temp_delays1(i1,1)
    %Zero mean, variance set to 0.0001 to check for lower variance - better fiber.
    if delays_old1(i1)>=0
        delays_counter1=delays_counter1+1
    end
end

for i2=1:n_loop2
    delays_old2(i2) = 0 + sqrt(1e-4)*temp_delays2(i2,1)
    %Zero mean, variance set to 0.0001 to check for lower variance - better fiber.
    if delays_old2(i2)>=0
        delays_counter2=delays_counter2+1
```

```

    end
end

for i3=1:n_loop3
    delays_old3(i3) = 0 + sqrt(1e-4)*temp_delays3(i3,1)
    %Zero mean, variance set to 0.0001 to check for lower variance - better fiber.
    if delays_old3(i3)>=0
        delays_counter3=delays_counter3+1
    end
end

delays_counter= delays_counter1+delays_counter2+delays_counter3
delays=zeros(1,delays_counter)

% Filtering the delays and choosing only the positive delays.
for cc1=1:n_loop1
    if delays_old1(cc1)>=0
        delays(bb)=delays_old1(cc1)
        bb=bb+1
    end
end

for cc2=1:n_loop2
    if delays_old2(cc2)>=0
        delays(bb)=delays_old2(cc2)
        bb=bb+1
    end
end

for cc3=1:n_loop3
    if delays_old3(cc3)>=0
        delays(bb)=delays_old3(cc3)
        bb=bb+1
    end
end

n = delays_counter

% Writing the number of delays generated in an output file
fid = fopen('G:\UNH-Program\Main-Matlab-Code\value_n-8-5.txt','w');
fprintf(fid,'%1.4f ',n);
fclose(fid)

```

```
% Checking that the number of delays does not exceed the maximum number supported
if n>1023
    'the value of n is greater than 1023'
    exit()
end

sum_delays=0

for aa=1:n
    sum_delays=sum_delays+delays(aa)
end

% Writing the delays to an output file
fid = fopen('G:\UNH-Program\Main-Matlab-Code\delays-log-8-5.txt','w');
fprintf(fid,'%1.4f ',delays);
fclose(fid)
```

C++ CODE OUTPUT DGD and PERFORMANCE PENALTY

This code uses the output from the from the MATLAB program as its input. The individual delays of the beat segments are used to generate the output DGD distribution. This code also calculates the RMS DGD of the output distribution and the associated eye closure that is used to generate performance penalties.

```
// test2C.cpp : Defines the entry point for the console application.
#include "stdafx.h"
#include <iostream.h>
#include <fstream.h>
#include <math.h>
#include <algorithm>

using namespace std;

const int MAX_SIZE = 10;
int numNormalizedElements = 0;

int main(int argc, char* argv[])
{
    // Initialize the variable below with MATLAB results to correspond to number
    // of beat segments
    float delays[1019];
    int n = 1019;

    // Reading in the delay file
    FILE* fin;
    fin = fopen("G:\\UNH-Program\\Main-C-Code-Folder-40G\\delays-log-8-5.txt", "r");
    for (int i=0; i<n; i++)
    {
        fscanf(fin, "%e ", &delays[i]);
    }
}
```

```

// Calculating the value of the maximum delay component
float sum_delays=0;
for (int aa=0;aa<n;aa++)
{
    sum_delays= sum_delays + delays[aa];
}

//Setting the bin_size and calculating the number of bins
double bin_size=0.0025;
int num_bins=ceil(sum_delays/bin_size);

//Defining the output distribution array
int num_bins_plus_one=num_bins+1;
double* output=NULL;
double* temp = NULL;
output = new double[num_bins_plus_one];
temp = new double[num_bins_plus_one];
for(int j=0;j<num_bins_plus_one;j++)
{
    output[j]=0;
    temp[j]=0;
}

// Hardcoding the output frequency of segment 1
output[0]=1;
temp[0]=1;

// Calculating the shift introduced by the first delay component
int num_steps=floor(delays[0]/bin_size);
int upper_limit=1;
int dummy =-1;

```

```

// Populating the output array with frequency: Main Logic
for (int k=0; k<n;k++)
{
    cout<<"Current delay being processed is "<<k<<endl;

    // Calculating the shift introduced by the current delay component
    num_steps=floor(delays[k]/bin_size);
    for (int l=0;l<upper_limit;l++)
    {
        output[l+num_steps]= temp[l]+temp[l+num_steps];
    }

    upper_limit=num_steps+upper_limit;
    for(int o=0; o<upper_limit; o++)
    {
        temp[o]=output[o];
    }
}

// Writing out the output DGD distribution
FILE* fid11;
fid11 = fopen("G:\UNH-Program\Main-C-Code-Folder-40G\output.txt","w");
for(int uu=0;uu<num_bins_plus_one;uu++)
{
    fprintf(fid11,"%e \n",output[uu]);
}
fclose(fid11);

// Calculating the highest frequency value of the output distribution
double highest =-1;
double next =-1;
int highestIndex=-1;
for (int q=0; q<num_bins_plus_one; q++)
{
    if (output[q]> highest)
    {
        highest = output[q];
        highestIndex =q;
    }
}

double* normalizedOutput=NULL;
numNormalizedElements = num_bins_plus_one - highestIndex;
normalizedOutput = new double[numNormalizedElements];
int tempIndex =0;

```

```

// Generating the normalized output distribution
for (int r =highestIndex; r<num_bins_plus_one; r++)
{
    normalizedOutput[tempIndex] = output[r]/highest;
    tempIndex++;
}

int finalIndex = numNormalizedElements;
printf("highest dgd dist value is %e \n", highest);

// Writing out the normalized output delay distribution
FILE* fid;
fid = fopen("G:\\UNH-Program\\Main-C-Code-Folder-40G\\C_Normalized-op-
delay.txt", "w");
for(int t=0;t<finalIndex;t++)
{
    fprintf(fid,"%e \n",normalizedOutput[t]);
}
fclose(fid);

// Calculating the RMS value of the output distribution
double sum_squares =0;
for (int u=0; u< numNormalizedElements;u++)
{
    sum_squares=sum_squares+(normalizedOutput[u]*normalizedOutput[u]);
}

double rms_y = pow((sum_squares / numNormalizedElements),0.5);
int rms_index = -1;
int rmsDevn =1000;
int tempRmsDevn =1000;
for (int v=0; v< numNormalizedElements;v++)
{
    tempRmsDevn= abs(floor(normalizedOutput[v]*1000)-
    floor(rms_y*1000));
    if(tempRmsDevn <rmsDevn)
    {
        rmsDevn=tempRmsDevn;
        rms_index = v;
    }
}

double rms_dgd = rms_index*bin_size;
printf("RMS DGD in ps is %e \n",rms_dgd);

```

```

// Writing out the RMS value and the highest DGD distribution value
FILE* fid1;
fid1 = fopen("G:\\UNH-Program\\Main-C-Code-Folder-
40G\\meanpmd_rmsdgd.txt","w");
fprintf(fid1, "RMS DGD in ps is %e \n",rms_dgd);
fprintf(fid1, "highest dgd dist value is %e \n",highest);
fclose(fid1);

// Generating the eye closure using Sinc functions for a 40 Gbps data rate
double total_delay_components=0;
double sinc_delay = 0;
for(int x=0;x<numNormalizedElements; x++)
{
    total_delay_components = normalizedOutput[x]+total_delay_components;
}

const double PI = 3.142857;

// Setting data rate as 40 Gbps
double freq = 40E9;

// Setting 5 sampling points at t=0, 25 ps, 50 ps, 75 ps and 100ps
double x_time_lower_limit=0;
double x_time_interval = 25E-12;
double x_time_upper_limit = 100E-12;
double sinc_bin_size = bin_size*1E-12;
int x_num_sinc_steps = ((x_time_upper_limit - x_time_lower_limit)/
x_time_interval) + 1 ;
double amplitude =1 ;

// Defining a two dimensional array to store Sinc function value at the 5 sampling
// points for each delay of the output distribution
double* YArray_2D = new
double[numNormalizedElements*x_num_sinc_steps];

// Defining 5 one dimensional arrays each storing the Sinc function value at a
// specific sampling point for all delays of the output distribution
double* YArray0 = new double[numNormalizedElements];
double* YArray1 = new double[numNormalizedElements];
double* YArray2 = new double[numNormalizedElements];
double* YArray3 = new double[numNormalizedElements];
double* YArray4 = new double[numNormalizedElements];
double time =0;

```



```

// Generating the Sinc plots
for (int y=0; y<numNormalizedElements; y++)
{
    for (int z=0; z<x_num_sinc_steps;z++)
    {
        amplitude = (normalizedOutput[y]/total_delay_components);
        sinc_delay = (y+1)*sinc_bin_size;
        if ((time-sinc_delay)==0)
        {
            *(YArray_2D + (z + y*x_num_sinc_steps))=0;
        }
        else
        {
            *(YArray_2D + (z + y*x_num_sinc_steps)) =
            amplitude*sin(PI* freq * (time-
            sinc_delay))/(PI*freq*(time-sinc_delay));
        }
        time = time + x_time_interval;
    }
    time =0;
}

// Defining arrays for that store captured data statistics at each sampling point
double max[5] ;
double sum[5];
double average[5];
double median[5];
double stdev[5];
double min[5];
double sum_stdev[5];

// Initializing stats arrays
for (int ee=0;ee<5;ee++)
{
    max[ee]=0;
    sum[ee]=0;
    min[ee]=10000;
    stdev[ee]=0;
    average[ee]=0;
    median[ee]=0;
    sum_stdev[ee]=0;
}

```

```

// Calculating average value at each sampling point
for(int cc=0; cc<x_num_sinc_steps;cc++)
{
    for(int bb=0; bb< numNormalizedElements;bb++)
    {
        if( *(YArray_2D + cc+ (x_num_sinc_steps *bb )) > max[cc])
        {
            max[cc]= *((YArray_2D +cc)+ (x_num_sinc_steps *bb));
        }

        {
            sum[cc]= ( *((YArray_2D +cc)+ (x_num_sinc_steps *bb
            ))) + sum[cc] ;
        }

        if( *((YArray_2D + cc)+ (x_num_sinc_steps *bb )) < min[cc])
        {
            min[cc]= *((YArray_2D +cc)+ (x_num_sinc_steps *bb ));
            if(min[cc]==0)
            {
                int myDummy=0;

            }

        }

    }

    average[cc] = sum[cc]/numNormalizedElements;
}
printf("MIN-MAX-AVG DONE\n");

```

```

// Calculating standard deviation value at each sampling point
double diff_with_mean_square =0;
for(int dd=0; dd<x_num_sinc_steps;dd++)
{
    for(int ee=0; ee< numNormalizedElements;ee++)
    {
        diff_with_mean_square =pow((*YArray_2D + dd+
(x_num_sinc_steps *ee )) - average[dd]),2);
        {
            sum_stdev[dd]=diff_with_mean_square + sum_stdev[dd];
        }
    }
    stdev[dd] = pow((sum_stdev[dd]/numNormalizedElements), 0.5);
}
printf("STDEVEV DONE\n");

// Calculating median value at each sampling point
// Creating a separate array for each Sinc step sampling point to simplify sorting
for(int ff=0; ff< numNormalizedElements;ff++)
{
    *(YArray0+ff) = *(YArray_2D + 0+ (x_num_sinc_steps *ff ));
    *(YArray1+ff) = *(YArray_2D + 1+ (x_num_sinc_steps *ff ));
    *(YArray2+ff) = *(YArray_2D + 2+ (x_num_sinc_steps *ff ));
    *(YArray3+ff) = *(YArray_2D + 3+ (x_num_sinc_steps *ff ));
    *(YArray4+ff) = *(YArray_2D + 4+ (x_num_sinc_steps *ff ));
}
printf("2D to 1D CONVERSION OF YARRAY_2D to 5 column arrays
DONE\n");

// Sorting each of the one dimensional arrays that have been created
sort(YArray0, YArray0+numNormalizedElements);
printf("SORT0 DONE\n");
sort(YArray1, YArray1+numNormalizedElements);
printf("SORT1 DONE\n");
sort(YArray2, YArray2+numNormalizedElements);
printf("SORT2 DONE\n");
sort(YArray3, YArray3+numNormalizedElements);
printf("SORT3 DONE\n");
sort(YArray4, YArray4+numNormalizedElements);
printf("SORT4 DONE\n");

```

```

// Calculating the median value at each sampling point using the sorted arrays
int medianIndex = (int) (numNormalizedElements/2);
median[0]= YArray0[medianIndex];
median[1]= YArray1[medianIndex];
median[2]= YArray2[medianIndex];
median[3]= YArray3[medianIndex];
median[4]= YArray4[medianIndex];

// Writing data statistics to an output file
FILE* fid3;
fid3 = fopen("G:\\UNH-Program\\Main-C-Code-Folder-40G\\40GStats.txt","w");
fprintf(fid3,"MAX \n ");
for (int jj=0; jj<x_num_sinc_steps; jj++)
{
    fprintf(fid3,"%e \n ",max[jj]);
}

fprintf(fid3,"AVERAGE \n ");
for (int ll=0; ll<x_num_sinc_steps; ll++)
{
    fprintf(fid3,"%e \n ",average[ll]);
}

fprintf(fid3,"MEDIAN \n ");
for (int nn=0; nn<x_num_sinc_steps; nn++)
{
    fprintf(fid3,"%e \n ",median[nn]);
}

fprintf(fid3,"STDEV \n ");
for (int mm=0; mm<x_num_sinc_steps; mm++)
{
    fprintf(fid3,"%e \n ",stdev[mm]);
}

fprintf(fid3,"MIN \n ");
for (int kk=0; kk<x_num_sinc_steps; kk++)
{
    fprintf(fid3,"%e \n ",min[kk]);
}

fclose(fid3);

printf("WRITING TO STATS FILE DONE\n");

```

```
// Deleting the dynamically created objects when done
delete YArray0;
YArray0=NULL;

delete YArray1;
YArray1=NULL;

delete YArray2;
YArray2=NULL;

delete YArray3;
YArray3=NULL;

delete YArray4;
YArray4=NULL;

delete YArray_2D;
YArray_2D =NULL;

delete normalizedOutput;
normalizedOutput=NULL;

delete output;
output =NULL;

delete temp;
temp=NULL;

return 0;
}
```